24. Allred DC, Clark GM, Elledge R, Fuqua SA, Brown RW, Chamness GC, Osborne CK, McGuire WL. Association of p53 protein expression with tumor cell proliferation rate and clinical outcome in node-negative breast cancer. J Natl Cancer Inst 1993;85:200–6.
25. Culig Z, Steiner H, Bartsch G, Hobisch A. Mechanisms of endocrine therapy-responsive and -unresponsive prostate tumours. Endocr Relat Cancer 2005;12:229–44.
26. Harkonen PL, Makela SI. Role of estrogens in development of prostate cancer. J Steroid Biochem Mol Biol 2004;92:297–305.
27. Vanacker JM, Bonnelye E, Chopin-Delannoy S, Delmarre C, Cavailles V, Laudet V. Transcriptional activities of the orphan nuclear receptor ERR α (estrogen receptor-related receptor-α). Mol Endocrinol 1999;13:764–73.
28. Zhang Z, Teng CT. Estrogen receptor α and estrogen receptor-related receptor α1 compete for binding and coactivator. Mol Cell Endocrinol 2001;172:223–33.
29. Shi H, Shigeta H, Yang N, Fu K, O'Brian G, Teng CT. Human estrogen receptor-like 1 (*ESRL1*) gene: genomic organization, chromosomal localization, and promoter characterization. Genomics 1997;44:52–60.
30. Cavallini A, Notarnicola M, Giannini R, Montemurro S, Lorusso D, Visconti A, Minervini F, Caruso MG. Oestrogen receptor-related receptor α (ERRα) and oestrogen receptors (ERα and ERβ) exhibit different gene expression in human colorectal tumour progression. Eur J Cancer 2005;41:1487–94.
31. Johnston SD, Liu X, Zuo F, Eisenbraun TL, Wiley SR, Kraus RJ, Mertz JE. Estrogen-related receptor β1 functionally binds as a monomer to extended half-site sequences including ones contained within estrogen-response elements. Mol Endocrinol 1997;11:342–52.
32. Carpenter R, Miller WR. Role of aromatase inhibitors in breast cancer. Br J Cancer 2005;93(Suppl 1):S1–S5.
33. Ellem SJ, Schmitt JF, Pedersen JS, Frydenberg M, Risbridger GP. Local aromatase expression in human prostate is altered in malignancy. J Clin Endocrinol Metab 2004;89:2434–41.
34. Forootan SS, Foster CS, Aachi VR, Adamson J, Smith PH, Lin K, Ke Y. Prognostic significance of osteopontin expression in human prostate cancer. Int J Cancer 2006;118:2255–61.
35. Lonard DM, Smith CL. Molecular perspectives on selective estrogen receptor modulators (SERMs): progress in understanding their tissue-specific agonist and antagonist actions. Steroids 2002;67:15–24.
36. Suetsugi M, Su L, Karlsberg K, Yuan YC, Chen S. Flavone and isoflavone phytoestrogens are agonists of estrogen-related receptors. Mol Cancer Res 2003;1:981–91.
37. Kim IY, Seong do H, Kim BC, Lee DK, Remaley AT, Leach F, Morton RA, Kim SJ. Raloxifene, a selective estrogen receptor modulator, induces apoptosis in androgen-responsive human prostate cancer cell line LNCaP through an androgen-independent pathway. Cancer Res 2002;62:3649–53.
38. El Etreby MF, Liang Y, Lewis RW. Induction of apoptosis by mifepristone and tamoxifen in human LNCaP prostate cancer cells in culture. Prostate 2000;43:31–42.
39. Kim IY, Kim BC, Seong do H, Lee DK, Seo JM, Hong YJ, Kim HT, Morton RA, Kim SJ. Raloxifene, a mixed estrogen agonist/antagonist, induces apoptosis in androgen-independent human prostate cancer cell lines. Cancer Res 2002;62:5365–9.
40. Raghow S, Hooshdaran MZ, Katiyar S, Steiner MS. Toremifene prevents prostate cancer in the transgenic adenocarcinoma of mouse prostate model. Cancer Res 2002;62:1370–6.
41. Steiner MS, Pound CR. Phase IIA clinical trial to test the efficacy and safety of Toremifene in men with high-grade prostatic intraepithelial neoplasia. Clin Prostate Cancer 2003;2:24–31.
42. Tremblay GB, Kunath T, Bergeron D, Lapointe L, Champigny C, Bader JA, Rossant J, Giguere V. Diethylstilbestrol regulates trophoblast stem cell differentiation as a ligand of orphan nuclear receptor ERR β. Genes Dev 2001;15:833–8.

Oncogene (2007) 26, 4453–4463

www.nature.com/onc

Identification of novel androgen response genes in prostate cancer cells by coupling chromatin immunoprecipitation and genomic microarray analysis

K Takayama[1,3], K Kaneshiro[2], S Tsutsumi[2], K Horie-Inoue[3], K Ikeda[3], T Urano[1,3], N Ijichi[3], Y Ouchi[1], K Shirahige[4], H Aburatani[2,5] and S Inoue[1,3]

[1]Department of Geriatric Medicine, Graduate School of Medicine, The University of Tokyo, Tokyo, Japan; [2]Genome Science Division, Research Center for Advanced Science and Technology, The University of Tokyo, Tokyo, Japan; [3]Division of Gene Regulation and Signal Transduction, Research Center for Genomic Medicine, Saitama Medical University, Saitama, Japan; [4]Division for Gene Research, Center for Biological Resources and Informatics, Tokyo Institute of Technology, Tokyo, Japan and [5]CREST, Japan Science and Technology Agency (JST), Tokyo, Japan

The androgen receptor (AR) plays a key role as a transcriptional factor in prostate development and carcinogenesis. Identification of androgen-regulated genes is essential to elucidate the AR pathophysiology in prostate cancer. Here, we identified androgen target genes that are directly regulated by AR in LNCaP cells, by combining chromatin immunoprecipitation (ChIP) with tiling microarrays (ChIP-chip). ChIP-enriched or control DNAs from the cells treated with R1881 were hybridized with the ENCODE array, in which a set of regions representing approximately 1% of the whole genome. We chose 10 bona fide AR-binding sites (ARBSs) ($P<1e-5$) and validated their significant AR recruitment ligand dependently. Eight upregulated genes by R1881 were identified in the vicinity of the ARBSs. Among the upregulated genes, we focused on UGT1A and CDH2 as AR target genes, because the ARBSs close to these genes (in UGT1A distal promoter and CDH2 intron 1) were most significantly associated with acetylated histone H3/H4, RNA polymerase II and p160 family co-activators. Luciferase reporter constructs including those two ARBSs exhibited ligand-dependent transcriptional regulator/enhancer activities. The present study would be powerful to extend our knowledge of the diversity of androgen genetic network and steroid action in prostate cancer cells.
Oncogene (2007) **26**, 4453–4463; doi:10.1038/sj.onc.1210229; published online 5 February 2007

Keywords: androgen receptor; androgen response element; chromatin immunoprecipitation; prostate cancer; UGT1A

Introduction

Androgen is a key regulator of male sexual differentiation as well as prostate development and carcinogenesis. Androgen-regulated gene expression is mediated by the action of androgen receptor (AR), which is a member of nuclear receptor superfamily that functions as a ligand-dependent transcription factor. Prostate cancer is originally an androgen-dependent tumor, whose growth and survival are under the control of AR signaling. Thus, androgen deprivation is the most common option of the cancer treatment. The therapy, however, eventually fails and most patients will relapse owing to adaptive progression of the surviving prostate cancer cells. The recurrent cancer is usually referred to as 'androgen independent' (Grossmann *et al.*, 2001). Nevertheless, advanced prostate cancer often continues to express AR and androgen-regulated genes, suggesting a functional role of AR in the recurrent stage. Alterations of the AR gene including mutation and amplification are also shown in some recurrent tumors, but these mechanisms will not explain the hormone-refractory responses in the majority of patients after androgen deprivation. Indeed, a modest increase in AR mRNA has been shown to be associated with the resistance to anti-androgen therapy in isogenic prostate cancer xenograft models (Chen *et al.*, 2004). Therefore, understanding the global aspects of AR signaling network and the distinct roles of AR target genes are essential for the development of new diagnostic procedures and therapeutic options for prostate cancer in various disease states.

AR regulates the expression of target genes by binding to androgen response elements (AREs) in the genome, or by interacting with other transcription factors bound to their specific recognition sites. AR-mediated gene transcription has been studied using prostate-specific antigen (PSA) as a prototypic model, and AREs in PSA promoter and enhancer have been shown to recruit various co-activators and general transcription factors including histone acetyltransferases,

Correspondence: Dr S Inoue, Department of Geriatric Medicine, Graduate School of Medicine, The University of Tokyo, 7-3-1 Hongo, Bunkyo-ku, Tokyo 113-8655, Japan.
E-mail: INOUE-GER@h.u-tokyo.ac.jp
Received 18 October 2006; revised 20 November 2006; accepted 21 November 2006; published online 5 February 2007

p160 family, mediator and RNA polymerase II (PolII) (Wang *et al*., 2005). Efforts have been paid to search various androgen target genes by using microarray techniques since last decade, identifying hundreds of genes with altered expression by hormone stimulation in cells. The gene expression profiling is powerful to depict the global function of androgen in a specified model; however, the technique will not be suitable to determine whether the alteration of gene expression is owing to direct or indirect action of AR transcription. Recent advance of human genome project enables to search putative AREs bioinformatically in the transcription regulatory regions of androgen target genes; yet, few AREs are identified as physiological elements in AR signaling (Horie-Inoue *et al*., 2004, 2006). Thus, the development of a new high-throughput method that identifies bona fide AR-binding sites (ARBSs) in the genome is a prerequisite for the elucidation of AR gene network.

Recently, a combined technique of chromatin immunoprecipitation (ChIP) analysis with DNA microarray has been established to identify chromatin-interacting domains of transcription factors in a genome-wide manner (Cawley *et al*., 2004; Bernstein *et al*., 2005). Regarding nuclear receptors, ligand-dependent estrogen receptor (ER)-binding sites have been recently shown by this ChIP-chip technique using Affymetrix-tiling oligonucleotide microarrays of chromosomes 21 and 22 (Carroll *et al*., 2005), or a custom-made promoter microarrays (Laganière *et al*., 2005). In this study, we have performed ChIP-chip using a sampler DNA microarray of the human genome, the so-called ENCODE chip. In this microarray, a set of regions representing approximately 1% (30 Mb) of the whole genome are included as the target for the pilot project that has been selected by the research consortium of the ENCyclopedia of DNA Elements (ENCODE Project Consortium, 2004). Fifty percent of the 30-Mb genomic regions, consisting of 14 regions (ENm001–ENm014), were manually selected, and the remaining 50% were composed of 30, 500 kb regions (ENr111–ENr334) selected according to a stratified random-sampling strategy based on gene density and level of non-exonic conservation.

Here, we find a discrete number of ARBSs in the selected regions of the ENCODE regions. Intriguingly, most of the AR-interacting regions have been shown to locate in non-promoter proximal regions; yet, they contained ARE sequences and were validated to recruit AR ligand dependently. In the vicinity of the functional ARBSs, we found several genes with upregulated transcript levels by hormone stimulation. Some of the AR target genes that have been identified in this study are previously known to be associated with AR expression, whereas some are novel targets. Our ChIP-chip analysis and transcriptional study indicate that non-promoter ARBSs play roles in the AR-dependent transcriptional regulation, potentially dissecting a series of AR-regulated mechanisms in a genome-wide manner.

Results

Screen of ARBSs on ENCODE DNA microarray

To perform a screen of ARBSs in AR-positive cells on tiling oligonucleotide microarrays, we first investigated the time course of ligand-dependent AR recruitment in human prostate cancer LNCaP cells. After 3-day hormone depletion, cells were stimulated with vehicle or a synthetic androgen R1881 (10 nM) for 2, 6 or 24 h. Cross-linked protein–DNA complexes extracted from the cells were immunoprecipitated with anti-AR antibody, and quantitative polymerase chain reaction (qPCR) for ARE regions in the proximal promoter and enhancer of PSA was performed using the purified precipitated DNAs as templates. AR binding in response to ligand stimulation exhibited maximal levels at 24 h (data not shown).

We next performed ChIP-chip analyses using the ENCODE tiling microarrays comprised of the total 30-Mb human genomic DNA, which corresponds to 1% of the genome. The chromatin DNAs immunoprecipitated by anti-AR or without ChIP (input control) were amplified unbiasedly by *in vitro* transcription (IVT), and the amplified DNAs were fragmented and biotin-labeled, then hybridized with the ENCODE chips for duplication. Using the Affymetrix Tiling Analysis Software, raw intensity data of duplicate arrays for each experimental group were transformed and signal and *P*-values for each genomic position interrogated were determined after quantile normalization. The results were mapped to genomic positions that could be visualized in the Affymetrix Integrated Genome Browser or the UCSC Genome Browser (NCBI Build 35). Applying a *P*-value cutoff of 1e-5 for a significant AR binding, we identified 10 ARBSs (Table 1) in the ENCODE genomic regions. Among them, five ARBSs were involved in the manually defined regions of the 30-Mb ENCODE regions (ARBSs no. 3–no. 7), whereas the remaining five binding sites were derived from the randomly selected regions.

Notably, most of the ARBSs were located within intronic regions or gene upstream regions at least 10 kb apart from the transcriptional start sites (TSSs) of their closest genes. One of the ARBSs included in the ENCODE chips was ARBS no. 1, which was located adjacent to UGT1A locus, in the 5′ upstream region >17 kb upstream of UGT1A1 gene TSS or in intron 1 of UGT1A3 on chromosome 2q37. As another example, ARBS no. 10 was situated in intron 1 of CDH2 on chromosome 18q11.2 (Figure 1).

We next investigated whether the 10 ARBSs included sequences highly similar to the previously established consensus AREs. Using a weighted matrix-based finder TRANSFAC (Matys *et al*., 2003) with the matrix conservation >75% or a sequence analysis utility of JASPER with the relative profile score threshold >70% (Sandelin *et al*., 2004), we identified canonical ARE sequences in all of the ARBSs (Table 2).

To verify whether the identified ARBSs in ChIP-chip were authentic ARBSs in the genome, we performed new independent ChIP experiments in LNCaP cells. We

Table 1 ARBSs identified in the encyclopedia of DNA element (ENCODE) regions by ChIP-chip experiments

ARBS no.	*ENCODE region*	*Chromosome*	*Start*	*Stop*	*Closest gene*	*Distance from TSS (bp)**	*Position*
1	ENr131	2	234 433 433	234 433 623	UGT1A1	−17 390	5′ upstream
2	ENr334	6	41 823 411	41 823 433	PGC	−323	5′ upstream
3	ENm010	7	26 807 344	26 807 566	SCAP2	−129 874	5′ upstream
4	ENm013	7	89 501 530	89 501 614	STEAP2	+15 922	intron 3
5	ENm013	7	89 980 335	89 980 369	PFTK1	−3010	5′ upstream
6	ENm001	7	115 551 316	115 551 473	TES	+106 864	3′ downstream
7	ENm001	7	116 022 567	116 022 922	MET	+116 336	intron 17
8	ENr233	15	41 640 443	41 640 980	KIAA0377	+23 671	intron 27
9	ENr233	15	41 739 974	41 740 495	CATSPER2	−11 904	5′ upstream
10	ENr213	18	23 990 311	23 990 793	CDH2	+20 637	intron1

Abbreviations: ARBs, androgen receptor-binding sites; TSS, transcriptional start site. *Distance from the TSS of the closet RefSeq gene to the corresponding ARBS based on the genomic position published in NCBI Build 35.

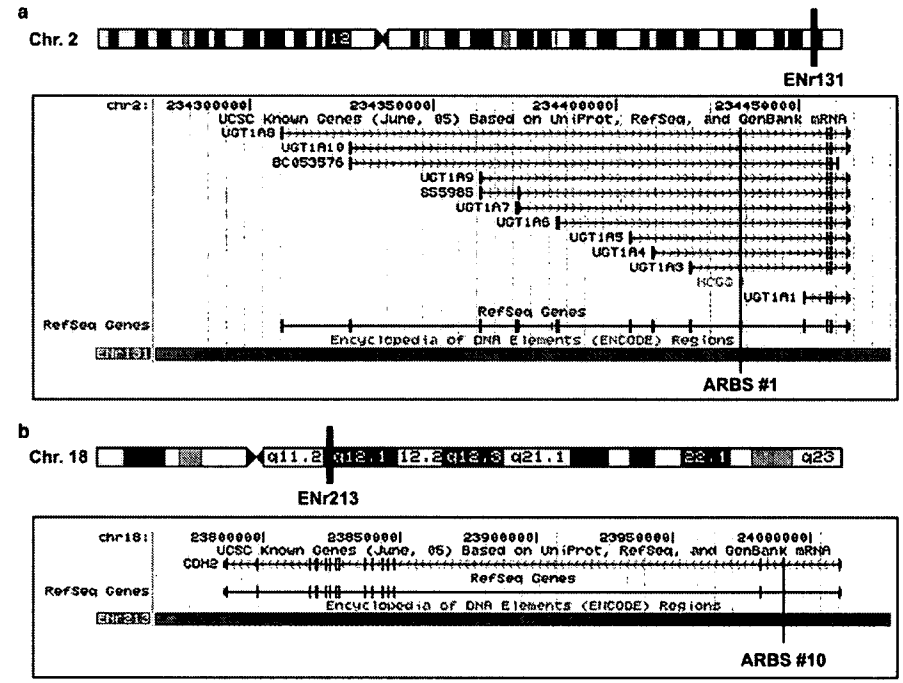

Figure 1 Identification of *in vivo* ARBSs in LNCaP cells on the encyclopedia of DNA elements (ENCODE) array by ChIP-chip analysis. (**a**) An expanded view of the UGT1A locus on the ENCODE region ENr131 from chromosome 2q37 is shown in its genuine 5′–3′ orientation. ARBS no. 1 is located on the 5′ upstream region of UGT1A1, or on intron 1 of other UGT1A isoforms. (**b**) An expanded view of the CDH2 on the ENCODE region ENr213 from chromosome 18q11.2 is shown in its genuine 3′–5′ orientation. ARBS no. 10 is located on intron 1 of CDH2.

confirmed that >10-fold enrichment of R1881-dependent AR binding was shown in the all regions involved in the defined 10 ARBSs, targeting the identified ARE sequences (Figure 2). Thus, with the cutoff value 1e-5, we validated that our ChIP-chip results did not include false positives.

Identification of androgen target genes adjacent to AR-binding sites

To identify novel androgen target genes by using ChIP-chip data, we examined the alteration of gene expression closest to the ARBSs in LNCaP cells in response to R1881 (Figure 3). Eight of 10 genes adjacent to the

Table 2 ARE sequences identified in the ARBSs detected by ENCODE chip

ARBS no.	*Gene*	*Distance from TSS (bp)*	*Position*	*Chromosome*	*Genomic location*	*Strand*	*ARE sequence*
1	UGT1A1	−17422	5′	2	234433576	+1	TGAACAttcTGTCCT
2	PGC	−399	5′	6	41823498	+1	GGAACAaatAGTTCT
3	SCAP2	−130006	5′	7	26807587	−1	AGAACCccaGGACCC
4	STEAP2	15941	INTRON 3	7	89501592	+1	GGAAAGaatTGTTCT
5	PFTK1	−2978	5′	7	89980382	−1	AGTAAGaagAGTTGC*
		−2947	5′	7	89980415	−1	ACAGCActcAGTACT*
6	TES	+106870	3′	7	115551402	+1	AAAACActcAGTTGC*
7	MET	+116298	INTRON 17	7	116022708	+1	TGCACAgtgTTTTAC*
8	KIAA0377	+27774	INTRON 27	15	41640739	−1	TAACCAtccTGTACC
9	CATSPER2	−11955	5′	15	41740290	−1	TAACCAtccTGTACC
10	CDH2	+20827	INTRON1	18	23990362	−1	GGTACAgaaTGTCAC
		+20805	INTRON1	18	23990384	−1	GGTACAgaaTGTCAC
		+20761	INTRON1	18	23990428	−1	GGTACAgcaTGTCAC
		+20739	INTRON1	18	23990450	−1	GGTACAgaaTGTCAC
		+20695	INTRON1	18	23990494	−1	GGTACAgcaTGTCAC
		+20673	INTRON1	18	23990516	−1	GGTACAgcaTGTCAC
		+20651	INTRON1	18	23990538	−1	GGTACAgaaTGTCAC
		+20629	INTRON1	18	23990560	−1	GGTACAgcaTGTCAC
		+20607	INTRON1	18	23990582	−1	GGTACAgcaTGTCAC
		+20541	INTRON1	18	23990648	−1	GGTACAgcaTGTCAC
		+20519	INTRON1	18	23990670	−1	GGTACAgcaTGTCAC
		+20651	INTRON1	18	23990538	−1	GGTACAgaaTGTCAC
		+20453	INTRON1	18	23990736	−1	GGTACAgaaTGTCAC

ARE sequences were primarily determined by a position-weighted matrix method TRANSFAC with the matrix conservation > 75% (Matys *et al.*, 2003). If no ARE was predicted by the first criteria, alternative ARE sequences (indicated as *) were determined by a sequence analysis utility of JASPER with the relative profile score threshold > 70% (Sandelin *et al.*, 2004). Genomic location of ARE sequence indicates the position of the center base.

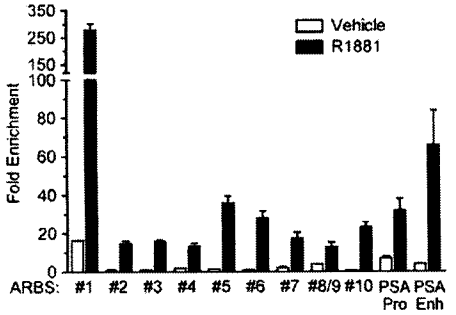

Figure 2 Validation of androgen-dependent AR enrichment by quantitative ChIP analysis on the identified ChIP-chip ARBSs in LNCaP cells. Hormone-deprivated cells were stimulated with R1881 (10 nM) or vehicle (0.1% ethanol) for 24 h. Cross-linked samples were immunoprecipitated with anti-AR antibody. The precipitated DNA fragments were subjected to qPCR. PCR primer sets were designed to include ARE sequences on individual ARBSs no. 1–no. 10. PCR products including ARBSs no. 8 and no. 9 were not distinguishable, as ARBSs no. 8 and no. 9 are located in genome duplication regions from the same origin. PSA promoter (PSA Pro) and enhancer (PSA Enh) regions including ARE sequences were used as positive controls. Data are fold enrichment compared with individual input non-enriched DNA (mean±s.d., $n=2$).

ARBSs exhibited a ligand-dependent increase in expression levels by > 2-fold compared with a vehicle-treated control by 48 h after treatment. Among them, UGT1A1 and Pepsinogen C (PGC) levels elevated by > 30- and > 1000-fold, respectively, with 48-h R1881 treatment (Figure 3a and b). Residual two of 10 genes adjacent to the ARBSs, SCAP2 and MET, exhibited a ligand-dependent decrease in expression levels (Figure 3c).

UGT1A gene locus encodes nine distinct isoforms with unique exon 1 based on the difference of TSSs (Gong *et al.*, 2001). Individual first exons are determinants for the structure of N-terminal UGT1A isoforms, which are important for substrate specificity. We examined whether androgen regulated the transcription of distinct UGT1A isoforms in LNCaP cells. Interestingly, only the mRNA levels of UGT1A1 (Figure 3a) and UGT1A3 isoforms, which have TSSs most adjacent to ARBS no. 1, were significantly increased up to 48 h after R1881 (10 nM) stimulation (UGT1A3 mRNA levels: 1.2±0.1 fold at 12 h, 5.8±0.2 fold at 24 h and 11.2±0.2 fold at 48 h after treatment). On the contrary, the mRNA levels of other UGT1A isoforms were not basically altered or rather decreased during the time course (data not shown).

Taken together, our data suggest that AR could regulate transcription of genes adjacent to ARBSs.

ARBSs are associated with histone acetylation and facilitate recruitment of RNA PolII

We next examined whether these ARBS regions recruited components indicative of transcriptional activation. ChIP analyses for acetylated histone H3/H4 (AcH3/H4) and RNA PolII were performed on the 10 ARBS regions in LNCaP cells (Figure 4). The AREs in PSA promoter and enhancer were used as positive

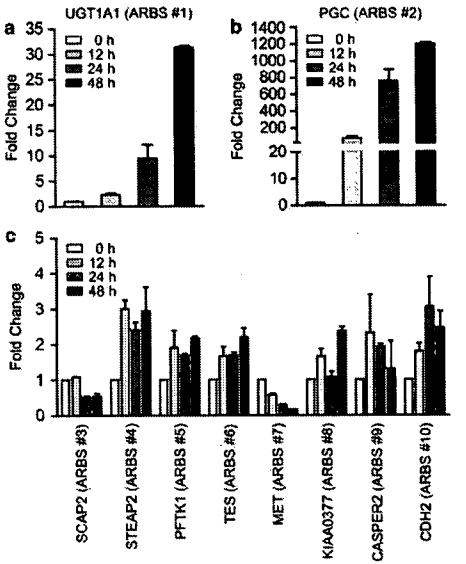

Figure 3 Androgen-dependent changes in expression of genes adjacent to the ChIP-chip ARBSs in LNCaP cells. Hormone-deprivated cells were stimulated with R1881 (10 nM) or vehicle for 12, 24 and 48 h. Quantitative RT–PCR analysis regarding the expression of 10 proximal genes close to ARBSs no. 1–no. 10 was performed using the reverse-transcribed cDNAs from the cells. Data are fold change compared with vehicle-treated cells at individual time point (mean±s.d., $n=2$). (a) UGT1A1 mRNA levels, (b) PGC mRNA levels and (c) mRNA levels of gene adjacent to ARBSs no. 3–no. 10.

controls. Histone acetylation was remarkable by R1881 treatment in ARBSs no. 1 and no. 10, in the vicinity of UGT1A1 and CDH2, respectively. Ligand-dependent RNA PolII recruitment was also significant in ARBS no. 1. In ARBS no. 10, PolII binding was enriched at basal levels and further enhancement of PolII binding was not observed by ligand stimulation (Figure 4c). Moderate histone acetylation and PolII recruitment in response to R1881 were also observed in ARBS no. 4, which was located in intron 3 of STEAP2. In the rest of seven ARBSs, all associated with ligand-dependent AcH3/H4 binding by > 2-fold and three of seven recruited PolII ligand dependently by > 2-fold. Although most of the identified ARBSs were located rather distal from known genes, our data suggest that a significant number of the ARBSs in the genome physically function as distal transcriptional regulatory domains during transcription of the adjacent genes.

Functional recruitment of p160 co-activators at ARBSs

The p160 SRC family co-activators play scaffold roles in forming co-activator complex involved in nuclear

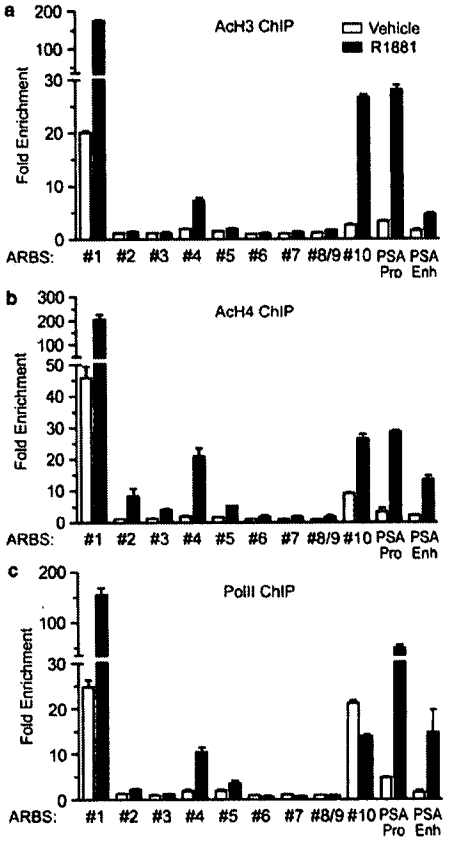

Figure 4 Some of the ChIP-chip ARBSs associate with histone acetylation and RNA PolII recruitment. Hormone-deprivated LNCaP cells were stimulated with R1881 (10 nM) or vehicle for 24 h. Cross-linked samples were immunoprecipitated with anti-acetylated H3/H4 (AcH3/AcH4) or anti-RNA PolII antibodies. The precipitated DNA fragments were subjected to qPCR. Identical primer sets were used as described in Figure 2. Data are fold enrichment compared to individual input non-enriched DNA (mean±s.d., $n=2$).

receptor-mediated transcription (Shang and Brown, 2002). In AR-mediated transcription, the p160 co-activators are shown to be recruited to AR complex and to facilitate AR transactivation by their histone acetylase activity (Shang *et al.*, 2002). To delineate the functional roles of endogenous p160 co-activators in AR-mediated transcription from the identified ARBSs no. 1–no. 10, we performed ChIP analysis using antibodies against SRC1, GRIP1 and AIB1 (Figure 5). It is notable that all of the p160 co-activators were recruited by > 10-fold in the ARE from PSA promoter.

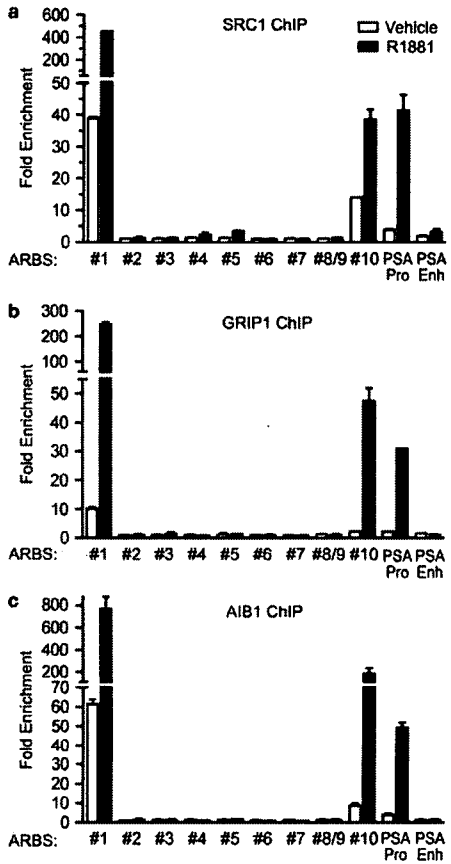

Figure 5 ChIP-chip ARBSs and p160 coactivator recruitment. Hormone-deprivated LNCaP cells were stimulated with R1881 (10 nM) or vehicle for 24 h. Cross-linked samples were immunoprecipitated with anti-SRC1, anti-GRIP1 or anti-AIB1 antibodies. The precipitated DNA fragments were subjected to qPCR. Identical primer sets were used as described in Figure 2. Data are fold enrichment compared to individual input non-enriched DNA (mean ± s.d., $n = 2$).

Consistent with the result of histone acetylation and RNA PolII recruitment, all of the p160 co-activators were recruited by >10-fold upon R1881 stimulation compared with vehicle in ARBS no. 1, adjacent to UGT1A1. The second potent binding site for AcH3/H4 and RNA PolII, ARBS no. 10 adjacent to CDH2, recruited SRC1 by >2-fold and GRIP1 and AIB1 by >20-fold upon ligand stimulation. Among other ARBSs, ARBS no. 5 close to PFTK1 recruited SRC1 by >2-fold in response to ligand stimulation. The data show that some of the authentic ARBSs may play roles as enhancers that recruit various transcriptional regulators and co-activators.

Distal and intronic ARBSs function as transcriptional regulators in androgen-dependent transcription

To further assess the possibility that the distal or intronic ARBSs function as bona fide transcriptional regulators in androgen-dependent transcription, we performed promoter activity assay using luciferase reporter constructs including ARE sequences derived from the ARBSs. Using the genomic DNA of LNCaP cells as a template, we amplified fragments included ARE sequences in ARBSs no. 1 and no. 10, corresponding to the 5′ upstream region of UGT1A1 (~−17 kb) and intron 1 of CDH2 (Figure 6a and b). Note that ARBS no. 1 is also located in intron 1 of other UGT1A isoforms. The amplified fragments were ligated to a luciferase reporter plasmid pGL3-vector containing SV40 promoter. Regarding the 5′ upstream region of UGT1A1, we also generated a mutated construct including two substitutions at the positions −2C and +2G from the 3-bp spacer (UGT1A1 5′ Mut-Luc). Using LNCaP cells transfected with reporter constructs, the luciferase activities of UGT1A1 5′-Luc and CDH2 Int 1-Luc were increased ~5- and ~8-fold by R1881 treatment, respectively, whereas MMTV luciferase construct exhibited >100-fold activation in response to ligand stimulation (Figure 6c). UGT1A1 5′ Mut-Luc did not exhibit androgen-dependent transcriptional activation. These results suggest that a significant number of non-promoter ARBSs also play essential roles in AR-mediated gene transcription.

Moreover, UGT1A protein expression could be regulated by androgen (Figure 6d). LNCaP cells after 72-h hormone deprivation were stimulated with R1881 or vehicle and cell lysates were prepared after 24 or 48 h. Although the isoform specificity of UGT1A was not shown by the antibody that we used, overall amounts of UGT1A protein were increased in response to androgen.

Discussion

This study aimed to identify novel androgen target genes in prostate cancer LNCaP cells by performing ChIP-chip analysis, identifying *in vivo* ARBSs in the selected ENCODE genomic regions. This scanning successfully identified 10 bona fide *in vivo* ARBSs with a $P < 1e\text{-}5$. Notably, all of the 10 ARBSs included ARE sequences as determined by the sequence analysis utilities based on TRANSFAC or JASPER transcription factor-binding profiles (Matys *et al*., 2003; Sandelin *et al*., 2004), and ChIP-PCR validation confirmed that those ARBSs had abilities to recruit AR ligand dependently. Our ChIP-chip approach is a powerful high-throughput method that can be applied to the whole genome-wide screen of ARBSs.

Efforts have been paid to identify transcription factor-binding motifs for years by searching a consensus-like sequence through *in silico* or *in vitro* studies in

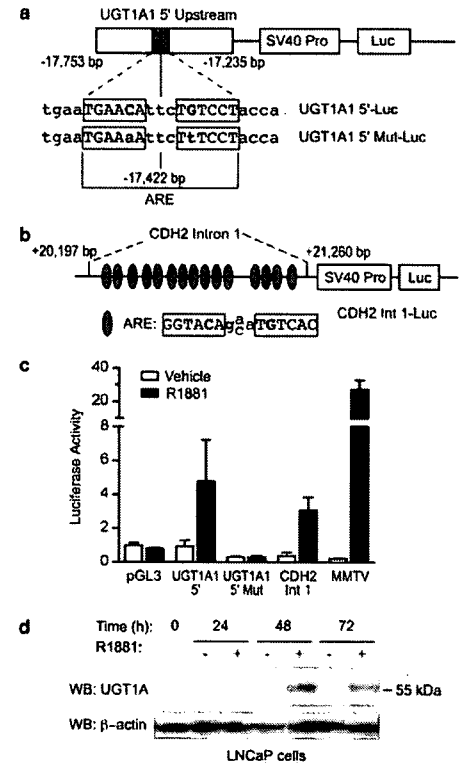

Figure 6 Transcriptional activity of UGT1A1 5′ upstream and CDH2 intronic ARBSs. (**a**) Construction of luciferase reporter plasmids containing UGT1A1 5′ upstream regions. A 519-bp fragment of the 5′ upstream of UGT1A1 (−17 753/−17 235 bp) amplified from LNCaP cells, and the 5′ fragment of UGT1A1 with mutation at the positions −2C and +2G from the 3-bp spacer in ARE sequences (ARBS no. 1) were cloned into pGL3 vector containing SV40 promoter (SV40 Pro), designated as UGT1A1 5′-Luc and UGT1A1 5′ Mut-Luc, respectively. (**b**) Construction of luciferase reporter plasmid containing CDH2 intron 1. A genomic fragment of CDH2 intron 1 (ARBS no. 10) derived from LNCaP cells (+20 197/+21 260 bp), containing 15 repeats of palindromic ARE sequences with the half-site GGTACA, was cloned into pGL3 vector (CDH2 Int 1-Luc). Note that the number of ARE sequences in LNCaP cells was larger than that in the genome database. (**c**) Androgen-stimulated luciferase activities of ARE sequences involved in UGT1A1 5′ upstream and CDH2 intron 1. LNCaP cells were stimulated with R1881 (10 nM) or vehicle 12 h after transfection with indicated plasmids together with a Renilla luciferase reporter gene, and incubated for another 24 h. Firefly luciferase activity was normalized to Renilla luciferase activity for each data set. MMTV luciferase reporter gene containing ARE sequences was used as a positive control. Data represent the mean ± s.d., $n = 3$. (**d**) Androgen-stimulated expression of UGT1A protein in LNCaP cells. Cells were stimulated with R1881 (10 nM) or vehicle for indicated times and whole cell lysates were separated by 8% SDS–PAGE. The PVDF membrane blotted with proteins were probed with anti-UGT1A or anti-β-actin antibodies.

the vicinity of transcription factor targets. In the days after the completion of the Human Genome Project, genomic DNA microarray has been developed and identification of *in vivo* binding targets of nuclear proteins is enabled by ChIP-chip analysis. For instance, in the ChIP-chip study for ERα on chromosomes 21 and 22, most of the binding sites were found at significant distances including several >100 kb removed from TSSs (Carroll *et al*., 2005). It has been suggested that these distal ERα-binding sites play an important role in estrogen-mediated regulation, as they could be physically associated with promoter-proximal regions. Similarly, in the present study, nine of 10 ARBSs that we identified by ChIP-chip were situated in the distal 5′ regions or intronic regions of known genes. Among those distal ARBSs, there were several sites that significantly recruited AcH3/H4 and RNA PolII (Figure 4). ARBSs no. 1 and no. 10, which are located at >17 kb upstream of UGT1A1 and in intron 1 of CDH2, respectively, could also associate with the p160 co-activators in a ligand-dependent manner (Figure 5). Based on our findings and previous evidence, a number of ARBSs may be located in non-promoter regions of the genome, and often associated with histone acethylation and co-activator recruitment.

In the vicinity of ChIP-chip identified ARBSs, we found several genes upregulated or downregulated by androgen stimulation. PGC, whose location is close to ARBS no. 2, is an androgen-upregulated gene that has been reported previously as a prognostic factor in prostate cancer (Diaz *et al*., 2002). It is an aspartyl protease and known as a protein involved in the digestion of proteins in the stomach. We identified a novel ARE sequence in ARBS no. 2, at −323 bp upstream of the TSS of PGC, indicating that ChIP-chip is particularly a powerful method to find out a novel transcription factor target regardless of the expression level of the target gene. As the ligand-dependent RNA PolII recruitment was not significant at ARBS no. 2 at the time we investigated (Figure 4c), other PGC regulatory region might be more important in the PolII activation; yet, ARBS no. 2 might play a role in the transcriptional regulation of PGC as the histone acetylation was at least promoted by ligand stimulation (Figure 4b). STEAP2, which includes ARBS no. 4 in intron 3, has been originally cloned as a STEAP homolog gene that encodes a transmembrane protein expressed in prostate cancer (Porkka *et al*., 2002). Although androgen responsiveness of STEAP2 was not reported previously, our data showed that it was a novel androgen target gene with a genuine ARBS in intron 3, which was also associated with histone acetylation.

ENCODE region ENm001 corresponds to chromosome 7q31, which is known as a fragile site with frequent loss of heterozygosity in advanced prostate cancer (Kawana *et al*., 2002). Among several genes at 7q31, TES (testis-derived transcript) has been shown as a candidate tumor suppressor gene in prostate cancer (Chene *et al*., 2004). In the present studies, we showed that TES was an androgen-upregulated gene with a

genuine ARBS (ARBS no. 6) in its 3′ downstream region (−58 kb from the 3′-end). TES protein contains three conserved cysteine-rich zinc-binding motifs called LIM domains, suggesting that TES may play a role in protein-protein interaction and focal adhesion (Coutts *et al.*, 2003). Methylation of the CpG island at the 5′ end of TES is frequently occurred in ovarian cancer cells, and overexpression of TES in culture cells was shown to be growth-inhibitory (Tobias *et al.*, 2001). In contrast, we showed that MET was an androgen-downregulated gene with a novel ARBS (ARBS no. 7) in intron 17. MET encodes a receptor-like tyrosine kinase, c-met proto-oncogene product, which can be activated by hepatocyte growth factor as a receptor (Cooper *et al.*, 1984). It has been reported that MET expression is upregulated by androgen deprivation and MET appears to be preferentially expressed in androgen-insensitive, high-grade prostate cancer cells (Pisters *et al.*, 1995; Humphrey *et al.*, 1995). It has been also shown that overexpression of AR in prostate cancer PC3 cells leads to MET downregulation (Maeda *et al.*, 2006). Based on our bindings, we could propose that both TES and MET at 7q31 are regulated by AR in a way to exhibit negative feedback for prostate cancer progression, while the former is a tumor suppressor gene and the latter is a proto-oncogene.

CDH2 encodes one of the calcium-dependent cell adhesion molecules, N-cadherin. Whereas another calcium-dependent cell adhesion molecules, E-cadherin, is expressed in epithelial cells, N-cadherin is expressed in nerve system, skeletal muscle and mesenchymal cells (Jaggi *et al.*, 2006). Recent evidence suggests that changes in cadherin expression or cadherin switching play a critical role during progression of various tumors including breast cancer (Hazan *et al.*, 1997) and prostate cancer (Tomita *et al.*, 2000). Loss of E-cadherin expression was seen in high-grade breast and prostate cancers, whereas high levels of N-cadherin expression was shown in invasive tumors. Androgen responsiveness of N-cadherin has been shown in neurons, in spinal motoneurons (Monks and Watson, 2001). Our finding demonstrates that CDH2 is an androgen target gene with a novel cluster of ARE repeats in intron 1.

Interestingly, we found a polymorphism in terms of the number of ARE sequences in intron 1 of CDH2. In regard to the 15-bp complete palindromes consisting of the half-site GGTACA motif, LNCaP cells had 15 ARE sequences as shown in Figure 6b, whereas the genomic data published in NCBI Genome Browser contained 13 ARE sequences. We also found that 15 and 14 ARE repeats were contained in the CDH2 intron 1 derived from prostate cancer DU145 cells and benign prostate hyperplasia BPH1 cells, respectively (data not shown). By generating luciferase constructs including the ARE repeats of the CDH2 intron 1 derived from DU145 and BPH1, we showed that the luciferase activities of those constructs were also induced by R1881 stimulation, although the response of BPH1 was smaller than that of LNCaP or DU145. Thus, the polymorphism of ARE repeats in intron 1 may be related to the intensity of androgen responsiveness.

In this study, we demonstrated that UGT1A was a novel androgen-regulated gene with a functional ARE sequence in the 5′ upstream region of UGT1A1 or intron 1 in other UGT1A isoforms. Among several UGT1A isoforms, only UGT1A1 and UGT1A3 have been shown as androgen-upregulated genes in LNCaP cells. Considering out results, it is possible that the isoform-specific androgen responsiveness is linked with the closeness of the functional ARE in ARBS no. 1 to each isoform TSS. Thus, ChIP-chip would be also useful to dissect the isoform specificity of transcription factor target genes that encode a number of isoforms.

The human UGT1A locus spans ~200 kb on chromosome 2q37 and encodes nine UGT1A enzymes that play a crucial role in glucuronidation of xenobiotics and endobiotic substrates such as bilirubin (Chen *et al.*, 2005). UGT1A proteins are expressed in liver, whereas also expressed in extrahaptic tissues like urinary bladder and large intestine (Giuliani *et al.*, 2005). UGT1A gene products are generated by a strategy of exon sharing, resulting in divergent isoforms with a unique N-terminal domain and commonly shared C-terminal 245 amino acids. As UGT proteins are detoxifying enzymes, it is natural that this gene expression is regulated by xenobiotic receptor including pregnenolone X receptor and constitutive androstane receptor (Sugatani *et al.*, 2001; Xie *et al.*, 2003). Reduction of UGT1A expression is involved in the early phase of neoplastic transformation, such as in liver and biliary cancer, bladder cancer and colon cancer (Strassburg *et al.*, 1997; Giuliani *et al.*, 2005). In contrast, decrease in UGT1A1 expression seems to be associated with the reduced risk of endometrial cancer (Duguay *et al.*, 2004). UGT1A1 promoter polymorphism with an $A(TA)_7TAA$ element instead of a normal $A(TA)_6TAA$ element is known to decrease the level of gene expression, and it has been shown that there was a significant inverse association with the seven dinucleotide repeat allele and endometrial cancer risk (Duguay *et al.*, 2004). UGT proteins also glucuronidate steroid hormones, as the UGT1A enzymes showing specificity for estrogens, whereas androgens are substrates for another type of UGT family, UGT2B proteins (Lepine *et al.*, 2004). It has been recently shown that UGT2B15 isoform is an estrogen-regulated gene that is involved in the glucuronidation of androgens as well as estrogens (Harrington *et al.*, 2006). Similarly, there is a possibility that UGT1A1 and UGT1A3 play a role in glucuronidation of androgens as well as estrogens.

In summary, we performed ChIP-chip analysis for *in vivo* ARBSs in prostate cancer LNCaP cells, on the ENCODE regions in the human genome. A number of novel androgen target genes were identified adjacent to the ChIP-chip-based ARBSs. The present results show that ChIP-chip has an advantage over transcript-based microarray analysis, identifying a number of bona fide AR target genes regardless of their expression levels based on the data of functional ARBSs. The androgen target genes identified by the present study would play various important roles in the maintenance of prostate cancer, including detoxification, protein degradation, cell motility/migration and tumor suppression/progression. Our study could be extended to the whole genome search of ARBSs in different cell systems using various ligands for the receptor. Identification of novel androgen target genes by ChIP-chip will reveal the whole entity of androgen signaling network, and will be applied to develop new clinical methods of prevention, diagnosis and treatment for prostate cancer.

Materials and methods

Reagents

Methyltrienolone 17β-hydroxy-17α-methyl-estra-4,9,11-trien-3-one (R1881) was purchased from NEN Life Science Products (Boston, MA, USA). Anti-AR (H-280), anti-SRC1 (M341), anti-GRIP1 (M343), anti-UGT1A (H-300) antibodies were purchased from Santa Cruz Biotechnology (Santa Cruz, CA, USA). Anti-AcH3 and anti-AcH4 were from Upstate Biotechnology (Lake Placid, NY, USA). Anti-RNA PolII (8WG16) was from Covance (Berkeley, CA, USA). Anti-β-actin monoclonal antibody was from Sigma (St Louis, MO, USA). Anti-AIB1 antibody was generated from rabbit serum using a glutathione *S*-transferase fusion protein with amino acids 1320–1420 of human AIB1 protein as an epitope.

Cell culture

Human prostate cancer LNCaP cells were purchased from American Type Culture Collection (Rockville, MD, USA). Cells were maintained in RPMI 1640 supplemented with 4.5 g/dl glucose, 1 mM sodium pyruvate, 10 mM HEPES and 10% fetal bovine serum (FBS). Before hormone addition, cells were cultured for 2 days in phenol red-free RPMI 1640 with 5% dextran-charcoal stripped FBS (dcc-FBS) and 1 day in phenol red-free medium supplemented with 2.5% dcc-FBS.

Chromatin immunoprecipitation

ChIP assay and qPCR were performed as previously described (Horie-Inoue *et al.*, 2004, 2006). LNCaP cells after 72-h hormone depletion were treated with 10 nM R1881 or vehicle (0.1% ethanol) for the indicated times. Cells were fixed in 1% formaldehyde for 5 min at room temperature. Chromatin was sheared to an average size of 500 bp by sonication using a Bioruptor ultrasonicator (Cosmo-Bio, Tokyo, Japan). Lysates were rotated at 4°C for overnight with specific antibodies. Salmon sperm DNA/protein A–agarose (Upstate Biotechnology, Lake Placid, NY, USA) was added and incubated for 2 h. Precipitated DNA was used as templates for qPCR using Applied Biosystems 7000 sequence detector (Foster City, CA, USA) based on SYBR Green I fluorescence. Genomic fragments containing ARE in the promoter and enhancer regions of PSA (−250/−39 bp and −4170/−3978 bp from the TSS, respectively) were used as positive controls for AR binding (Horie-Inoue *et al.*, 2004). Sequences of PCR primers are described in Supplementary Table 1.

DNA amplification and microarray preparation

ChIP-enriched DNA was amplified by two-step IVT as described previously (Katou *et al.*, 2006). Briefly, alkali phosphatase-treated ChIP DNA was incubated with terminal transferase for poly-dT tailing, annealed with T7-poly A primer (5′-GCATTAGCGGCCGCGAAATTAATACGACTCACTATAGGGAGAAAAAAAAAAAAAAAA[C/T/G]-3′), and used as a template for second-strand cDNA synthesis. Using this template DNA, first IVT amplification was performed by T7 RNA polymerase (Ambion Inc., Austin, TX, USA). The first-strand cDNA was synthesized using the amplified cRNA as a template. Second-strand cDNA synthesis and IVT amplification were carried out again. Second amplified RNA was converted into double-strand cDNA with random primers, fragmented with DNase I and end labeled with biotin. Hybridization was performed on the Affymetrix GeneChIP ENCODE01 1.0 Arrays (Santa Clara, CA, USA) using 2 μg of ChIP-enriched and non-enriched input control DNA.

Analysis of microarray data

Array intensity data were analysed by the Affymetrix Tiling Analysis Software based on the algorithm by Cawley *et al.* (2004), and the results were mapped to genomic positions in human genome assembly hg 17 (NCBI Build 35) or in Affymetrix Integrated Genome Browser. In ENCODE01 1.0 Arrays, sets of one probe pair, a perfect matched (PM) probe and a mismatch probe (MM) both 25 bases long are tiled at an average resolution of 22 bp as measured from the central position of adjacent 25-mer oligos, creating an overlap of approximately 3 bp. The (PM-MM) intensity value was recorded for each probe pair as a new probe value, and the distribution of probe value was adjusted to equal across all samples by conducting quantile normalization on each duplicate arrays for two groups, including non-enriched genomic input DNA or ChIP-enriched DNAs by AR antibody. To determine whether a probe x is ChIP-enriched, Wilcoxon rank sum test was applied to rank all the probe pairs within a 550-bp sliding window from x by their $\log_2(\max(PM\text{-}MM),1)$ values for checking whether the sum of ranks of all probe pairs in the ChIP samples were significantly higher than that in the controls (a P-value cutoff of 1e-5). For each window, a signal ratio was also estimated by the Hedges–Lehmann method computing the median of folds enrichment among the probe sets within the window.

Reverse transcription-qPCR

Total RNA was extracted from hormone-treated or 0.1% ethanol-treated cells for indicated times using ISOGEN reagent (Nippon Gene, Tokyo, Japan). First strand cDNA was generated from RNase-free DNase I-treated total RNA by using SuperScript II Reverse Transcriptase (Invitrogen, Carlsbad, CA, USA) and oligo-dT_{20} primer. Androgen responsiveness was analysed by quantitative reverse transcription-PCR (RT-qPCR) using Applied Biosystems 7000 sequence detector based on SYBR Green I fluorescence. Primer design and PCR protocol were as previously described (Horie-Inoue *et al.*, 2004, 2006). Sequences of PCR primers are described in Supplementary Table 2.

Sequence analysis

The sequences of human RefSeq transcripts (hg 17, NCBI build 35) were retrieved from UCSC genome browser (http://www.genome.ucsc.edu/) (Kent *et al.*, 2002). The presence of ARE sequences in the genomic DNA of every ChIP-enriched region were determined by a position weighted matrix method TRANSFAC (Matys *et al.*, 2003) with the matrix conservation >75%. If no ARE sequence was predicted by this criteria, the search was performed by a sequence analysis utility of JASPER, an open-access database for eukaryotic transcription factor binding profiles, with the relative profile score threshold >70% (Sandelin *et al.*, 2004).

Luciferase assay

Luciferase reporter genes containing ARE sequences in ARBSs no. 1 and no. 10 identified by ChIP-chip were constructed by ligating the fragments derived from UDP-glucuronosyltransferase (UGT) 1A1 5′ upstream region (−17753/−17235 bp from the TSS) and cadherin-2 (CDH2) intron 1 region (+20197/+21260 bp from the TSS) into pGL3 vector (Promega, Madison, WI, USA) at the sites between *MluI* and *XhoI*, designated as UGT1A1 5′-Luc and CDH2 Int 1-Luc, respectively. A mutated UGT1A1 5′ region construct (UGT1A1 5′ Mut-Luc) was also generated, including the identical region of UGT1A1 5′-Luc except two substitutions of conserved C and G for A and T, respectively, at the 2-bp apart positions from the 3-bp spacer of ARE sequence. Mouse mammary tumor virus luciferase construct (MMTV-Luc) was used as a positive control for AR transcription activity (Ogawa *et al*., 1995). LNCaP cells were plated at a density of 10000 cells/well in a 24-well culture plate and cultured for 3 days in phenol red-free RPMI 1640 with 5% dcc-FBS. Cells were transfected with plasmids using the transfection reagent FuGENE6 (Roche Applied Science, Indianapolis, IN, USA), then 12 h later treated with R1881 (10 nM) or vehicle (0.1% ethanol) for 24 h. Luciferase activity of cell lysate was determined by the Dual Luciferase Assay Kit (Promega, Madison, WI, USA). A renilla luciferase reporter Tk-PRL was co-transfected as a control for evaluating transfection efficiency. Data represent means ± s.d. from triplicate sets.

Western blotting

Whole cell lysates were prepared using lysis buffer (50 mM Tris–HCl, pH 8.0, 150 mM NaCl, 1% TritonX-100, 1.5 mM $MgCl_2$, 10 μg/ml aprotinin, 10 μg/ml leupeptin, 1 mM PMSF). Protein concentrations were analyzed using the BCA protein assay kit (Pierce Biotechnology, Rockford, IL, USA). Fifty microgram of proteins were resolved by 8% SDS-polyacrylamide gel electrophoresis and electroblotted onto Immobilon-P Transfer Membrane (Millipore, Billerica, MA, USA). Membranes were incubated with primary antibodies followed by incubation with secondary antibodies. Antibody–antigen complexes were detected using the Western Blotting Chemiluminescence Luminol Reagent (Santa Cruz Biotechnology, Santa Cruz, CA, USA).

Acknowledgements

We thank T Suzuki and R Nozawa for their technical assistance. This work was supported in part by grants-in-aid from the Ministry of Health, Labor and Welfare; from the Japan Society for the Promotion of Science; from The Promotion and Mutual Aid Corporation for Private Schools of Japan. This work was supported in part by a grant of the Genome Network Project from the Ministry of Education, Culture, Sports, Science and Technology.

References

Bernstein BE, Kamal M, Lindblad-Toh K, Bekiranov S, Bailey DK, Huebert DJ *et al.* (2005). Genomic maps and comparative analysis of histone modifications in human and mouse. *Cell* **120**: 169–181.

Carroll JS, Liu XS, Brodsky AS, Li W, Meyer CA, Szary AJ *et al.* (2005). Chromosome-wide mapping of estrogen receptor binding reveals long-range regulation requiring the forkhead protein FoxA1. *Cell* **122**: 33–43.

Cawley S, Bekiranov S, Ng HH, Kapranov P, Sekinger EA, Kampa D *et al.* (2004). Unbiased mapping of transcription factor binding sites along human chromosomes 21 and 22 points to widespread regulation of noncoding RNAs. *Cell* **116**: 499–509.

Chen CD, Welsbie DS, Tran C, Baek SH, Chen R, Vessella R *et al.* (2004). Molecular determinants of resistance to antiandrogen therapy. *Nat Med* **10**: 33–39.

Chen S, Beaton D, Nguyen N, Senekeo-Effenberger K, Brace-Sinnokrak E, Argikar U *et al.* (2005). Tissue-specific, inducible, and hormonal control of the human UDP-glucuronosyltransferase-1 (UGT1) locus. *J Biol Chem* **280**: 37547–37557.

Chene L, Giroud C, Desgrandchamps F, Boccon-Gibod L, Cussenot O, Berthon P *et al.* (2004). Extensive analysis of the 7q31 region in human prostate tumors supports TES as the best candidate tumor suppressor gene. *Int J Cancer* **111**: 798–804.

Cooper CS, Park M, Blair DG, Tainsky MA, Huebner K, Croce CM *et al.* (1984). Molecular cloning of a new transforming gene from a chemically transformed human cell line. *Nature* **311**: 29–33.

Coutts AS, MacKenzie E, Griffith E, Black DM. (2003). TES is a novel focal adhesion protein with a role in cell spreading. *J Cell Sci* **116**: 897–906.

Diaz M, Rodriguez JC, Sanchez J, Sanchez MT, Martin A, Merino AM *et al.* (2002). Clinical significance of pepsinogen C tumor expression in patients with stage D2 prostate carcinoma. *Int J Biol Markers* **17**: 125–129.

Duguay Y, McGrath M, Lepine J, Gagne JF, Hankinson SE, Colditz GA *et al.* (2004). The functional UGT1A1 promoter polymorphism decreases endometrial cancer risk. *Cancer Res* **64**: 1202–1207.

ENCODE Project Consortium, EP (2004). The ENCODE (ENCyclopedia of DNA Elements) Project. *Science* **306**: 636–640.

Giuliani L, Ciotti M, Stoppacciaro A, Pasquini A, Silvestri I, De Matteis A *et al.* (2005). UDP-glucuronosyltransferases 1A expression in human urinary bladder and colon cancer by immunohistochemistry. *Oncol Rep* **13**: 185–191.

Gong QH, Cho JW, Huang T, Potter C, Gholami N, Basu NK *et al.* (2001). Thirteen UDP glucuronosyltransferase genes are encoded at the human UGT1 gene complex locus. *Pharmacogenetics* **11**: 357–368.

Grossmann ME, Huang H, Tindall DJ. (2001). Androgen receptor signaling in androgen-refractory prostate cancer. *J Natl Cancer Inst* **93**: 1687–1697.

Harrington WR, Sengupta S, Katzenellenbogen BS. (2006). Estrogen regulation of the glucuronidation enzyme UGT2B15 in estrogen receptor-positive breast cancer cells. *Endocrinology* **147**: 3843–3850.

Hazan RB, Kang L, Whooley BP, Borgen PI. (1997). N-cadherin promotes adhesion between invasive breast cancer cells and the stroma. *Cell Adhes Commun* **4**: 399–411.

Horie-Inoue K, Bono H, Okazaki Y, Inoue S. (2004). Identification and functional analysis of consensus androgen response elements in human prostate cancer cells. *Biochem Biophys Res Commun* **325**: 1312–1317.

Horie-Inoue K, Takayama K, Bono HU, Ouchi Y, Okazaki Y, Inoue S. (2006). Identification of novel steroid target genes through the combination of bioinformatics and functional analysis of hormone response elements. *Biochem Biophys Res Commun* **339**: 99–106.

Humphrey PA, Zhu X, Zarnegar R, Swanson PE, Ratliff TL, Vollmer RT *et al.* (1995). Hepatocyte growth factor and its receptor (c-MET) in prostatic carcinoma. *Am J Pathol* **147**: 386–396.

Jaggi M, Nazemi T, Abrahams NA, Baker JJ, Galich A, Smith LM *et al.* (2006). N-cadherin switching occurs in high Gleason grade prostate cancer. *Prostate* **66**: 193–199.

Katou Y, Kaneshiro K, Aburatani H, Shirahige K. (2006). Genomic approach for the understanding of dynamic aspect of chromosome behavior. *Methods Enzymol* **409**: 389–410.

Kawana Y, Ichikawa T, Suzuki H, Ueda T, Komiya A, Ichikawa Y *et al.* (2002). Loss of heterozygosity at 7q31.1 and 12p13-12 in advanced prostate cancer. *Prostate* **53**: 60–64.

Kent WJ, Sugnet CW, Furey TS, Roskin KM, Pringle TH, Zahler AM *et al.* (2002). The human genome browser at UCSC. *Genome Res* **12**: 996–1006.

Laganière J, Deblois G, Lefebvre C, Bataille AR, Robert F, Giguère V. (2005). From the cover: location analysis of estrogen receptor alpha target promoters reveals that FOXA1 defines a domain of the estrogen response. *Proc Natl Acad Sci USA* **102**: 11651–11656.

Lepine J, Bernard O, Plante M, Tetu B, Pelletier G, Labrie F *et al.* (2004). Specificity and regioselectivity of the conjugation of estradiol, estrone, and their catecholestrogen and methoxyestrogen metabolites by human uridine diphosphoglucuronosyltransferases expressed in endometrium. *J Clin Endocrinol Metab* **89**: 5222–5232.

Maeda A, Nakashiro K, Hara S, Sasaki T, Miwa Y, Tanji N *et al.* (2006). Inactivation of AR activates HGF/c-Met system in human prostatic carcinoma cells. *Biochem Biophys Res Commun* **347**: 1158–1165.

Matys V, Fricke E, Geffers R, Gossling E, Haubrock M, Hehl R *et al.* (2003). TRANSFAC: transcriptional regulation, from patterns to profiles. *Nucleic Acids Res* **31**: 374–378.

Monks DA, Watson NV. (2001). N-cadherin expression in motoneurons is directly regulated by androgens: a genetic mosaic analysis in rats. *Brain Res* **895**: 73–79.

Ogawa H, Inouye S, Tsuji FI, Yasuda K, Umesono K. (1995). Localization, trafficking, and temperature-dependence of the Aequorea green fluorescent protein in cultured vertebrate cells. *Proc Natl Acad Sci USA* **92**: 11899–11903.

Pisters LL, Troncoso P, Zhau HE, Li W, von Eschenbach AC, Chung LW. (1995). c-met Proto-oncogene expression in benign and malignant human prostate tissues. *J Urol* **154**: 293–298.

Porkka KP, Helenius MA, Visakorpi T. (2002). Cloning and characterization of a novel six-transmembrane protein STEAP2, expressed in normal and malignant prostate. *Lab Invest* **82**: 1573–1582.

Sandelin A, Alkema W, Engstrom P, Wasserman WW, Lenhard B. (2004). JASPAR: an open-access database for eukaryotic transcription factor binding profiles. *Nucleic Acids Res* **32**: D91–94.

Shang Y, Brown M. (2002). Molecular determinants for the tissue specificity of SERMs. *Science* **295**: 2465–2468.

Shang Y, Myers M, Brown M. (2002). Formation of the androgen receptor transcription complex. *Mol Cell* **9**: 601–610.

Strassburg CP, Manns MP, Tukey RH. (1997). Differential down-regulation of the UDP-glucuronosyltransferase 1A locus is an early event in human liver and biliary cancer. *Cancer Res* **57**: 2979–2985.

Sugatani J, Kojima H, Ueda A, Kakizaki S, Yoshinari K, Gong QH *et al.* (2001). The phenobarbital response enhancer module in the human bilirubin UDP-glucuronosyltransferase UGT1A1 gene and regulation by the nuclear receptor CAR. *Hepatology* **33**: 1232–1238.

Tobias ES, Hurlstone AF, MacKenzie E, McFarlane R, Black DM. (2001). The TES gene at 7q31.1 is methylated in tumours and encodes a novel growth-suppressing LIM domain protein. *Oncogene* **20**: 2844–2853.

Tomita K, van Bokhoven A, van Leenders GJ, Ruijter ET, Jansen CF, Bussemakers MJ *et al.* (2000). Cadherin switching in human prostate cancer progression. *Cancer Res* **60**: 3650–3654.

Wang Q, Carroll JS, Brown M. (2005). Spatial and temporal recruitment of androgen receptor and its coactivators involves chromosomal looping and polymerase tracking. *Mol Cell* **19**: 631–642.

Xie W, Yeuh MF, Radominska-Pandya A, Saini SP, Negishi Y, Bottroff BS *et al.* (2003). Control of steroid, heme, and carcinogen metabolism by nuclear pregnane X receptor and constitutive androstane receptor. *Proc Natl Acad Sci USA* **100**: 4150–4155.

Supplementary Information accompanies the paper on the Oncogene website (http://www.nature.com/onc).

Characterization and Identification of a Steroid Receptor-Binding Protein, SRB-RGS

Mitsunori IKEDA,*[a] Satoshi INOUE,[b,c] Masami MURAMATSU,[c] and Yohsuke MINATOGAWA[a]

[a] Department of Biochemistry, Kawasaki Medical School; 577 Matsushima, Kurashiki, Okayama 701–0192, Japan: [b] Department of Geriatrics, Graduate School of Medicine and Faculty of Medicine, University of Tokyo; 7–3–1 Hongo, Bunkyo-ku, Tokyo 113–0033, Japan: and [c] Research Center for Genomic Medicine, Saitama Medical School; 1397–1 Inariyama, Yamane, Hidaka 350–1241, Japan.

Received June 30, 2006; accepted April 8, 2007; published online April 10, 2007

We cloned the cDNA of a novel steroid receptor-binding protein, SRB-RGS, which suppressed the estrogen receptor (ER)α-mediated and other promoter-driven transcriptional activities. This study revealed the interaction between the full-length SRB-RGS and full-length ERα or ERβ by a coimmunoprecipitation assay. The full-length SRB-RGS and full-length ERα interacted in COS-7 cell by a mammalian two-hybrid system. The interaction between intrinsic SRB-RGS and ERs in the nuclear ER extract from the rat uteri was observed by the gel-shift assay. These results strongly suggested that SRB-RGS interacts with ERs bound to DNA (estrogen response element) in the nuclei of the cells. SRB-RGS suppressed very efficiently the ERα-, ERβ-, and ERα+ERβ-mediated transcriptional activities. Green fluorescence of enhanced green fluorescence protein (EGFP)-tagged SRB-RGS was localized both in the nucleus and in the cytoplasm. Intrinsic SRB-RGS was immunostained in the nucleus and the cytoplasm of HeLa cells. The putative SRB-RGS deduced from cDNA sequence was identified by the immunostaining and Western blotting by using the anti-SRB-RGS antibody. Overexpression of SRB-RGS induced the cell death in the HeLa cells. The nucleotide sequence of SRB-RGS cDNA that we cloned previously is identical with that of the newly isolated RGS3 cDNA. SRB-RGS could interact with ERs bound DNA in the nuclei of the cells and suppressed the ERs-mediated transcriptional activities.

Key words estrogen receptor; gene expression; transcriptional suppression; localization; cell death; RGS3

The nuclear hormone receptors are a superfamily of ligand-inducible transcription factors. They include the receptor proteins for steroids, thyroid hormone, vitamin D, and retinoids. Steroid hormone receptors are structurally related and composed of six major functional domains. Domain A/B in the NH_2-terminal region of the protein is the constitutive activation 1 (AF-1). Domain C, the DNA-binding domain, is arranged in two zinc-stabilized DNA-binding finger motifs. Region D contains a nuclear localization signal. The ligand-binding and ligand-dependent transcriptional activation function 2 (AF-2) is located in domain E/F of the COOH-terminal region of the protein.[1—3] For the activation of transcription, steroid hormone receptors recruit coactivators such as SRC-1/p160, p300/CBP, ARA70, Tip60, and RIP140, through binding to AF-1 and AF-2 of the receptors. This kind of coactivator recruits histone acetyltransferase (HAT) or bear HAT activity on itself. Recruitment of HAT allows the local decondensation of chromatin. In the next step, the DRIP/TRAP complex binds to the AF-2 of the receptor and mediates transcriptional activation. This kind of coactivator does not recruit HAT. Thus, these coactivators facilitate the transcription process.[4—9] The thyroid hormone receptor (TR) and retinoid X receptor (RXR) in the absence of ligand bind to the corepressors, such as N-CoR and SMRT, respectively, suppressing transcriptional activity. The corepressors recruit histone deacetylase (HDAC).[10—13] The chromatin-modifying complexes, ATP-dependent remodeling complexes and HAT or HDAC complexes regulate chromatin structure and transcription so that they might be coordinated to create a DNA template that is accessible to the general transcription apparatus.[14]

We employed a yeast two-hybrid system for cloning the cDNA of the protein that interacted with domains C and D of the rat estrogen receptorα (rERαC/D) from the rat ovary cDNA library and cloned the cDNA of a novel steroid receptor-binding (SRB) protein bearing the regulator of the G-protein signaling (RGS) domain[15] at the COOH-terminal, designated as SRB-RGS. RGS proteins are GTPase accelerating proteins, which interact with the Gα-subunits that are linked to seven transmembrane G-protein coupled receptor. SRB-RGS bears a PDZ domain that is a multi-functional protein–protein interaction module that plays important roles in organizing signal transduction complexes, clustering membrane proteins, and maintaining cell polarity at the NH_2-terminal, as well.[16,17] rERαC/D interacted *in vitro* with partial SRB-RGS1-495 amino acid (a.a.). SRB-RGS suppressed the transcriptional activities of ERα and the other promoters.[18]

We could show that the full-length SRB-RGS interacted with either the full-length ERα or ERβ by a coimmunoprecipitation assay. The full-length SRB-RGS and full length ERα interacted in COS-7 cell by a mammalian two-hybrid system. The interaction between intrinsic SRB-RGS and ERs in the nuclear ER extract from the rat uteri was suggested by the gel-shift assay. The human (h) ERα-, hERβ-, hERα+hERβ-mediated transcriptional activities were suppressed by overexpression of SRB-RGS. Enhanced fluorescence protein (EGFP)-tagged SRB-RGS was localized in the nucleus and the cytoplasm of the HeLa cells and the COS-7 cells. Similar results were shown by immunostaining of the HeLa cells. Intrinsic SRB-RGS was identified by the immunostaining and Western blotting. Overexpression of SRB-RGS induced the cell death in the HeLa cells. SRB-RGS could interact with ERs bound DNA in the nucleus and suppressed the ERs-mediated transcriptional activities.

* To whom correspondence should be addressed. e-mail: ikeda@bcc.kawasaki-m.ac.jp

MATERIALS AND METHODS

Materials Anti-hERα rabbit polyclonal antibody HC-20, raised against a peptide mapping at the COOH-terminus of ERα of human origin and anti-hERβ antibody N-19, goat polyclonal antibody raised against a peptide mapping at the NH_2-terminus of ERβ of human origin, were purchased from Santa Cruz Biotechnology (Santa Cruz, CA, U.S.A.). [^{35}S]methionine was purchased from Amersham Biosciences Co. (Piscataway, NJ, U.S.A.). [α-^{33}P]dATP was purchased from Perkin Elmer Life and Analytical Sciences (Boston, MA, U.S.A.).

Preparation and Purification of the Antiserum against the SRB-RGS Peptide The anti-SRB-RGS peptide antiserum was prepared by Sawady Technology Co. (Tokyo, Japan) immunizing a rabbit. The immune serum was assayed by enzyme-linked immunoassay with detection at greater than 10000-fold dilution by the manufacturer. The immune and the preimmune sera were purified on protein A Sepharose™ CL-4B (Amersham Biosciences Co.). The purified sera are called as the anti-SRB-RGS antibody and the preimmune serum, respectively.

Construction of Plasmids The expression vectors of SRB-RGS, pcDNASRB-RGS or β-galactosidase (β-gal), pcDNAβ-gal (pCMVβ-gal) were constructed by inserting SRB-RGS cDNA, β-gal cDNA from pCH110, respectively into the malti-cloning site (MCS) of pcDNA3 (Invitrogen Co., Groningen, The Netherlands) driven by a cytomegalovirus (CMV) promoter in mammalian cells and by the T7 promoter in the *in vitro* transcription translation system.[18] The expression vector for EGFP-tagged SRB-RGS, pEGFP-SRB-RGS was constructed by inserting the PCR-amplified cDNA fragment of SRB-RGS into the HindIII site in the MCS of pEGFP-C1 (Clontech Co., Palo Alto, CA, U.S.A.). The expression vectors of DsRed1-tagged hERα and hERβ, pDsRed-hERα and pDsRed-hERβ were constructed by inserting PCR-amplified cDNA fragments from pCXN2-hERα and pCXN2-hERβ,[19] respectively into the MCS of pDsRed1-C1 (Clontech Co.). The construction of the expression vectors of hERα, pcDNA-hERα, and hERβ, pcDNA-hERβ were constructed by inserting PCR-amplified cDNA fragments from pCXN2-hERα and pCXN2-hERβ, respectively into the MCS of pcDNA3. The constructions of pASrERαC/D, pASrERα and pACTrERαC/D were described previously.[18,20] pACTSRB-RGS was constructed by inserting the EcoRI cDNA fragment of pcDNASRB-RGS into the EcoRI site in the MCS of pACT2 after adding 8 nucleotides at the NcoI site. pACTSRB-RGS 1-495 a.a. was constructed by inserting a PCR-amplified cDNA fragment of SRB-RGS 1-495 a.a. into the EcoRI site in the MCS of pACT2. pASSRB-RGS was constructed by inserting the EcoRI fragment of pcDNASRB-RGS into the EcoRI site in the MCS of pAS2-1. The expression vectors of the fusion proteins of GAL4 DNA-binding domain (GAL4 DNA-BD) and hERα, pM-hERα and VP16 activation-domain (VP16AD) and SRB-RGS, pVP16SRB-RGS were constructed by inserting PCR-amplified cDNA fragments from pcDNA-hERα and pcDNASRB-RGS, respectively into the MCS of the expression vectors of GAL4 DNA-BD, pM and VP16AD, pVP16 (Clontech Co.), respectively.

An Interaction Study between SRB-RGS and ERs by a Yeast Two-Hybrid System A yeast two-hybrid interaction study was performed as mentioned previously.[18,20,21] Briefly, the colonies of *Saccharomyces cerevisiae* Y187 (Y187) transfected with pAS2-1, pASrERα, pASSRB-RGS and pLAM5′-1 and the colonies of *Saccharomyces cerevisiae* CG-1945 (CG-1945) transfected with pACT2, pACTrERα, and pACTSRB-RGS 1-495 a.a. were incubated together in the same YPD medium (20 g/l polypeptone, 10 g/l yeast extract, 20 g/l glucose) at 30 °C for 10 h with shaking, and an aliquot of the mating culture was placed on a synthetic dropout minimal medium (SD)/-leucine/-tryptophane/-histidine+5 mM 3-amino-1,2,4-triazole (3-AT) plate in the absence or presence of 10^{-6} M estradiol. The transformants were assayed for β-gal activity by the colony-lift filter assay. Interacting positives turned blue.

***In Vitro* Interaction between SRB-RGS and ERs by Coimmunoprecipitation** [^{35}S]methionine-labeled proteins were prepared by using an *in vitro* transcription translation system. pcDNASRB-RGS+pcDNA-hERα or pcDNASRB-RGS+pcDNA-hERβ as the templates and [^{35}S]methionine were added to the reaction mixture (TnT^{R} Quick Coupled Transcription/Translation System, Promega Co., Madison, WI, U.S.A.) in the respective tubes. The each reaction mixture was incubated at 30 °C for 1.5 h and then with protein G PLUS-agarose (Santa Cruz Biotechnology) for 1 h on ice. After centrifugation, the supernatants were incubated with the anti-hERα antibody HC-20, the anti-hERβ antibody N-19 or anti-SRB-RGS antibody for 2 h on ice and then with protein G PLUS-agarose for 1 h on ice. The protein G PLUS-agarose was washed with 10 mM Tris–HCl, 1 mM EDTA (pH 7.4) (TE) containing 0.4 M NaCl and 0.1% Nonidet P-40 (for SRB-RGS+hERβ) or 10 mM Tris–HCl, 1 mM EDTA (pH 7.4) (TE) containing 0.2 M NaCl and 0.05% Nonidet P-40 (for SRB-RGS+hERα). The labeled proteins bound to the protein G PLUS-agarose were analyzed by 9% SDS-polyacrylamide gel electrophoresis (PAGE) and an autoradiography by using the Fluoro image analyzer FLA-3000 (Fuji Film Co., Tokyo, Japan).

Cell Culture and Transfection COS-7 cells and HeLa cells were purchased from The Institute of Physical and Chemical Research (RIKEN) (Wako, Japan). They were routinely maintained in Dulbecco's modified Eagle's minimal essential medium (DMEM) (Sigma Co., St. Louis, MO, U.S.A.) supplemented with 10% fetal bovine serum (FBS) (Medical & Biological Laboratories Co., Nagoya, Japan). The cells were maintained in 5% CO_2 at 37 °C. The COS-7 cells or the HeLa cells in screw-capped flasks (25 cm^2) or 35-mm dishes (10.8 cm^2) were transiently transfected with plasmids by lipofectamine2000 (Invitrogen Co.). The cells were incubated for 48 h after transfection.

Chloramphenicol Acetyltransferase Assay The chloramphenicol acetyltransferase (CAT) assay for ER transcriptional activity, using a FAST CAT Yellow (deoxy) CAT assay kit (Molecular Probes, Eugene, OR, U.S.A.), and the β-gal assay were performed as mentioned previously.[18] Briefly, the medium for COS-7 cells in a screw-capped flask (25 cm^2) was replaced by phenol red-free MEM (Nissui Pharmaceutical Co., Tokyo, Japan) supplemented with 10% dextran-coated charcoal-treated (DCC) FBS for 48 h before transfection. The COS-7 cells were cotransfected with plasmids as indicated and incubated for 48 h in the presence of 10^{-7} M

estradiol after transfection. The cell extract was prepared according to the manufacturer's manual. A portion of the cell extract was incubated with fluorescent deoxychloramfenicol substrate and acetyl CoA (Sigma Co.) at 37 °C for 2 h. The acetylated derivative and the substrate were quantified by measuring the absorbance using the fluorescence spectrophotometer Model F-3010 (Hitachi Co., Tokyo, Japan). For the β-gal assay, the other portion of the cell extract was incubated with *o*-nitrophenyl β-galactopyranoside at 37 °C for 30 min. The relative CAT activities were calculated according to the manufacturer's manual and normalized by β-gal activities. The CAT activity for the cells cotransfected with the empty plasmid, pcDNA3 instead of pcDNA-hERα (or pcDNA-hERβ) was subtracted from each CAT activity.

Quantitative Real-Time RT-PCR pcDNA-hERα (or pcDNA-hERβ), pEREtkCAT and pcDNAβ-gal were cotransfected with pcDNASRB-RGS (or pcDNA3) to COS-7 cells and incubated under the same condition as mentioned below in Fig. 2 (the CAT assay for the ER transcriptional activites). Total RNA was prepared by RNeasy Plus Mini kit (Qiagen GmbH, Hilden, Germany) according to the manufacturer's manual from 2.5×10^6 COS-7 cells. Briefly, the homogenized lysate was centrifuged in a DNA Eliminator spin column to eliminate contaminating DNA and then in a RNeasy spin column to get total RNA. A_{260}/A_{280} value was approximately 2.2. The total RNA was converted to cDNA by iScript cDNA synthesis kit (Bio-Rad Co., Hercules, CA, U.S.A.) using a modified MMLV-derived reverse transcriptase, oligo (dT) and random hexamer primers. SYBR green-based real-time RT-PCR was carried out by SYBR GREEN PCR Master Mix (Applied Biosystems, Warrington, U.K.) using Mx3000P™ Multiplex Quantitative PCR System (Stratagene Co., La Jolla, LA, U.S.A.). The following primer pairs were used: 5′-ATC AGG ATA TGT GGC GGA TGA-3′ (forward) and 5′-CTG ATT TGT GTA GTC GGT TTA TGC A-3′ (reverse) for amplification of β-gal, 5′-CCA CCA ACC AGT GCA CCA TT-3′ (forward) and 5′-GGT CTT TTC GTA TCC CAC CTT TC-3′ (reverse) for amplification of hERα and: 5′-AGA GTC CCT GGT GTG AAG CAA G-3′ (forward) and 5′-GAC AGC GCA GAA GTG AGC ATC-3′ (reverse) for amplification of hERβ. The plasmids pcDNAβ-gal, pcDNA-hERα and pcDNA-hERβ were used as standards of quantification for β-gal, hERα and hERβ cDNAs, respectively. Reactions were incubated at 95 °C for 10 min followed by 40 cycles of 95 °C for 15 s and 60 °C for 1 min. Controls incubated no-reverse transcriptase reactions in which reverse transcriptase were omitted from the reverse transcriptase reaction.

Mammalian Two-Hybrid System Mammalian two-hybrid assay for interaction between ERα and SRB-RGS was performed using Mammalian Matchmaker Two-Hybrid Assay kit (Clontech Co.). Briefly, COS-7 cells were cotransfected with plasmids as indicated and incubated in the absence or presence of 10^{-7} M estradiol. The cell extracts were incubated with fluorescent deoxychloramfenicol substrate and acetyl CoA as mentioned above. The relative CAT activities were normalized by β-gal activities as mentioned above.

Observation of Subcellular Localization of SRB-RGS and TUNEL-Positive Cells by Confocal Laser-Scanning Microscopy The HeLa cells or COS-7 cells in 35-mm dishes (10.8 cm^2) were grown on glass cover slips in phenol red-free MEM supplemented with 10% DCC FBS, and the plasmids were transiently cotransfected by lipofectamine2000. They were incubated for 48 h in the presence or absence of 10^{-7} M estradiol or 10 μM Z-VAD-FMK (the caspases inhibitor) (Peptide Institute Inc., Minoh, Osaka, Japan) after transfection. The cells washed with PBS and fixed in 4% paraformaldehyde for 1 h. After the cover slips were mounted on to glass sides after or without propidium iodide (PI) staining of the cells, the cells were viewed on a confocal laser-scanning microscopy Model Fluoview FV300 (Olympus Co., Tokyo, Japan).

The ApoTag^R Red *In Situ* Apoptosis Detection kit (Intergen Co., Purchase, NY, U.S.A.) was used for the assessment of DNA fragmentation in the cells transfected with the plasmids after fixation of the cells on glass cover slips. Briefly, DNA fragments, which had been labeled with the digoxigenin-nucleotide, were then allowed to bind an anti-digoxigenin antibody conjugated to Rhodamine. The cells were viewed on a confocal laser-scanning microscopy as mentioned above.

Immunostaining of the Cells HeLa cells were grown on glass cover slips in 35-mm dishes and fixed in 4% paraformaldehyde for 1 h. After permiabilization with 2% Triton X-100 in PBS for 10 min. at room temperature, the cells were blocked with 20% FBS in PBS and incubated with the anti-SRB-RGS antibody (or the preimmune serum) and then the fluorescein-5-isothiocyanate (FITC)-conjugated goat IgG to rabbit immunoglobulin (IgG, IgA, IgM) (ICN pharmaceuticals, Aurora, OH, U.S.A.) followed by PI staining. They were observed on a confocal laser-scanning microscopy as mentioned above.

SDS-PAGE Analysis of [^{35}S]Methionine-Labeled SRB-RGS Expressed in COS-7 Cells Transfected with pcDNASRB-RGS COS-7 cells at 48 h after transfection with pcDNASRB-RGS or the empty plasmid, pcDNA3 were labeled for 4 h in methionine- and cystine-free DMEM (Gibco/Invitrogen Co., Carlsbad, CA, U.S.A.) containing [^{35}S]methionine (100 μCi/ml). The labeled cells were lysed in a solubilization buffer containing 10 mM Tris–HCl (pH 7.4), 0.15 M NaCl, 1% Nonidet P-40, 0.1% SDS, a protease inhibitor cocktail for mammalian tissues (Sigma Co.), designated as the whole cell lysate. The anti-SRB-RGS antibody was added to the whole cell lysate, and incubated for 1 h on ice. The immune complexes were adsorbed to protein G PLUS-agarose, washed extensively with a washing buffer [10 mM Tris–HCl (pH 7.4), 0.15 M NaCl, 0.1% Nonidet P-40, 0.1% SDS, and the protease inhibitor cocktail], and then analyzed with 7% SDS-PAGE followed by an autoradiography as mentioned above.

Western Blotting Analysis HeLa cells without transfection of any plasmids were lysed in the solubilization buffer as mentioned above and dialyzed against TE. The lysate was subjected on 7% SDS-PAGE and transferred to a nitrocellulose membrane (Bio-Rad Co.). The analysis was performed with ECL plus Western blotting detection system (Amersham Biosciences UK Limited, Little Chalfont, U.K.). Briefly, the membrane was immersed in 5% non-fat dried milk, 0.1% Tween 20 in PBS and incubated with the anti-SRB-RGS antibody and then peroxidase-linked anti-rabbit IgG. Peroxydase activity was developed according to the manufacturer's manual. The chemiluminescent signal of the band was visualized using a Lumino image analyzer LAS-1000 plus (Fuji Film Co.).

Table 1. An Interaction Study between the Estrogen Receptor and SRB-RGS by a Yeast Two-Hybrid System

Plasmid 1 in Y-187	Plasmid 2 in CG-1945							
	pACT2		pACTrERα		pACTSRB-RGS		pACTSRB-RGS 1-495 a.a.	
	$-E_2$	$+E_2$	$-E_2$	$+E_2$	$-E_2$	$+E_2$	$-E_2$	$+E_2$
pAS2-1	−	−	−	−	nd		nd	
pASrERα	nd		−	+	nd		+	+
pASSRB-RGS	nd		−	−	nd		nd	
pASrERαC/D	nd		−	−	±	±	+	+
pLAM5′-1	nd		nd		nd		−	−

Saccharomyces cerevisiae Y187 and CG-1945 were transfected with plasmids 1 and 2, respectively, followed by yeast mating. The growth and β-galactosidase (β-gal) assay of the cells were determined as described previously.[19] The growth was performed in the presence ($+E_2$) or absence ($-E_2$) of 10^{-6} M estradiol. The growth and β-gal assay of yeast cells were expressed as positive (+), negative (−), and faintly positive (±). rERαC/D: the bait for a yeast two-hybrid screening. SRB-RGS 1-495 a.a.: the open reading flame of the cDNA fragment (clone4-32) isolated by a yeast two-hybrid screening. pLAM5′-1: human lamin $C_{(66\text{-}230)}$ in pAS2-1 as a control bait. nd: not determined.

Gel-Shift Assay The gel-shift assay was performed as mentioned previously.[2,20]

Animal and Tissue Preparation: Female SD rats (8 week-old) were obtained from Charles River Co. (Yokohama, Japan), and were sacrificed by cervical dislocation. The uteri were removed and immediately frozen in liquid nitrogen. They were used immediately or stored at −80 °C before use. These experiments were approved by Animal Research Committee of Kawasaki Medical School and conducted according to the "Guide for the Care and Use of Laboratory Animals" of Kawasaki Medical School.

Preparation of the Nuclear Receptor Fraction from the Rat Uteri: The operations were carried out at 0—4 °C. The nuclear receptor fraction was prepared following treatment of the rats with estradiol (100 μg/kg). The uteri were homogenized with TEGMPi buffer[2] and filtered through Nytex (100—124 μm). The filtrate was centrifuged at 2500×g for 10 min. The pellet was washed twice with homogenization buffer and resuspended in the buffer containing 0.4 M KCl and allowed to extract for 30 min. The suspension was centrifuged at 105000×g for 50 min.

Synthetic Oligonucleotides: A wild type 25-base pair synthetic oligonucleotide containing a *Xenopus* vitellogenin A2 estrogen response element (VRE) were prepared as followed: The synthetic oligonucleotide 5′-TCAGGTCACTGTGACCTGACTTTGG-3′ was annealed to the complementary primer 5′-CCAAAGTC-3′. [^{33}P]VRE or the unlabeled VRE was synthesized by end-filling of the annealed oligonucleotide with Klenow fragment (Takara Co., Kusatsu, Japan) in the presence of 20 μM each of dCTP, dGTP, dTTP, dATP with or without 5 μM of [α-^{33}P]dATP, respectively.

Gel-Shift Assay: The nuclear receptor fraction were incubated with [^{33}P]VRE, electrophoresed through non-denaturing PAGE (5.6%), and autoradiographed as mentioned above.

RESULTS

Interaction Study of the Estrogen Receptors and SRB-RGS Yeast Two-Hybrid Assay: We examined the interaction between ERs and SRB-RGS by a yeast two-hybrid system. Full-length rERα (or rERαC/D, the bait for a yeast two-hybrid screening) and SRB-RGS 1-495 a.a. [the open reading frame of the cDNA fragment (clone4-32) isolated by a yeast two-hybrid screening] interacted in both the absence and presence of estradiol in the culture medium of the yeast two-hybrid system. No interaction between full-length rERα and full-length SRB-RGS was observed in this system (Table 1).

Coimmunoprecipitation Assay: We examined whether [^{35}S]methionine-labeled SRB-RGS, hERα or hERβ were translated correctly by an *in vitro* transcription and translation system adding pcDNASRB-RGS, pcDNA-hERα or pcDNA-hERβ, respectively, as the templates and [^{35}S]methionine to the reaction mixture containing the rabbit reticulocyte lysate. The labeled products immunoprecipitated by the respective antibodies and protein G-agarose showed their apparent molecular weights on SDS-PAGE (data not shown), suggesting that they were translated correctly in this system.

The interaction study of full-length SRB-RGS and full-length ERs was examined by a coimmunoprecipitation assay. Estradiol was not added to the medium for the interaction study using immunoprecipitation assay on the basis of the above observation by a yeast two-hybrid system. [^{35}S]methionine-labeled SRB-RGS and hERα were synthesized in the same reaction mixture of an *in vitro* transcription and translation system and immunoprecipitated by an anti-hERα antibody HC-20 or an anti-SRB-RGS antibody, and analyzed by SDS-PAGE and autoradiography. Similarly, an interaction between hERβ and SRB-RGS was examined. [^{35}S]methionine-labeled SRB-RGS and hERβ synthesized as mentioned above were immunoprecipitated by the anti-hERβ antibody N19 or the anti-SRB-RGS antibody, and analyzed by SDS-PAGE and autoradiography. SRB-RGS or ERs were coimmunoprecipitated by the anti-SRB-RGS antibody (Fig. 1A lanes 2, 6), anti-hERα antibody (Fig. 1A lane 3) or anti-hERβ antibody (Fig. 1A lane 7), respectively, whereas they were hardly coimmunoprecipitated by the vehicle that contained the preimmune serum (Fig. 1A lanes 1, 5). These observations showed that full-length SRB-RGS bound to either full-length hERα or hERβ *in vitro*.

Mammalian Two-Hybrid Assay: The interaction of full-length SRB-RGS and full-length hERα in the COS-7 cells was examined by a mammalian two-hybrid assay in the absence or presence of estradiol. As indicated at the bottom of Fig. 1B, the expression vectors of the fusion proteins of GAL4 DNA-binding domain (GAL4 DNA-DB) and hERα, pM-hERα (or an empty vector, pM) and VP16 activation-domain (VP16 AD) and SRB-RGS, pVP16 SRB-RGS (or an empty vector, pVP16) were also cotransfected with the re-

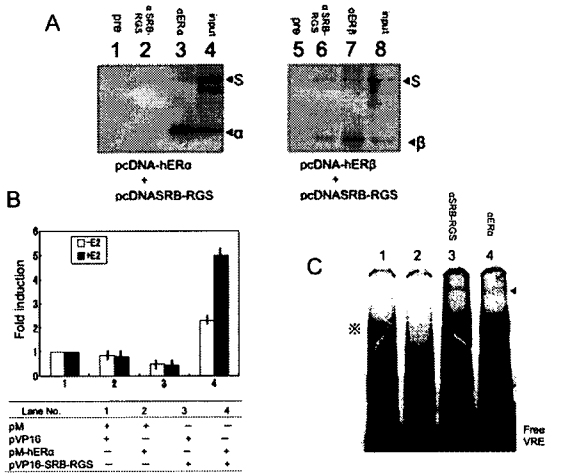

Fig. 1. An Interaction Study between SRB-RGS and the Estrogen Receptors

(A) Coimmunoprecipitation assay: [^{35}S]methionine-labeled proteins were prepared by using either pcDNASRB-RGS+pcDNA-hERα (lanes 1—4) or pcDNASRB-RGS+pcDNA-hERβ (lanes 5—8) as templates in respective tubes with the *in vitro* transcription and translation system. Respective reaction mixtures were incubated with the preimmune serum (pre; lanes 1, 5), the anti-SRB-RGS antibody (αSRB-RGS; lanes 2, 6), the anti-hERα antibody HC-20 (αERα; lane 3), or the anti-hERβ antibody N19 (αERβ; lane 7), precipitated with the protein G PLUS-agarose, and washed with TE containing 0.2 M NaCl and 0.05% Nonidet P-40 (lanes 1—3) or TE containing 0.4 M NaCl and 0.1% Nonidet P-40 (lanes 5—7). The bound proteins were analyzed by SDS-PAGE and autoradiography. Lanes 4 and 8 represent one ninth of the total amount of input [^{35}S]methionine-labeled proteins in each reaction tube. S: SRB-RGS. α: hERα. β: hERβ. (B) A mammalian two-hybrid assay: An interaction study between hERα and SRB-RGS was performed by mammalian two-hybrid system. Briefly, COS-7 cells were cotransfected with plasmids as indicated and incubated in the absence (white bar) or presence (black bar) of 10^{-7} M estradiol (E_2). The cell extracts were incubated with fluorescent deoxychloramfenicol substrate and acetyl CoA. The relative CAT activities were normalized by β-gal activities. (C) Gel shift assay: The effect of the anti-SRB-RGS antibody on VRE-binding nuclear ERs was examined by the gel-shift assay as described under "Materials and Methods". ERs-[^{33}P]VRE complexes were formed prior to addition of preimmune serum (lanes 1, 2), the anti-SRB-RGS antibody (αSRB-RGS; lane 3), and the anti-hERα HC-20 (αERα; lane 4). Lane 2 also contains large excess of unlabeled VRE. The asterisk indicates specific ERs-VRE bands. The arrowhead indicates antibody-shifted ERs-VRE complexes.

porter plasmid, pG5CAT which contains the CAT gene downstream of five consensus GAL4 binding sites and the minimal adenovirus E1b promoter to COS-7 cells. The interaction between hERα and SRB-RGS was expressed as relative CAT activity normalized by β-gal activity. The CAT activity remained low when cells were transfected with the empty plasmids (pM and pVP16AD), or when either of these plasmids was transfected together with pM-hERα or pVP16 SRB-RGS. In contrast, when pM-hERα was transfected together with pVP16 SRB-RGS, the CAT activities of the reporter were induced approximately 5-fold and 2.3-fold in the presence or absence of 10^{-7} M estradiol, respectively (Fig. 1B). In the presence and absence of 10^{-7} M estradiol, SRB-RGS interacted with hERα in the nucleus of the COS-7 cell.

Gel-Shift Assay: The interaction of intrinsic SRB-RGS and ERs in the nuclear receptor fraction from the rat uteri was examined by the gel-shift assay. The nuclear receptor fraction incubated with [^{33}P]VRE was separated from the free oligonucleotide on nondenaturing PAGE. Retarded bands were observed (the asterisk in Fig. 1C lane 1). The band disappeared as a result of competition with excess of unlabeled VRE (lane 2). A super-shift of the retarded bands was observed by incubation with the anti-SRB-RGS antibody or anti-ERα antibody HC-20 (the arrow-head lanes 3 or 4, respectively). The [^{33}P]VRE-binding band included SRB-RGS and ERα, suggesting that SRB-RGS interacted with ERα bound to VRE.

Effects of SRB-RGS on the ERα-, ERβ- and ERα+ERβ-Mediated Transcriptional Activities The COS-7 cells were transfected with pcDNASRB-RGS (or the empty plasmid, pcDNA3) and labeled with [^{35}S]methionine. The whole cell lysates of the COS-7 cells were immunoprecipitated with the anti-SRB-RGS antibody and the protein G PLUS-agarose. The precipitates were analyzed with SDS-PAGE and autoradiography. The band of the [^{35}S]methionine-labeled protein in the immunoprecipitate had the same mobility as [^{35}S]methionine-labeled SRB-RGS prepared by an *in vitro* transcription translation system. There was no band corresponding to the mobility of SRB-RGS in the lysate of the cells transfected with pcDNA3. In the COS-7 cells transfected with pcDNASRB-RGS, the SRB-RGS protein was translated with the correct amino acid sequence (data not shown).

Both ERα and ERβ are coexpressed in the same cells of estrogen target tissues. In some target tissues, each ER is distributed separately in the different cells.[22,23] We examined the effects of SRB-RGS overexpression on the ERα-, ERβ-, and ERα+ERβ-mediated transcriptional activities in COS-7 cells. We introduced the smallest and still effective amount of pcDNASRB-RGS to suppress the ERs-mediated transcriptional activities. In this condition, the CMV promoter-driven transcriptional activity (the CMV promoter-driven expression of β-gal) was not suppressed (data not shown). Therefore, the expression vector of β-gal driven by CMV promoter, pcDNAβ-gal was cotransfected to normalize transfection efficiency. As indicated at the bottom of Fig. 2, the expression

vectors of hERα, pcDNA-hERα and/or hERβ, pcDNA-hERβ (or the empty plasmid of them, pcDNA3) and the reporter plasmid for ERs-mediated transcriptional activities, pEREtkCAT were also cotransfected with the expression vector of SRB-RGS, pcDNASRB-RGS (or the empty plasmid, pcDNA3) to COS-7 cells. Using the reporter plasmids pEREtkCAT, it was demonstrated that, among hERα, hERβ, and hERα+hERβ, hERα had the strongest transcriptional activity. (Fig. 2 No. 1), hERβ had the weakest one (Fig. 2 No. 3), and hERα+hERβ had the middle-range one (Fig. 2 No. 5). ERβ inhibits ERα-mediated transcription in the presence of ERα, whereas, in the absence of ERα, it can partially replace ERα.[24] Our results (Fig. 2 Nos. 1, 3, 5) are consistent with theirs. The hERα-, hERβ-, hERα+hERβ-mediated transcriptional activities were suppressed to 41, 21, and 25%, respectively by overexpression of SRB-RGS (Fig. 2 Nos. 2, 4, and 6, respectively). SRB-RGS suppressed very effectively on the transcriptional activities of ERs, especially ERβ.

pcDNA-hERα (or pcDNA-hERβ) and pEREtkCAT were cotransfected with pcDNASRB-RGS (or pcDNA3) and pcDNAβ-gal to normalize transfection efficiency to COS-7 cells as indicated above. Quantitative real-time RT-PCR was performed to examine the effects of introduction of pcDNASRB-RGS on the expression of hERα and hERβ mRNAs. When the mRNA quantity in the cells transfected with pcDNA3 is represented as 100% in each ER, the means±S.D. of three independent experiments in the values in the cells transfected with pcDNASRB-RGS are 120±50% for hERα and 104±27% for hERβ. Introduction of pcDNASRB-RGS to the cells did not affect significantly the expression of hERα and hERβ mRNAs, suggesting that the suppression effects of SRB-RGS on the ERs-mediated transcriptional activities were not due to decrease of ERs expression in the COS-7 cells.

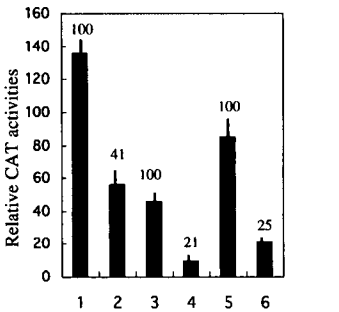

No.	1	2	3	4	5	6
pcDNA-hERα	0.01	0.01	-	-	0.005	0.005
pcDNA-hERβ	-	-	0.01	0.01	0.005	0.005
pEREtkCAT	1	1	1	1	1	1
pcDNA3	0.2	-	0.2	-	0.2	-
pcDNA SRB-RGS	-	0.2	-	0.2	-	0.2
pCMVβ-gal	0.01	0.01	0.01	0.01	0.01	0.01

Fig. 2. Effects of SRB-RGS Overexpression on ERα-, ERβ-, and ERα+ERβ-Mediated Transcriptional Activities

The COS-7 cells were transiently transfected with plasmids as indicated at the bottom. The empty plasmid, pcDNA3 was added to obtain the same input DNA amount. pcDNAβ-gal was cotransfected to normalize transfection efficiency. After transfection, the cells were incubated for 48 h in the presence of 10^{-7} M estradiol. The CAT activity for the cells cotransfected with the empty plasmid, pcDNA3 instead of pcDNA-hERα and/or pcDNA-hERβ was subtracted from each CAT activity. The numbers on top of the bars in the graphs represent the percent activity for each ER group. In each ER group, the activity in the cells transfected with pcDNA3 is represented as 100%. Values are the means±S.D. of three independent experiments.

Subcellular Localization and Identification of SRB-RGS To elucidate the subcellular localization of SRB-RGS, the expression vector of EGFP-tagged SRB-RGS, pEGFPSRB-RGS, was cotransfected with (B) or without (A) the expression vectors of DsRed1-tagged hERα or hERβ, pDsRed-hERα or pDsRed-hERβ, respectively, to HeLa cells (A) or COS-7 cells (B), as indicated in Fig. 3. Transfection of pcDNASRB-RGS (3 μg) or pEGFPSRB-RGS (3 μg) to HeLa cells induced the cell death as mentioned below in Fig. 4. Therefore, relatively small amount of the plasmid (0.2 μg) was transfected to the HeLa cells. Fluorescence was observed by a confocal laser-scanning microscopy after PI staining (Fig. 3A). Green fluorescence of EGFP-tagged SRB-RGS was observed both in the nucleus stained by PI and in the cytoplasm, but not in the plasma membrane, of the HeLa cells. By even small amount of pEGFPSRB-RGS, some HeLa cells showed the appearance of cell shrinkage (an apoptotic appearance). Therefore, pEGFPSRB-RGS (2 μg) was cotransfected to COS-7 cells with pDsRed-hERα (2 μg) or pDsRed-hERβ (2 μg). Green fluorescence of EGFP-tagged SRB-RGS was observed both in the nucleus, where hERα or hERβ localized, and in the cytoplasm, of the COS-7 cells (Fig. 3B). Subcellular localization of SRB-RGS was similar despite the presence or absence of ERs and/or estradiol in the HeLa cells and COS-7 cells.

We examined subcellular localization of intrinsic SRB-RGS and identification of intrinsic SRB-RGS by immunostaining of HeLa cells without transfection of plasmids. HeLa cells were immunostained with the anti-SRB-RGS antibody or PBS containing preimmune serum and then fluorescein-5-isothiocyanate (FITC)-conjugated anti-rabbit immunoglobulin (green fluorescence) as a secondary antibody and observed on a confocal laser-scanning microscopy after staining of the nucleus with PI (red fluorescence). SRB-RGS was stained in the cytoplasm and in the nucleus stained with PI in HeLa cells (Fig. 3C). These observations showed that intrinsic SRB-RGS localized in the cytoplasm and the nucleus, but not in the plasma membrane. In some cells, the cytoplasm was immunostained, but the nucleus was not. SRB-RGS may be localized in either the nucleus or the cytoplasm of the cell and shuttle between the nucleus and the cytoplasm under some condition. These findings by intrinsic SRB-RGS (Fig. 3C) were consistent with the observations in the HeLa cell or the COS-7 cells transfected with pEGFPSRB-RGS (Figs. 3A, B).

The whole cell lysate from HeLa cells without transfection with pcDNASRB-RGS was analyzed by Western blotting using the anti-SRB-RGS antibody and then peroxidase linked anti-rabbit IgG. Consequently, an apparent band with the mobility corresponding to SRB-RGS was detected (Fig. 3D, a white arrow). The band of SRB-RGS was observed in the whole cell lysate from COS-7 cells without transfection of pcDNASRB-RGS as well (data not shown).

These findings (Figs. 3C, D and Fig. 1C) showed that the intrinsic SRB-RGS was expressed in the cells. The putative SRB-RGS deduced from cDNA sequence [18] was identified.

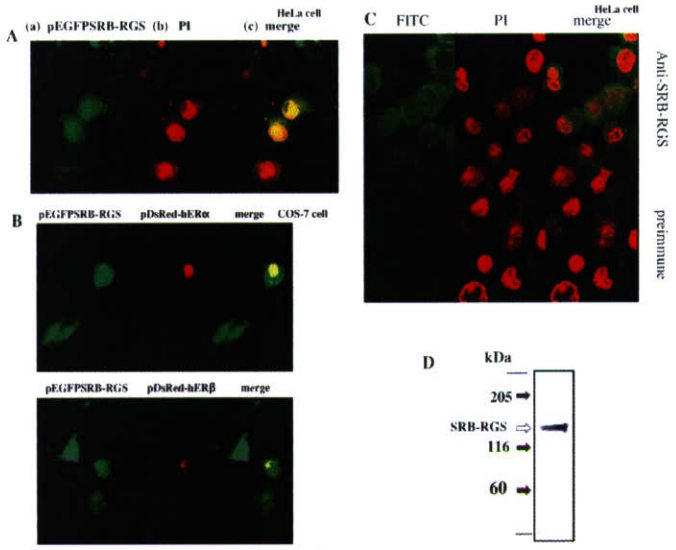

Fig. 3. Subcellular Localization and Identification of SRB-RGS

(A, B) Subcellular localization of EGFP-tagged SRB-RGS. The HeLa cells (A) or COS-7 cells (B) were transiently transfected with pEGFPSRB-RGS (A: 0.2 μg, B: 2 μg) with (B) or without (A) pDsRed-hERα (2 μg) or pDsRed-hERβ (2 μg). Fluorescence was observed by a confocal laser-scanning microscopy after (A) or without (B) staining of the nucleus with PI. (C) Immunostainning of intrinsic SRB-RGS. HeLa cells without transfection of any plasmids were stained with the anti-SRB-RGS antibody or PBS containing preimmune serum and then fluorescein-5-isothiocyanate (FITC)-conjugated anti-rabbit immunoglobulin (green fluorescence). They were viewed on a confocal laser-scanning microscopy after PI staining of the nucleus (red fluorescence). (A—C) The same microscopic field of the cells was shown in Green fluorescence (SRB-RGS), Red fluorescence (nucleus) and merge. (D) Identification of intrinsic SRB-RGS by Western blotting. The HeLa cells without transfection of pcDNASRB-RGS were lysed in the solubilization buffer as mentioned in Materials and Methods. The lysate was subjected on 7% SDS-PAGE and transferred to a nitrocellulose membrane. The membrane was incubated with the anti-SRB-RGS antibody and then peroxidase-linked anti-rabbit IgG. The band on the membrane was visualized as the chemiluminescent signal by development of the peroxidase activity.

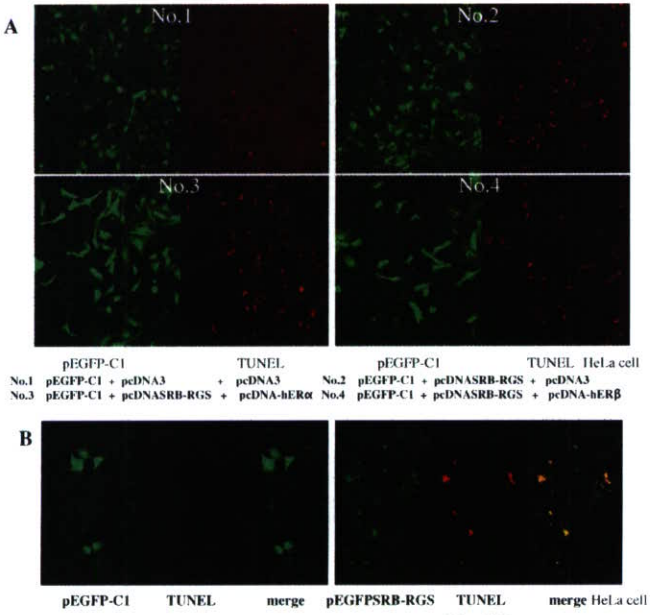

Fig. 4. The Cell Death in HeLa Cells Induced by SRB-RGS

The HeLa cells were grown on glass cover slips and transiently transfected with the plasmids. (A) No. 1 pcDNA3 (3 μg)+pcDNA3 (3 μg), No. 2 pcDNASRB-RGS (3 μg)+pcDNA3 (3 μg), No. 3 pcDNASRB-RGS (3 μg)+pcDNA-hERα (3 μg) and No. 4 pcDNASRB-RGS (3 μg)+pcDNA-hERβ (3 μg) were individually cotransfected with pEGFP-C1 (3 μg) to normalize the transfection efficiency to HeLa cells. (B) HeLa cells were transfected with pEGFP-C1 (3 μg) or pEGFPSRB-RGS (3 μg). The TUNEL assay was performed on the cells to assess DNA fragmentation, as mentioned in Materials and Methods, and the cells were viewed on a confocal laser-scanning microscopy. Red fluorescence: staining by TUNEL assay. pEGFP-C1: the empty plasmid of pEGFPSRB-RGS. pcDNA3: the empty plasmid of pcDNASRB-RGS, pcDNA-hERα and pcDNA-hERβ.

A blast search of SRB-RGS on a mouse genome database of National Center for Biotechnology Information (NCBI) (U.S.A.) revealed that SRB-RGS gene locates on a mouse chromosome 5, splitting into some exons. SRB-RGS gene actually locates on a rat, mouse and human chromosomes according to the genome databases, supporting strongly the identification of intrinsic SRB-RGS in the cells.

Induction of the Cell Death in HeLa Cells by Overexpression of SRB-RGS Overexpression of SRB-RGS in HeLa cells induced the appearances of cell shrinkage and nuclear fragmentation (apoptotic appearances). We examined whether the shrinked cells were TUNEL-positive. As indicated at the bottom of Fig. 4A, No. 1: pcDNA3 (3 μg)+pcDNA3 (3 μg), No. 2: pcDNASRB-RGS (3 μg)+pcDNA3 (3 μg), No. 3: pcDNASRB-RGS (3 μg)+pcDNA-hERα (3 μg), and No. 4: pcDNASRB-RGS (3 μg)+pcDNA-hERβ (3 μg) were individually cotransfected with pEGFP-C1 (3 μg) to normalize the transfection efficiency to HeLa cells. Consequently, the ratios of the TUNEL-positive cells in the cells transfected with pcDNASRB-RGS to the control (No. 1) increased to 4.9-, 3.4- and 4.4-fold (Nos. 2, 3 and 4, respectively) (the ratios of means in two microscopic fields normalized by the transfection efficiency) (Fig. 4A). By transfection of pcDNA3 (3 μg) or pcDNASRB-RGS (3 μg), 3.4 or 16.0%, respectively, of the total HeLa cells were TUNEL-positive (data not shown). Introduction of ERs did not significantly change the ratio of the cell death. The cell death was ERs-independent. To examine further whether overexpression of SRB-RGS caused cell death in the cells, HeLa cells were transfected with pEGFPC-1 or pEGFPSRB-RGS in the absence or presence of Z-VAD-FMK (the caspases inhibitor), and a TUNEL assay was performed. The cells which overexpressed EGFP (the green fluorescent cells) were TUNEL-negative, whereas almost all cells which overexpressed EGFP-tagged SRB-RGS (the green fluorescent cells) were TUNEL-positive (red fluorescence) (Fig. 4B), showing the introduction of SRB-RGS to the cells induced the cell death. The ratio of TUNEL-positive cells did not decrease in HeLa cells which overexpressed EGFP-tagged SRB-RGS in the presence of Z-VAD-FMK (data not shown). The cell death induced by SRB-RGS was caspases-independent.

The significant apoptotic appearance such as cell shrinkage and nuclear fragmentation was not observed by overexpression of SRB-RGS in COS-7 cells. pcDNASRB-RGS (or pcDNA3) (0.2 μg or 3 μg) was cotransfected with pEGFP-C1 (3 μg) to COS-7 cells. The ratios of the TUNEL-positive cells did not increased by overexpression of SRB-RGS (data not shown), suggesting that the suppression effects of SRB-RGS overexpression on the ERα-, ERβ- and ERα+ERβ-mediated transcriptional activities in COS-7 cells (Fig. 2) were not due to the cell death of the COS-7 cells.

DISCUSSION

We attempted to characterize the physiological functions of SRB-RGS in this paper. Our studies provide evidence that SRB-RGS bound to ERs *in vitro* and in the nuclei of the cells (Figs. 1A, B) even when ERs bind to DNA (Fig. 1C), and suppressed the ERs-mediated transcription activities (Fig. 2). SRB-RGS induced the cell death in the HeLa cells ERs- and caspase-independently (Fig. 4). In addition, SRB-RGS was localized in nucleus and cytoplasm, and identified in HeLa cells (Fig. 3).

SRB-RGS and ERs were coimmunoprecipitated by the anti-SRB-RGS antibody, anti-hERα antibody or anti-hERβ antibody. Full-length SRB-RGS interacted with full-length ERs even in the absence of estradiol *in vitro* (Fig. 1A). SRB-RGS 1-495 a.a. and full-length rERα interacted in either the absence or presence of estradiol in a yeast two-hybrid system (Table 1). Full-length hERα interacted with full-length SRB-RGS in the COS-7 cells in either the absence or presence of estradiol in a mammalian two-hybrid system as well (Fig. 1B). These findings suggested that estradiol was not a trigger of interaction between SRB-RGS and ERs. They may interact constitutively, or some unknown trigger may be necessary for the interaction. Full-length SRB-RGS hardly interacted with rERα in yeast cells (Table 1). SRB-RGS and ERs prepared in mammalian systems (an *in vitro* transcription translation system, a mammalian two-hybrid system, the nuclear extract from the rat uterus) could interact with each other (Figs. 1A, B, C). The chemical modification of SRB-RGS and/or ERs, such as phosphorylation, may be a trigger for the interaction *in vivo*. In fact, SRB-RGS has the many phosphorylation sites in the NH_2-terminal region (the ER-binding region).[18] The transcriptional activities of estrogen receptors might be enhanced after dissociation of chemically modified SRB-RGS.

We introduced the smallest and still effective amount of pcDNASRB-RGS to suppress the ERs-mediated transcriptional activities to the cells. In this condition, the CMV promoter-driven transcriptional activity (pcDNAβ-gal) was not suppressed (data not shown). This finding and the results of quantitative real time RT-PCR of the expression of hERα (or hERβ) mRNA (mentioned above) showed that introduction of pcDNASRB-RGS did not affect the ERs expression driven by CMV promoter (pcDNA-hERα or pcDNA-hERβ), suggesting the suppression effects were not due to decrease of ERs expression in the cells. SRB-RGS was localized in the nucleus (Fig. 3), bound to hERα in the nucleus of the cell (Fig. 1B), and interacted with ERs bound to DNA (estrogen response element) (Fig. 1C). SRB-RGS may suppress the ER-mediated transcriptional activities through the interaction with ERs bound to DNA (Fig. 2). SRB-RGS might affect the signal transduction of the membrane-associated receptors in the cytoplasm. Proteins with both PDZ and RGS domains were reported, such as RGS12[25] and PDZ-RGS3.[26] SRB-RGS was the first protein among them to report the suppression of the transcriptional activities.

Recently, it was shown that the nucleotide sequence of SRB-RGS (DDBJ/GenBank/EMBL Accession AB055153) is identical with that of the newly isolated full-length rRGS3 cDNA (NCBI secondary DNA database Accession NM019340). Previous partial hRGS3 (1-519 a.a., corresponding to SRB-RGS 399-967 a.a.) was localized in the cytoplasm, whereas the truncated variant of previous partial hRGS3 termed hRGS3T (previous hRGS3 314-519 a.a., corresponding to SRB-RGS 763-967 a.a.) was found predominantly in the nucleus and partially in the plasma membrane.[27] SRB-RGS could enter the nucleus without ERs (Fig. 3). In fact, previous partial hRGS3 and hRGS3T have the nuclear localization signal (NLS) sequences.

Overexpression of hRGS3T, but not previous hRGS3, followed by serum deprivation resulted in apoptosis of CHO cells.[27] Overexpression of SRB-RGS induced the cell death in HeLa cells without serum deprivation (Fig. 4). SRB-RGS might induce the cell death through caspases-independent affection to survival signals of the cell.

Acknowledgements This study was supported in part by Research Project Grants (Nos. 14-112, 15-104A, 16-105M) from Kawasaki Medical School. We thank Yasue Miyasako, Hiroko Yamamoto, Akane Tsubouti, Tomoko Takada, Mayu Asahi, Marie Sugimoto, Masako Jinbo, Masako Matsuura, Kumiko Ohchi, Yohsuke Utihi (Department of Clinical Engineering, Kawasaki College of Allied Health Professions) for their technical assistance. We also thank Dr. Yoshinobu Tone (Department of Biochemistry, Kawasaki Medical School) for his helpful advices.

REFERENCES

1) Green S., Chambon P., *Trends Genet.*, **4**, 309—314 (1988).
2) Ikeda M., Ogata F., Curtis S. W., Lubahn D. B., French F. S., Wilson E. M., Korach K. S., *J. Biol. Chem.*, **268**, 10296—10302 (1993).
3) Mangelsdorf D. J., Thummel C., Beato M., Herrlich P., Schutz G., Umesono K., Blumberg B., Kastner P., Mark M., Chambon P., Evans R. M., *Cell*, **83**, 835—839 (1995).
4) Onate S. A., Tsai S. Y., Tsai M.-J., O'Malley B. M., *Science*, **270**, 1354—1357 (1995).
5) Ogryzko V. V., Schiltz R. L., Russanova V., Howard B. H., Nakatani Y., *Cell*, **87**, 953—959 (1996).
6) Bannister A. J., Kouzarides T., *Nature* (London), **384**, 641—643 (1996).
7) Yeh S., Chang C., *Proc. Natl. Acad. Sci. U.S.A.*, **93**, 5517—5521 (1996).
8) Fondell J. D., Ge H., Roeder R. G., *Proc. Natl. Acad. Sci. U.S.A.*, **93**, 8392—8333 (1996).
9) Freedman L. P., *Cell*, **97**, 5—8 (1999).
10) Nagy L., Kao H.-Y., Chakravarti D., Lin R. J., Hassing C. A., Ayer D. E., Schreiber S. L., Evans R. M., *Cell*, **89**, 373—380 (1997).
11) Heinzel T., Lavinsky R. M., Mullen T.-M., Soderstrom M., Laherty C. D., Torchia J., Yang W.-M., Brard G., Ngo S. D., Davie J. R., Seto E., Eisenman R. E., Rse D. W., Glass C. K., Rosenfeld M. G., *Nature* (London), **387**, 43—48 (1997).
12) Alland L., Muhle R., Hou H., Jr., Potes J., Chin L., Schreiber-Agus N., DePinho R. A., *Nature* (London), **387**, 49—55 (1997).
13) McKenna N. J., O'Malley B. W., *Cell*, **108**, 465—474 (2002).
14) Narlikar G. J., Fan H.-T., Robert E., Kingston R. E., *Cell*, **108**, 475—487 (2002).
15) Siderovski D. P., Strockbine B., Behe C. I., *Crit. Rev. Biochem. Mol. Biol.*, **34**, 215—251 (1999).
16) Linare J.-L., Wendling C., Tomasetto C., Rio M.-C., *FEBS Lett.*, **480**, 249—254 (2000).
17) Hata Y., Nakanishi H., Takai Y., *Neurosci. Res.*, **32**, 1—7 (1998).
18) Ikeda M., Hirokawa M., Satani N., Kinoshita T., Watanabe Y., Inoue H., Tone S., Ishikawa T., Minatogawa Y., *Gene*, **273**, 207—214 (2001).
19) Ogawa S., Inoue S., Watanabe T., Hiroi H., Orimo A., Hosoi T., Ouchi Y., Muramatsu M., *Biochem. Biophys. Res. Commun.*, **243**, 122—126 (1998).
20) Ikeda M., Okai M., Miyoshi T., Minatogawa Y., *Horm. Metab. Res.*, **34**, 425—430 (2002).
21) Wang H., Peter G., Xeng X., Tang M., Ip W., Khan S., *J. Biol. Chem.*, **270**, 23322—23329 (1995).
22) Chaidarun S. S., Swearingen B., Alexander J. M., *J. Clin. Endocrinol. Metab.*, **83**, 3308—3315 (1998).
23) Kuiper G. G., Carlsson B., Grandien K., Enmark E., Haggblad J., Nilsson S., Gustafsson J.-Å., *Endocrinology*, **138**, 863—870 (1997).
24) Lindberg M. K., Monverare S., Skrtic S., Gao H., Dahlman-Wright K., Gustafsson J.-Å., Ohlsson C., *Mol. Endocrinol.*, **17**, 203—208 (2003).
25) Snow B. E., Antonio L., Suggs S., Gutstein H. B., Siderovski D. P., *Biochem. Biophys. Res. Commun.*, **233**, 770—777 (1997).
26) Lu Q., Sun E. E., Klein R. S., Flanagan J. G., *Cell*, **105**, 69—79 (2001).
27) Dulin N. O., Pratt P., Tiruppathi C., Niu J., Voyno-Yasenetkaya T., Dunn M. J., *J. Biol. Chem.*, **275**, 21317—21323 (2000).

ELSEVIER

Bone 40 (2007) 451–456

BONE

www.elsevier.com/locate/bone

A functional single nucleotide polymorphism in the vitamin-K-dependent gamma-glutamyl carboxylase gene (Arg325Gln) is associated with bone mineral density in elderly Japanese women

Hiroyuki Kinoshita [a], Kimie Nakagawa [b], Ken'ichiro Narusawa [c], Masae Goseki-Sone [d], Mariko Fukushi-Irie [d], Lena Mizoi [d], Hideyo Yoshida [e], Toshio Okano [b], Toshitaka Nakamura [c], Takao Suzuki [e], Satoshi Inoue [a], Hajime Orimo [f], Yasuyoshi Ouchi [a], Takayuki Hosoi [g,h,*]

[a] *Department of Geriatric Medicine, Graduate School of Medicine, University of Tokyo, Japan*
[b] *Department of Hygienic Sciences, Kobe Pharmaceutical University, Japan*
[c] *Department of Orthopedic Surgery, School of Medicine, University of Occupational and Environmental Health, Japan*
[d] *Department of Food and Nutrition, Japan Women's University, Japan*
[e] *Epidemiology and Health Promotion Research Group, Tokyo Metropolitan Institute of Gerontology, Japan*
[f] *Health Science University, Japan*
[g] *Endocrinology Section, Tokyo Metropolitan Geriatric Hospital, Japan*
[h] *Department of Advanced Medicine, National Center for Geriatrics and Gerontology, Japan*

Received 28 March 2006; revised 6 August 2006; accepted 9 August 2006
Available online 6 October 2006

Abstract

The vitamin-K-dependent gamma-glutamyl carboxylase (GGCX) carboxylates vitamin-K-dependent proteins including bone Gla protein (osteocalcin) and matrix Gla protein, which play important roles in bone metabolism. Therefore, GGCX polymorphism might explain in part individual susceptibility to osteoporosis. In the present study, polymorphisms in the exons of this gene were screened in Japanese elderly women and a non-synonymous single nucleotide polymorphisms (SNP) were found; c.8762 G>A; (Arg325Gln). When the kinetic parameters of GGCX325-Gln and GGCX325-Arg were compared *in vitro*, Vmax/Km was significantly higher for GGCX325-Gln (944.4±9.21 pmol/30 min/mg/mM FLEEL) than for GGCX325-Arg (671.9+10.79 pmol/30 min/mg/mM FLEEL) ($p=0.018$). Then, association study of this polymorphism with forearm bone mineral density (BMD) of Japanese postmenopausal women ($n=500$, age 73.6±5.74) was conducted. As a result, the body mass index (BMI)-adjusted Z score in the subpopulation older than 75 years ($n=207$) was higher in those with 325-Gln (0.650±0.883, mean±SD) than those with 325-Arg/Gln or 325-Arg (0.133±0.650) ($p=0.0383$). This is the first report to demonstrate the different activities of GGCX between the common genotypes and their association with BMD.

Keywords: Vitamin-K-dependent gamma-glutamyl carboxylase; Single nucleotide polymorphism; Osteoporosis; Bone mineral density; Bone metabolism

Introduction

Osteoporosis is defined as a skeletal disorder characterized by compromised bone strength predisposing a person to an increased risk of fracture [1]. Because osteoporosis consequently leads to deterioration in activities of daily living (ADL) and quality of life (QOL), prevention and treatment are becoming more important in the current aging society.

Several risk factors for osteoporotic fractures have been established [2], which include the family history of fractures. Epidemiological studies also support the heritability of BMD [3], indicating the contribution of the genetic factors to the pathogenesis of osteoporosis. Therefore, the elucidation of genetic factors for this disease has been awaited. Recently, genetic factors for osteoporosis have been investigated with

* Corresponding author. Department of Advanced Medicine, National Center for Geriatrics and Gerontology, 36-3 Gengo, Morioka-cho, Ohbu-shi, Aichi 474-8511, Japan. Fax: +81 562 46 9595.
E-mail address: hosworld@cb3.so-net.ne.jp (T. Hosoi).

8756-3282/$ - see front matter © 2006 Elsevier Inc. All rights reserved.
doi:10.1016/j.bone.2006.08.007

polymorphisms of genes. Quite a few numbers of association studies have been done with so-called candidate gene approaches [4] and genome-wide approaches [5]. Polymorphisms of many genes were shown to have significant association with BMD. However, the contribution of each gene in determining BMD is small and the result is not always reproducible [6,7]. One of the ways to circumvent the problems and to make outcome biologically and clinically relevant would be to use polymorphisms whose functional variations can be studied.

The vitamin-K-dependent gamma-glutamyl carboxylase (GGCX or VKGC; EC 6.4.-.-) is a microsomal enzyme and is necessary for post-translational modification of vitamin-K-dependent proteins to exert their functions. The genomic structure of GGCX was elucidated in 1997 [8]. Concurrent with conversion of glutamate residue (Glu) to gamma-carboxyl glutamate residue (Gla), vitamin K hydroquinone is oxidized to vitamin K 2,3-epoxide by GGCX, then vitamin K 2,3-epoxide is reduced to vitamin K hydroquinone by vitamin K2,3-epoxide reductase (VKOR) [9]. In addition to vitamin-K-dependent coagulation factors, growth arrest-specific protein (gas6), proline-rich Gla protein-1 (PRGP-1), PRGP-2, bone Gla protein (BGP = osteocalcin) and matrix Gla protein (MGP) are also vitamin-K-dependent proteins [10]. BGP and MGP are abundant in bones [11] and assumed to play important roles in bone metabolism. Therefore, variation in the quality, i.e., carboxylation status, as well as the quantity of these proteins may contribute to variations in the susceptibility of individuals to osteoporosis and other skeletal disorder.

It is reported that the rare mutations of GGCX gene with amino acid substitution (Leu395Arg, Trp501Ser) cause consequential abnormal enzymatic activity, and these lead to vitamin-K-dependent protein defects and severe bleeding disorders [12,13]. However, any association between common variants of the GGCX gene with diseases has not been investigated. In addition, there have been no report comparing the function of products from the polymorphic genes. In this study, we compared the carboxylase activity of the products of the GGCX gene with each non-synonymous SNP and conducted association studies with forearm BMD according to the "common disease, common variant hypothesis" [14].

Materials and methods

Subjects

DNA samples were obtained from peripheral blood of 500 postmenopausal Japanese women living in an area of Japan. Mean ages with SD were 73.6 ± 5.7 years (range 65–90 years). None of the subjects were under the treatment with Warfarin.

All subjects were non-related volunteers and provided informed consent before the study. No participant had medical complications or was undergoing treatment for conditions known to affect bone metabolism, such as pituitary diseases, hyperthyroidism, primary hyperparathyroidism, renal failure, adrenal diseases, or rheumatic diseases, and none were receiving estrogen replacement therapy. The BMD of the radial bone (expressed in g/cm^2) of each participant was measured by dual energy X-ray absorptiometry (DXA) using DTX-200 (Osteometer Meditech Inc., Hawthorne CA, USA). Z scores were calculated using installed software (DTX-200) on the basis of Japanese women and adjusted for body mass index (BMI) utilizing regression analysis.

The ethics committee of the Tokyo Metropolitan Geriatric Hospital approved this study according to the Declaration of Helsinki.

SNPs screening and genotyping

DNA samples were extracted from leukocytes in peripheral blood. SNP screening in the exons of the GGCX gene was conducted with DNA samples of randomly chosen 20 subjects. All of the exons of the GGCX gene were amplified by polymerase chain reaction (PCR) with primers designed as reported previously [15]. Then, denaturing high performance liquid chromatography (DHPLC) with WAVE (Transgenomic Japan, Tokyo, Japan) was used to detect SNPs [16]. The detected variations in the PCR products were validated by direct sequencing utilizing Gene Rapid (Amersham Biosciences Corp, Piscataway, NJ). Then, the genotyping was performed by WAVE.

Construction of human GGCX cDNA (c.8762 = A and c.8762 = G) expression plasmid

Human GGCX cDNA (c.8762 = A) in p*CMV5* was obtained from American Type Culture Collection (ATCC Number 68666, GenBank M81592) (Manassas, VA). Site-directed mutagenesis was performed with a QuickChange XL Site-Directed Mutagenesis Kit (Stratagene, LA Jolla, CA) to prepare GGCX cDNA (c.8762 = G) in p*CMV5*. A pair of mutagenesis primers, 5′-TCCTACTGCCCCC-GAAGGTTGCAACAA-3′ and 5′-TTGTTGCAACCTTCGGGGGCAG-TAGGA-3′ (underlined nucleotides are the mutagenesis target) was used for this process. Direct sequencing of the full length of each c.8762 = G and c.8762 = A was performed utilizing Gene Rapid (Amersham Biosciences Corp, Piscataway, NJ) to ascertain the sequence. Then, the ligation to pcDNA3.1/V5-His/lacZ was performed.

Preparation of microsome fraction from COS-7 cells

Microsomal fraction was prepared from the transfected COS-7 cells as reported previously [17]. COS-7 cells cultured for 24 h were transfected with pcDNA3.1/V5-His/lacZ-GGCX (c.8762 = A; 325Gln) or pcDNA3.1/V5-His/lacZ-GGCX (c.8762 = G; 325Arg) using the LipofectAMINE (Invitrogen Corp., Carlsbad, CA). The transfected cells were cultured for 5 days in 10% FBS D-MEM medium containing G418 300 μg/ml. The cells (5×10^7 cells) were washed with PBS (−) (calcium and magnesium free PBS), scraped and collected in PBS (−) containing 20% glycerol and 1× PIC (protease inhibitor cocktail: 2 mM dithiothreitol, 2 mM EDTA, 0.5 μg/ml leupeptin, 1 μg/ml pepstatin A, 2 μg/ml caprotinin). Cells were homogenized in a glass homogenizer (3 × 10 strokes) and centrifuged at 500×g for 7 min. The pellet was re-homogenized and washed 3 times with the same buffer. Pooled supernatants were centrifuged at 105,000×g for 1 h at 4°C to separate the microsomal fraction. The pellet was resuspended in PBS (−) containing 0.5% (w/v) CHAPS, 0.2% (w/v) phosphatidylcholine, 1× PIC and 20% (v/v) glycerol by sonication.

Carboxylase activity assays

Carboxylase activity was assayed by previously described methods [18–20]. FLEEL was purchased from Bachem (Philadelphia, PA). L-a-Phosphatidylcholine (type V-E) and CHAPS were from Sigma Aldrich Japan (Tokyo, Japan). Vitamin K_2 (menaquinone-4) was from Eisai Co., Ltd. (Tokyo, Japan). The peptide ProFIX19 which contains the sequence AVFLDHENANKILNRPKRY was synthesized by Genenet Co., Ltd. (Fukuoka, Japan). $NaH^{14}CO_3$ (specific activity, 58 mCi/mmol) was from Amarsham Biosciences Corp. (NJ).

The amount of $^{14}CO_2$ incorporated into exogenous substrates was measured in reaction mixtures at 125 μl containing substrate at the indicated concentration, 222 μM reduced vitamin K2 (vitamin KH_2), 16 μM propeptide ProFIX19, 1.4 mM $NaH^{14}CO_3$ (5 μCi), 25 mM MOPS (pH 7.0), 500 mM NaCl, 0.16% (w/v) phosphatidylcholine, 0.16% (w/v) CHAPS, 8 mM DTT and 0.8 M ammonium sulfate, unless stated otherwise. All of the assay components except for the microsomal fraction were prepared as a master mixture. $^{14}CO_2$ incorporation into peptide substrates for over 30 min was assayed in a scintillation counter. Stimulation experiments with vitamin KH_2 were performed at a constant concentration of the enzyme sample and substrate (3.6 mM FLEEL) with increasing concentrations vitamin KH_2, as indicated. All assays were performed in quadruplicate.

Statistical analysis

The allele frequency, haplotype frequency and indices of linkage disequilibrium such as D, D' and r^2 were calculated by SNPAlyze ver3.2 Pro (DYNACOM, Tokyo, Japan). The Pearsons's goodness of fit test with one degree of freedom was used to examine Hardy–Weinberg equilibrium among GGCX genotypes.

The following analysis were performed by StatView 5.0 software (SAS Institute Inc., Cary, NC) and significance was defined as $p < 0.05$. ANOVA was used to compare baseline characteristics (age, height, weight and BMI) among GGCX genotypes. The Mann–Whitney's U test was utilized to examine the effects of GGCX genotypes on BMI adjusted Z scores. The unpaired t-test was used to compare the carboxylase activity.

Results

SNP search and genotyping

Table 1 summarizes the SNPs detected in our SNP search. These were already registered in the dbSNP (http://www.ncbi.nlm.nih.gov/SNP/) (Table 1a) and each genotype showed Hardy–Weinberg equilibrium ($p > 0.05$). The linkage disequilibrium coefficients, D' values, in c.8762 G>A, c.9167 C>T and c.9191 C>T were higher than 0.98, indicating that these three SNPs are in a strong linkage disequilibrium and constitute a haplotype block [21] (Table 1b). The genotype c.8762 = AA perfectly corresponded to c.9167 = TT, c.8762 = AG to c.9167 = CT and c.8762 = GG to c.9167 = CC, i.e., c.8762 G>A and c.9167 C>T were completely linked together. The SNP c.8762 G>A was a non-synonymous SNP, changing amino acid 325 Arg to Gln (Table 1a). Therefore, the genotypes were described as 325-Arg, 325-Arg/Gln, or 325-Gln afterward in this report. We focused on this non-synonymous polymorphism in further analyses. Genotype distribution in the subjects was as follows; 325-Arg = 265, 325-Arg/Gln = 203 and 325-Gln = 32. The baseline characteristics (age, height, weight and BMI) were not significantly different among these genotypes (Table 2).

Table 1
Summary of GGCX SNPs

a. Detected SNPs

Name	Base position	Allele frequency	Amino acid change	dbSNP[a]
c.8762 G>A	8762 (exon8)	G:A = 0.73:0.2 7	Arg325Gln	Rs699664
c.9167 C>T	9167 (exon9)	C:T = 0.73:0.2 7	none (406Arg)	Rs2592551
c.9191 C>T	9191 (exon9)	C:T = 0.93:0.0 7	none (414Thr)	Rs101799 04

b. Tests for linkage disequilibrium between GGCX SNPs

SNP1	SNP2	SNP3	D	D'	r^2
c.8762 G>A	c.9167 C>T		0.195 7	1.000 0	1.000 0
c.8762 G>A		c.9191 C>T	−0.017 9	0.999 9	0.026 2
	c.9167 C>T	c.9191 C>T	−0.017 9	0.999 9	0.026 2

The D, D', and r^2 were calculated by SNPAlyze ver3.2 Pro.
The D' value was an absolute value ($0 \leq D' \leq 1$).
[a] Numbers are from dbSNP database of NCBI (http://www.ncbi.nlm.nih.gov/SNP/).

Table 2
Baseline characteristics of subjects

Genotype	325-Gln	325-Arg/Gln	325-Arg	p value
Number	32	203	265	
Age	74.1 ± 5.9	73.1 ± 5.7	73.9 ± 5.7	0.344
Height (cm)	144.4 ± 5.0	144.8 ± 5.9	145.3 ± 5.7	0.534
Weight (kg)	48.7 ± 5.6	50.4 ± 8.7	51.1 ± 8.2	0.265
BMI (kg/m^2)	23.3 ± 2.4	24.0 ± 3.5	24.2 ± 3.4	0.409

Data were shown as mean ± SD.
The p values were calculated by ANOVA.

Carboxylase activity

Efficient transfection into COS-7 cells was confirmed by measuring luciferase activity from co-transfected internal control vector (pRL-*CMV*) (data not shown). Moreover, production of GGCX by transfected COS-7 cells was visualized

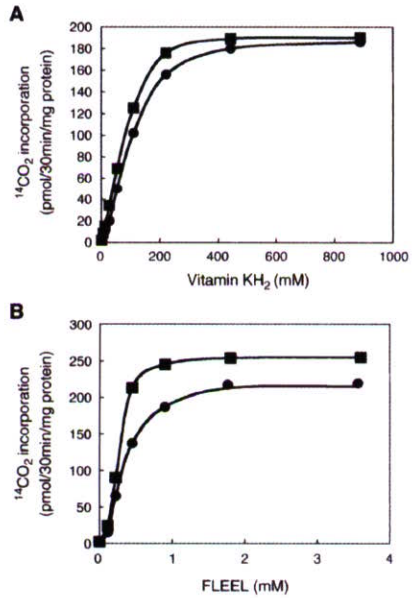

Fig. 1. Influence of vitamin KH_2 or FLEEL on the carboxylase activity of GGCX 325Gln or 325Arg. (A) Carboxylation of 3.6 mM FLEEL at vitamin KH_2 concentrations between 0 and 888 mM was measured by $^{14}CO_2$ incorporation for both 325Gln (filled squares) and 325Arg (filled circles). (B) Carboxylation in 222 mM vitamin KH_2 at FLEEL concentrations between 0 and 3.6 mM was measured by $^{14}CO_2$ incorporation for both 325Gln (filled squares) and 325Arg (filled circles).

as a 130 kDa band in Western blot analysis using antibodies to V5 and His (data not shown).

GGCX 325-Gln (c.8762=A) was determined to have a Km for vitamin KH_2 of 71.34±6.20 μM (mean±SD). The Km of GGCX 325-Arg (c.8762=G) for vitamin KH_2 was 90.31±4.63 μM, about 1.3-fold higher than that of 325-Gln (p=0.029). The Vmax determined for 325-Arg (186±7.88 pmol/30 min/mg) was lower than that of 325Gln (191±9.45 pmol/30 min/mg) (p=0.033). The Vmax/Km for vitamin KH_2 with 325-Arg (2.06±0.12 pmol/30 min/mg/μM) was thus reduced by 24% compared with 325Gln (2.68±0.20 pmol/30 min/mg/μM) (p=0.032) (Fig. 1 and Table 3a).

Kinetic constants for FLEEL carboxylation were determined in the presence of saturating concentrations of ProFIX19. The Km of 325-Gln for FLEEL was 0.27±0.02 mM. The Km of 325-Arg for FLEEL was 0.32±0.03 mM, about 1.3-fold higher than that of 325-Gln (p=0.016). Comparison of Vmax for FLEEL carboxylation showed that the reaction rate of 325-Arg (215±5.28 pmol/30 min/mg) was about 1.2-fold slower than that of 325-Gln (255±6.33 pmol/30 min/mg) (p=0.011). The Vmax/Km for FLEEL with 325-Arg (671.9±10.79 pmol/30 min/mg/mM) was thus reduced about 30% compared with 325Gln (944.4±9.21 pmol/30 min/mg/mM) (p=0.018) (Fig. 1 and Table 3b). These results indicate that 325-Gln has higher carboxylase activity than 325-Arg.

Association study of BMD

The subjects with 325-Gln had the highest adjusted Z score but the difference was not statistically significant in all subjects; 0.297±0.866 (mean±SD), 0.030±0.959 and 0.057±0.882 for 325-Gln, 325-Arg/Gln, or 325-Arg, respectively. From this result, we assumed that the effect of GGCX polymorphism c.8762 G>A is allele G dominant, and compared 325-Gln vs. 325-Gln/Arg+325-Arg.

Table 3
Comparison of the kinetic parameters of GGCX 325-Gln and 325-Arg

a. Using vitamin KH_2 as a substrate

Substrate	Enzyme	Km (μM)	Vmax (pmol/30 min/mg)	Vmax/Km (pmol/30 min/mg/μM)
Vitamin KH_2 [a]	325Gln	71.34±6.20	191±9.45	2.68±0.20
	325Arg	90.31±4.63	186±7.88	2.06±0.12
p value		0.029	0.033	0.032

b. Using FLEEL as a substrate

Substrate	Enzyme	Km (μM)	Vmax (pmol/30 min/mg)	Vmax/Km (pmol/30 min/mg/mM)
FLEEL [b]	325Gln	0.27±0.02	255±6.33	944.4±9.21
	325Arg	0.32±0.03	215±5.28	671.9±10.79
p value		0.016	0.011	0.018

All assays were performed in quadruplicate.
Data were shown as mean±SD. The p values were calculated by the unpaired t-test.
[a] Determined at 3.6 mM FLEEL.
[b] Determined at 222 mM vitamin KH_2.

Table 4
Comparison of BMI-adjusted Z score of BMD among the genotypes of GGCX Arg325Gln

Genotype	325-Gln	325-Arg or 325-Arg/Gln	p value
All	0.297±0.866 (32)	0.045±0.915 (468)	0.132
<75	0.022±0.926 (18)	−0.017±0926 (275)	0.861
>75	0.650±0.883 (14)	0.133±0.650 (193)	0.038

The data are expressed as mean±SD.
The p values were calculated by the Mann–Whitney's U test.

The adjusted Z score seemed higher in the subjects with 325-Gln than those with other genotypes. However, the difference was not statistically significant (Table 4). Then we divided the subjects into two groups according to the age; above and below 75 years. As a result, the adjusted Z score in the subpopulation older than 75 years (n=207) was higher in those with 325-Gln (0.650±0.883, mean±SD) than those with 325-Gln/Arg or 325-Arg (0.133±0.064) (p=0.0383). On the other hand, this association was not found in the subpopulation younger than 75 years.

Discussion

This is the first report to demonstrate the different activities of GGCX between the common genotypes. Although the association study of these genotypes with BMD provided a statistically significant results, the limited size of the samples should make us cautious and modest and requires further studies. Because the site of the BMD measurement in this study was limited to the radius, the association of GGCX genotype with BMD of spine and proximal femur would be another important issue. In addition, low BMD does not explain all of the pathophysiology of bone fragility in osteoporotic patients. Our results would explain a part of BMD determinants not the osteoporosis of itself, and suggest that the GGCX gene polymorphism may be involved in the pathogenesis of osteoporosis.

The physiological roles of vitamin-K-dependent Gla proteins in bone metabolism have not been elucidated yet, but it was reported that under-carboxylated osteocalcin (ucOC) was negatively correlated with BMD [22] and that administration of vitamin K decreased ucOC and worked to increase BMD [23]. Another vitamin-K-dependent protein, MGP (matrix Gla protein) has been reported to be a regulator of calcification in several studies. For example, MGP-deficient mice exhibited inappropriate calcification of various cartilages including the growth plate, which eventually led to short stature [24]. In addition, it was suggested that under-carboxylated MGP was biologically inactive and may increase the risk for vascular calcification [25]. Therefore, properly carboxylated MGP is assumed to be necessary to protect vascular system from calcification and skeletal system from abnormal ossification [26]. People with 325-Gln might have a higher efficiency of carboxylation of these proteins with the given status of vitamin K, considering that carboxylase activity of 325-Gln was higher than that of 325-Arg *in vitro*. Because this variation of carboxylase activity between the genotypes was examined using only a standard substrate, FLEEL, in this study, functional significance of the polymorphisms in physiological target molecules and tissues should be investigated further. For example, *in vitro* studies using other substrates as well as measurements of the serum levels and carboxylation status of vitamin-K-dependent proteins would be informative.

In order to be carboxylated, vitamin-K-dependent proteins are assumed to be bound specifically to 343–355 residues of GGCX with high affinity. Among these residues, 343 (Cys) and 345 (Tyr) were suggested to be located near the catalytic center [27]. Moreover, it was also reported that chemical modification of 323-Cys and 343-Cys decreased its carboxylase activity [28]. Considering a study of human GGCX membrane topology, human GGCX probably may span the endoplasmic reticulum membrane 5 times and the interval of fourth and fifth transmembrane region may be composed of amino acids 313–361 [29]. Since amino acids 323-Cys, 325-Arg/Gln, 343-Cys, 345-Tyr and 343–355 are involved in the interval of fourth and fifth transmembrane regions (313–361), the amino acid substitution of 325 residue (Arg/Gln) may affect enzymatic activity directly or indirectly through influencing the function of these residues.

The higher Km value of GGCX 325-Arg would mean that higher intake of vitamin K may cancel the effects of this genotype. Therefore, the influence of GGCX polymorphisms should be studied further from the viewpoints of gene–environment interactions as well as ethnic/race differences. When the association study with the GGCX gene polymorphism is designed among different ethnicities, the intake of vitamin Ks should be handled carefully, because there are large ethnic differences in vitamin K status as we reported previously [30]. On the other hand, the difference in Vmax between the 325-Gln and 325-Arg suggests that the GGCX polymorphism might affect the carboxylase activity at the pharmacological level of vitamin K and might contribute to the difference of individual sensitivity to vitamin K treatment for osteoporosis.

The reason for age-dependent effect of GGCX polymorphism is not obvious, but we reported the similar age-dependent effects of functional SNP in tissue non-specific alkaline phosphatase gene [31]. It is reported that dietary vitamin K intake decreases with age, and elevated levels of ucOC may result from subclinical vitamin K deficiency and are frequently observed in the elderly [32]. The administration of vitamin K increased osteocalcin's hydroxyapatite binding capacity, decreased urinary calcium and hydroxyproline excretion in postmenopausal women but no effect was observed in premenopausal women [33]. These evidences may explain partly that the effects of different carboxylase activity between 325-Gln and 325-Arg might become obvious in advancing aging.

In conclusion, we reported here for the first time the different activities of GGCX between the common genotypes which were associated with BMD in elderly Japanese women. There are two major limitations in this study as discussed above; the limited sample size and the lack of extensive functional studies. Further studies are absolutely necessary to delineate any conclusion regarding the GGCX polymorphism and osteoporosis.

Acknowledgments

This work was supported in part by the grants from the Japanese Ministry of Health, Labor and Welfare. We thank Ms. M. Kumasaka for her expert technical assistance.

References

[1] NIH. Consensus development panel on osteoporosis prevention, diagnosis, and therapy osteoporosis prevention, diagnosis, and therapy. JAMA 2001;285:785–95.
[2] Kanis JA. Diagnosis of osteoporosis and assessment of fracture risk. Lancet 2002;359:1929–36.
[3] Pocock NA, Eisman JA, Hopper JL, Yeates MG, Sambrook PN, Eberl S. Genetic determinants of bone mass in adults. A twin study. J Clin Invest 1987;80:706–10.
[4] Andrew T, Macgregor AJ. Genes and osteoporosis. Curr Osteoporos Rep 2004;2:79–89.
[5] Long JR, Xiong DH, Recker RR, Deng HW. The genetics of osteoporosis. Drugs Today (Barc) 2005;41:205–18.
[6] Pols HA, Uitterlinden AG. Genetic polymorphisms and clinical practice: the example of osteoporosis. Acta Clin Belg 2002;57:266–70.
[7] Shen H, Liu Y, Liu P, Recker RR, Deng HW. Nonreplication in genetic studies of complex diseases—Lessons learned from studies of osteoporosis and tentative remedies. J Bone Miner Res 2005;20:365–76.
[8] Wu SM, Stafford DW, Frazier LD, Fu YY, High KA, Chu K, et al. Genomic sequence and transcription start site for the human gamma-glutamyl carboxylase. Blood 1997;89:4058–62.
[9] Wu SM, Stanley TB, Mutucumarana VP, Stafford DW. Characterization of the gamma-glutamyl carboxylase. Thromb Haemost 1997;78:599–604.
[10] Berkner KL. The vitamin K-dependent carboxylase. J Nutr 2000;130:1877–80.
[11] Price PA. Gla-containing proteins of bone. Connect Tissue Res 1989;21:51–7.
[12] Brenner B, Sanchez-Vega B, Wu S-M, Lanir N, Stafford DW, Solera J. A missense mutation in a gamma-glutamyl carboxylase gene causes combined deficiency of all vitamin K-dependent blood coagulation factors. Blood 1998;92:4554–9.
[13] Spronk HMH, Farah RA, Buchanan GR, Vermeer C, Soute BAM. Novel mutation in the gamma-glutamyl carboxylase gene resulting in congenital combined deficiency of all vitamin K-dependent blood coagulation factors. Blood 2000;96:3650–2.
[14] Doris PA. Hypertension genetics, single nucleotide polymorphisms, and the common disease: common variant hypothesis. Hypertension 2002;39:323–31.
[15] Oldenburg J, von Brederlow B, Fregin A, Rost S, Wolz W, Eberl W, et al. Congenital deficiency of vitamin K dependent coagulation factors in two families presents as a genetic defect of the vitamin K-epoxide-reductase-complex. Thromb Haemost 2000;84:937–41.
[16] Hayward-Lester A, Oefner PJ, Sabatini S, Doris PA. Accurate and absolute quantitative measurement of gene expression by single-tube RT-PCR and HPLC. Genome Res 1995;5:494–9.
[17] Czerwiec E, Begley GS, Bronstein M, Stenflo J, Taylor K, Furie BC, et al. Expression and characterization of recombinant vitamin K-dependent gamma-glutamyl carboxylase from an invertebrate, Conus textile. Eur J Biochem 2002;269:6162–72.
[18] Ulrich MMW, Furie B, Jacobs M, Vermeer C, Furie BC. Vitamin K-dependent carboxylation. A synthetic peptide based upon the gamma-carboxylation recognition site sequence of the prothrombin propeptide is an active substrate for the carboxylation in vitro. J Biol Chem 1988;263:9697–702.
[19] Morris DP, Soute BAM, Vermeer C, Stafford DW. Characterization of the purified vitamin K-dependent gamma-glutamyl carboxylase. J Biol Chem 1993;268:8735–42.
[20] Mutucumarana VP, Stanfford DW, Stanley TB, Jin D, Solera J, Brenner B, et al. Expression and characterization of the naturally occurring

mutation L394R in human gamma-glutamyl carboxylase. J Biol Chem 2000;275:32572–7.
[21] Gabriel SB, Schaffner SF, Nguyen H, Moore JM, Roy J, Blumenstiel B, et al. The structure of haplotype blocks in the human genome. Science 2002;296:2225–9.
[22] Szulc P, Arlot M, Chapuy MC, Duboeuf F, Meunier PJ, Delmas PD. Serum undercarboxylated osteocalcin correlates with hip bone mineral density in elderly women. J Bone Miner Res 1994;9:1591–5.
[23] Shiraki M, Shiraki Y, Aoki C, Miura M. Vitamin K2 (menatetrenone) effectively prevents fractures and sustains lumbar bone mineral density in osteoporosis. J Bone Miner Res 2000;15:515–21.
[24] Luo G, Ducy P, McKee MD, Pinero GJ, Loyer E, Behringer RR, et al. Spontaneous calcification of arteries and cartilage in mice lacking matrix GLA protein. Nature 1997;386:78–81.
[25] Spronk HM, Soute BA, Schurgers LJ, Cleutjens JP, Thijssen HH, De Mey JG, et al. Matrix Gla protein accumulates at the border of regions of calcification and normal tissue in the media of the arterial vessel wall. Biochem Biophys Res Commun 2001;289:485–90.
[26] Shanahan CM, Proudfoot D, Farzaneh-Far A, Weissberg PL. The role of Gla proteins in vascular calcification. Crit Rev Eukaryot Gene Expr 1998;8:357–75.
[27] Pudota BN, Hommema EL, Hallgren KW, McNally BA, Lee S, Berkner KL. Identification of sequences within the gamma-carboxylase that represent a novel contact site with vitamin K-dependent proteins and that are required for activity. J Biol Chem 2001;276:46878–86.
[28] Tie JK, Jin DY, Loiselle DR, Pope RM, Straight DL, Stafford DW. Chemical modification of cysteine residues is a misleading indicator of their status as active site residues in the vitamin K-dependent gamma-glutamyl carboxylation reaction. J Biol Chem 2004;279:54079–87.
[29] Tie J, Wu SM, Jin D, Nicchitta CV, Stafford DW. A topological study of the human gamma-glutamyl carboxylase. Blood 2000;96:973–8.
[30] Kaneki M, Hodges S, Hosoi T, Fujiwara S, Lyons A, Cren ST, et al. Japanese fermented bean as the major determinant for the large geographical differences in circulating levels of vitamin K2 and its possible implication in hip fracture incidence. Nutrition 2001;17:315–21.
[31] Goseki-Sone M, Sogabe N, Fukushi-Irie M, Mizoi L, Orimo Hideo, Suzuki T, et al. Functional analysis of the single nucleotide polymorphisms 787T>C9 in the *Tissue-nonspecific alkaline phosphatase* gene associated with BMD. J Bone Miner Res 2005;20:773–82.
[32] Vermeer C, Jie KS, Knapen MH. Role of vitamin K in bone metabolism. Annu Rev Nutr 1995;15:1–22.
[33] Knapen MH, Hamulyak K, Vermeer C. The effect of vitamin K supplementation on circulating osteocalcin (bone Gla protein) and urinary calcium excretion. Ann Intern Med 1989;111:1001–5.

Available online at www.sciencedirect.com
ScienceDirect
Biochemical and Biophysical Research Communications 358 (2007) 813–818
BBRC
www.elsevier.com/locate/ybbrc

Estrogen-related receptor α modulates the expression of adipogenesis-related genes during adipocyte differentiation

Nobuhiro Ijichi [a], Kazuhiro Ikeda [a], Kuniko Horie-Inoue [a], Ken Yagi [b], Yasushi Okazaki [b], Satoshi Inoue [a,c,*]

[a] *Division of Gene Regulation and Signal Transduction, Research Center for Genomic Medicine, Saitama Medical University, Saitama, Japan*
[b] *Division of Functional Genomics and Systems Medicine, Research Center for Genomic Medicine, Saitama Medical University, Saitama, Japan*
[c] *Department of Geriatric Medicine, Graduate School of Medicine, The University of Tokyo, 7-3-1 Hongo, Bunkyo-ku, Tokyo 113-8655, Japan*

Received 27 April 2007
Available online 11 May 2007

Abstract

Estrogen-related receptor α (ERRα) is an orphan nuclear receptor that regulates cellular energy metabolism by modulating gene expression involved in fatty acid oxidation and mitochondrial biogenesis in brown adipose tissue. However, the physiological role of ERRα in adipogenesis and white adipose tissue development has not been well studied. Here, we show that ERRα and ERRα-related transcriptional coactivators, peroxisome proliferator-activated receptor γ (PPARγ) coactivator-1α (PGC-1α) and PGC-1β, can be up-regulated in 3T3-L1 preadipocytes at mRNA levels under the adipogenic differentiation condition including the inducer of cAMP, glucocorticoid, and insulin. Gene knockdown by ERRα-specific siRNA results in mRNA down-regulation of fatty acid binding protein 4, PPARγ, and PGC-1α in 3T3-L1 cells in the adipogenesis medium. ERRα and PGC-1β mRNA expression can be also up-regulated in another preadipocyte lineage DFAT-D1 cells and a pluripotent mesenchymal cell line C3H10T1/2 under the differentiation condition. Furthermore, stable expression of ERRα in 3T3-L1 cells up-regulates adipogenic marker genes and promotes triglyceride accumulation during 3T3-L1 differentiation. These results suggest that ERRα may play a critical role in adipocyte differentiation by modulating the expression of various adipogenesis-related genes.

Keywords: Estrogen-related receptor α (ERRα); Preadipocytes; 3T3-L1; Pluripotent mesenchymal cells; Adipocyte differentiation

Obesity is a significant risk factor for various metabolic diseases [1], as it has been recently shown that the hyperplasic adipose tissue itself alters systemic homeostasis [2]. The study for the mechanism of adipogenesis is important to understand the pathophysiology of obesity.

Estrogen-related receptors (ERRs) are orphan nuclear receptors that may regulate transcription of metabolic genes [3,4]. Among them, ERRα and ERRγ are particularly expressed in mitochondria-rich tissues [5,6], and ERRα stimulates gene expression associated with mitochondrial biogenesis and energy production [6]. ERRα-deficient mice show the reduction of fat mass and the resistance to high-fat diet-induced obesity [7], indicating that ERRα can participate in the development of white adipose tissue. The ERR coactivator peroxisome proliferator-activated receptor γ (PPARγ) coactivator-1α and β (PGC-1α and PGC-1β) are also considered as key regulators in the energy production pathways and may play a role in the regulation of mitochondrial status and functions [8–10]. Besides these previous findings, the contribution of ERRs to adipogenesis remains to be investigated.

To understand the functional roles of ERRs on adipogenesis, we investigated the expression of ERRs and adipogenic factors in 3T3-L1 and DFAT-D1 preadipocytes and C3H10T1/2 pluripotent mesenchymal cells [11,12] under

* Corresponding author. Address: Department of Geriatric Medicine, Graduate School of Medicine, The University of Tokyo, 7-3-1 Hongo, Bunkyo-ku, Tokyo 113-8655, Japan. Fax: +81 42 985 7209.
E-mail address: INOUE-GER@h.u-tokyo.ac.jp (S. Inoue).

0006-291X/$ - see front matter © 2007 Elsevier Inc. All rights reserved.
doi:10.1016/j.bbrc.2007.04.209

the adipogenic condition. We showed that ERRα mRNA was up-regulated in these cells during adipogenesis. Gene knockdown of ERRα repressed the induction of adipogenesis-related genes in 3T3-L1 cells during differentiation. Moreover, stable expression of ERRα in 3T3-L1 cells elevates the expression levels of adipogenic marker genes and promotes triglyceride accumulation during differentiation. The present study suggests that ERRα is one of the critical regulators in the signal transduction of adipogenesis.

Materials and methods

Cell culture and adipocyte differentiation. 3T3-L1 and C3H10T1/2 cells were obtained from American Type Culture Collection (Manassas, VA). DFAT-D1 cells were established from mature adipocytes of adult ddY mouse [12]. For adipogenic induction, cells (2 days after confluence) were cultured in the differentiation medium, DMEM containing 10% FBS together with the mixture of 0.5 mM isobutylmethylxanthine (IBMX, Sigma), 1 μM dexamethasone (Dex, Sigma) and 10 μg/ml bovine insulin (Sigma) (MDI mixture). On day 2 after the induction, cells were cultured in the post-differentiation medium, DMEM containing 10% FBS and 10 μg/ml insulin, and the medium was changed every 2 days (DFAT-D1) or 3 days (3T3-L1 and C3H10T1/2).

Oil-Red-O staining. Lipid accumulation was evaluated by staining with Oil-Red-O for 1 h as described previously [12].

Quantitative RT-PCR (qPCR). qPCR was performed as described previously [13]. The sequences of PCR primers are described in Table 1. The experiments were independently repeated at least three times, each performed in triplicate.

siRNA transfection. Synthetic small interfering RNA (siRNA) duplexes against mouse ERRα (ESRRA-NM_007953) and the luciferase reporter plasmid pGL2 (Luciferase GL2 Duplex) were purchased from Dharmacon (Lafayette, CO). During adipogenic induction, 3T3-L1 cells were transfected with 50 nM siRNA using Lipofectamine 2000 (Invitrogen) three times at days 0, 2, and 5.

Plasmid construction. Human ERRα cDNA (hERRα amino acids 2-475) was cloned from human brain cDNA (Clontech) by RT-PCR using the following primers: forward, 5′-CCTGAATTCTCCAGCCAGGTG GTGGGCATT-3′; reverse, 5′-ACTGAATTCTCAGTCCATCATGGC CTCGA-3′. The PCR product was N-terminally tagged with FLAG and cloned into blunted EcoRI sites of pCXN2 [14] (pCXN2-FLAG-hERRα). The construction of the plasmid was confirmed by sequencing.

Generation of stable cell lines and Western blotting. 3T3-L1 cells were transfected with pCXN2-FLAG-hERRα or empty pCXN2 plasmid and neo-resistant clones were isolated by G418 (0.8 mg/ml). hERRα mRNA expression was verified by qPCR using following primers: forward, 5′-GACTACAAGGACGATGATGACAAG-3′; reverse, 5′-CTCTGT CTCCGAGGAACCCTTT-3′.

For Western blotting, whole cell lysates were resolved by 10% denaturing SDS–PAGE and the blotted membrane (Immobilon-P Transfer Membrane, Millipore) was incubated with anti-FLAG M2 (Sigma).

Results

Up-regulation of ERRα mRNA by adipogenic induction in 3T3-L1 preadipocytes

Mouse 3T3-L1 preadipocytes have been used as a model for the adipogenesis study. 3T3-L1 cells exhibit the phenotype of adipocyte differentiation after 4-6 days of confluent culture treated with the standard adipogenic cocktail comprised of IBMX, Dex and insulin (MDI mixture) [15,16]. Using this experimental model, we investigated the expression of adipogenesis-related genes by qPCR. Oil-Red-O staining showed that triglyceride accumulation was initiated at day 2 after adipogenic induction in 3T3 cells (Fig. 1A). Consistent with the result of Oil-Red-O staining, mRNA expression of adipocyte differentiation markers aP2 and PPARγ was time-dependently elevated in 3T3-L1 cells following adipogenic induction (Fig. 1B and C). In contrast, mRNA level of uncoupling protein 1 (UCP1), which is abundantly expressed in brown adipose tissue (BAT) and known to function in adaptive thermogenesis, was transiently up-regulated by ~12-fold at day 2 after the induction (Fig. 1D). We also investigated the mRNA expression of nuclear receptor coactivators PGC-1α and PGC-1β following adipogenic stimulation. Both genes were eventually up-regulated at day 8, but the mRNA elevation of PGC-1β was observed earlier following the differentiation condition in comparison to the late induction of PGC-1α (Fig. 1E and F).

Next, we examined the mRNA expression of ERRs in 3T3-L1 preadipocytes in the adipogenesis condition. ERRα mRNA level was time-dependently up-regulated following the induction (Fig. 2A). On the contrary, ERRβ and ERRγ mRNA levels were decreased in first 5 days after the stimulation and returned to their initial levels at day 8 (Fig. 2B and C). Notably, among the three ERR subtypes, the absolute mRNA amount of ERRα was largest in 3T3-L1 preadipocytes (Table 2).

Table 1
Oligonucleotides used in qPCR

Gene	Accession No.	Description	qPCR primers (5′–3′)	
			Forward	Reverse
aP2	NM_024406	Fatty acid binding protein 4	gcgtggaattcgatgaaatca	cccgccatctagggttatga
PPARγ	NM_011146	Peroxisome proliferator activated receptor γ	cccgccatctagggttatga	ttccgaagaaccatccgatt
UCP1	NM_009463	Uncoupling protein 1	cgtaccaagctgtgcgatgt	aagccacaaaccctttgaaaaag
ERRα	NM_007953	Estrogen-related receptor α	ggagtacgtcctgctgaaagct	cacagcctcagcatcttcaatg
ERRβ	NM_011934	Estrogen-related receptor β	cgatatccccgagggagatatc	ccagttgatgaggaacacaagct
ERRγ	NM_011935	Estrogen-related receptor γ	gaccctactgtcccgacagt	aactctcggtcagccaagtca
PGC-1α	NM_008904	PPARγ coactivator-1α	ggcacgcagccctattcat	cacggagagttaaaggaagagcaa
PGC-1β	NM_133249	PPARγ coactivator-1β	catctgggaaaagcaagtacga	cctcgaaggttaaggctgatatca

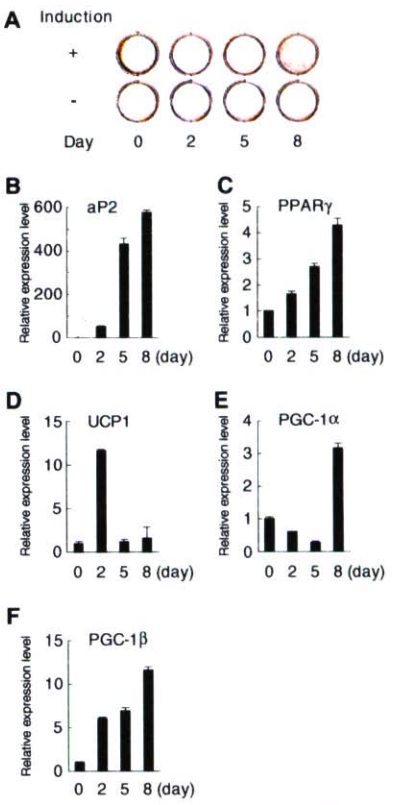

Fig. 1. Up-regulation of adipogenesis-related genes in 3T3-L1 preadipocytes under the adipogenic condition. (A) Oil-Red-O staining of 3T3-L1 cells. Two days after confluence (day 0), 3T3-L1 cells were treated with or without a MDI mixture (0.5 mM IBMX, 1 μM dexamethasone and 10 μg/ml insulin). At day 2 and 5, the medium was exchanged to DMEM/10% FBS containing 10 μg/ml insulin or vehicle. Oil-Red-O staining was performed at indicated times. (B–F) Gene expression profiles of fatty acid binding protein 4 (aP2) (B), PPARγ (C), UCP1 (D), PGC-1α (E) and PGC-1β (F) genes in 3T3-L1 cells in response to MDI treatment. mRNA expression levels of each gene were examined by qPCR and the results were shown as fold change over the expression level at day 0.

ERRα siRNA represses induction of adipocyte differentiation markers in adipogenic condition

To assess the role of ERRα on adipocyte differentiation, we investigated the effect of ERRα knockdown on the expression of adipogenesis-related genes. 3T3-L1 preadipocytes were transfected with siRNA targeted for ERRα mRNA (siERRα) in the adipogenic condition and the expression of several adipogenesis-related genes were evaluated by qPCR (Fig. 3). SiERRα reduced ERRα mRNA

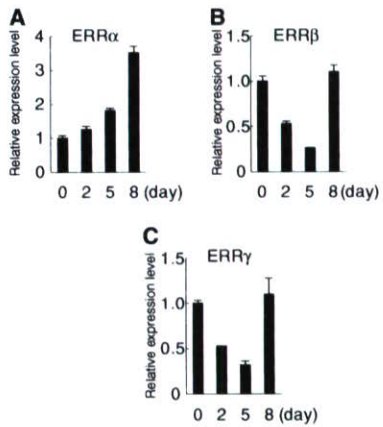

Fig. 2. Gene expression profiles of estrogen-related receptors (ERRs) in the 3T3-L1 cells under the adipocyte differentiation condition. 3T3-L1 cells were induced to differentiate as described in Fig. 1. mRNA expression levels of ERRα (A), ERRβ (B), and ERRγ (C) at indicated time points were examined by qPCR and the results were shown as fold change over the expression level at day 0.

levels by ~50% in 3T3-L1 cells compared to control siLuc, the siRNA targeted for the luciferase gene (Fig. 3A). In the adipogenic condition, siERRα attenuated the time-dependent induction of aP2 by ~50% in days 2–8 of culture compared to siLuc (Fig. 3B). Regarding PPARγ and PGC-1α mRNA, up-regulation itself was not remarkable in days 2–5 after the stimulation with siRNAs, yet siERRα repressed these mRNA induction by 35–45% at day 8 (Fig. 3C and D). These results showed that ERRα could be a modulator of the expression of adipogenesis-related genes.

Alteration of expression profile in DFAT-D1 preadipocytes and C3H10T1/2 pluripotent cells following adipogenesis

Since we found the alteration of gene expression in 3T3-L1 preadipocytes following the adipogenic induction, we next investigated whether the MDI mixture condition might also modulate gene expression in other preadipocytes or in other differentiation stages. We used mouse DFAT-D1 preadipocytes and C3H10T1/2 pluripotent cells, the former were established from ddY mouse fat and have the potential to differentiate mature adipocytes [12] whereas, the latter are pluripotent mouse embryonic fibroblasts that can differentiate into adipose, muscle, bone, or cartilage under specific conditions [17,18]. It was shown that these cell lines could differentiate into adipocytes in response to the MDI mixture [11,19]. Although not remarkable compared to 3T3-L1 cells, both DFAT-D1 and C3H10T1/2 cells exhibited intracellular lipid accumulation to some extent in the culture with the MDI mixture

Table 2
Gene expression profiles in 3T3-L1, DFAT-D1, and C3H10T1/2 cells under the adipogenic differentiation condition

Cells:	3T3-L1				DFAT-D1					C3H10T1/2			
		Fold induction[b]				Fold induction[b]					Fold induction[b]		
Gene	Day 0[a]	Day 2	Day 5	Day 8	Day 0[a]	Day 2	Day 4	Day 6	Day 8	Day 0[a]	Day 2	Day 5	Day 8
aP2	9.9E−3	50.6	430.0	574.7	2.0E−3	1.5	2.9	3.5	1.8	1.3E−3	31.9	180.2	961.4
PPARγ	4.1E−3	1.7	2.7	4.3	8.8E−4	2.8	2.2	1.9	1.5	1.3E−2	2.2	3.0	3.1
UCP1	3.4E−2	11.7	1.2	1.6	4.4E−6	2.3	1.6	2.9	1.3	1.0E−5	1.0	0.9	0.1
ERRα	2.9E−3	1.2	1.8	3.5	4.3E−5	2.6	2.2	3.1	1.6	5.0E−3	1.6	1.8	2.7
ERRβ	1.1E−4	0.5	0.3	1.1	1.1E−6	2.2	2.0	2.4	1.5	5.7E−4	1.5	0.9	0.9
ERRγ	7.9E−5	0.5	0.3	1.1	2.6E−6	2.2	2.0	3.8	1.8	6.2E−5	3.1	1.2	1.6
PGC-1α	8.6E−4	0.6	0.3	3.2	1.6E−5	0.8	1.4	1.6	0.9	8.2E−5	1.6	0.4	0.7
PGC-1β	1.1E−3	6.1	6.9	11.7	1.3E−5	2.0	5.8	8.5	3.3	2.1E−4	5.5	7.1	13.1

[a] Data represent the mean of mRNA amounts at day 0 normalized to GAPDH level.
[b] Data represent the relative mRNA level at the indicated times over day 0.

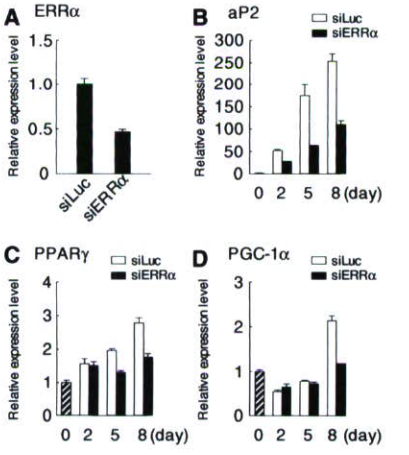

Fig. 3. Knockdown of ERRα mRNA expression leads to down-regulation of adipogenic marker genes in 3T3-L1 cells under the adipogenesis condition. (A) Reduction of ERRα expression by siRNA targeted for ERRα (siERRα). 3T3-L1 cells were transfected with 50 nM siERRα or firefly luciferase (siLuc), respectively. After 48 h, total RNA was isolated and subjected to qPCR, and the results were shown as fold change over ERRα mRNA level at day 0. (B–D) Repression of adipogenic marker genes in siERRα-treated 3T3-L1 cells under the adipogenesis condition. 3T3-L1 cells were induced to differentiate as described in Fig. 1. except for transfection of 50 nM siERRα or siLuc at day 0, 2, and 5. mRNA expression levels of the aP2 (B), PPARγ (C) and PGC-1α (D) at indicated time points were examined by qPCR and the results were shown as fold change over the expression level of each gene at day 0.

as assessed by Oil-Red-O staining (data not shown). Regarding adipogenesis-related genes, both aP2 and PPARγ mRNAs were up-regulated in DFAT-D1 and C3H10T1/2 cells under the adipogenic condition (Table 2). Especially, the fold induction of aP2 mRNA in C3H10T1/2 cells was higher than that in 3T3-L1 cells. Similar to 3T3-L1 cells, ERRα and PGC-1β mRNAs were also up-regulated in both cells following the adipogenic induction. The induction of PGC-1α was not remarkable in these cells compared to 3T3-L1 cells following the MDI stimulation, yet a slight elevation of PGC-1α mRNA was observed during the experimental period in both cells. Interestingly, ERRβ and ERRγ mRNA levels were moderately elevated in DFAT-D1 and C3H10T1/2 cells but not in 3T3-L1 cells. Cumulatively, the expression of the ERR family and its related coactivators PGC-1α and PGC-1β may be closely associated with the adipogenic signals in the process of adipocyte differentiation.

Stable expression of ERRα up-regulates adipogenic marker genes and increases triglyceride accumulation during 3T3-L1 differentiation

To further characterize the function of ERRα in adipocyte differentiation, we generated 3T3-L1 clones stably expressing FLAG-hERRα (3T3-L1-hERRα) or empty vector (3T3-L1-vector). Exogenous expression of hERRα protein was confirmed by Western blotting using anti-FLAG in 3T3-L1-hERRα clones E1 and E10, but not in 3T3-L1-vector clones C2 and C3 (Fig. 4A). mRNA expression of hERRα was also validated by qPCR using specific primers for FLAG-hERRα (Fig. 4B).

Using these 3T3-L1 clones, the alteration of adipogenesis-related gene expression was investigated by qPCR during MDI-induced differentiation as performed in Fig. 1. In general, aP2, PPARγ, and PGC-1α mRNA expression was time-dependently increased in 3T3-L1-hERRα cells during differentiation (Fig. 4B–D). In particular, E1 clones exhibited a ~8-fold and ~6-fold increase in both aP2 and PPARγ mRNA levels at day 8, respectively, compared with 3T3-L1-vector C3 cells (Fig. 4B). In regard to PGC-1α, the mRNA levels in E10 cells were also markedly increased compared with 3T3-L1-vector cells (~7-fold or ~15-fold elevation versus 3T3-L1-vector C2 or C3 cells at day 8, respectively) (Fig. 4C). Furthermore, Oil-O-Red staining revealed that the levels of triglyceride accumulation in 3T3-L1-hERRα cells were increased compared with 3T3-L1-vector cells during differentiation (Fig. 4D).

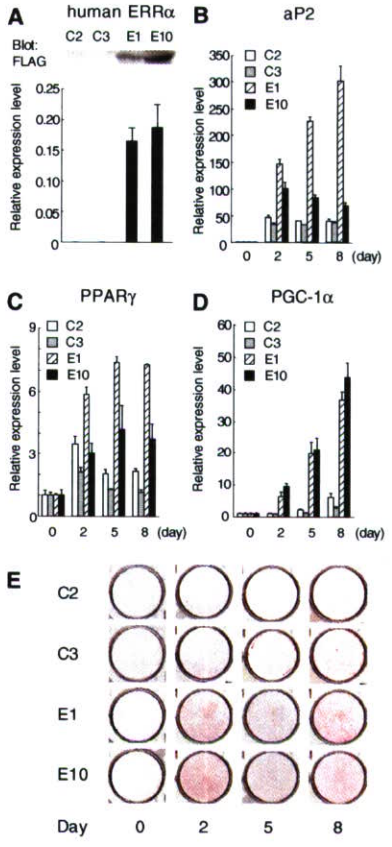

Fig. 4. Stable expression of ERRα up-regulates adipogenic marker genes and increases triglyceride accumulation during 3T3-L1 differentiation. (A) Generation of 3T3-L1 cells stably expressing FLAG-hERRα (3T3-L1-hERRα). Top panel, Expression of exogenous human ERRα protein in 3T3-L1 clones analyzed by immunoblotting using anti-FLAG (M2). C2, C3, clones expressing empty vector (3T3-L1-vector); E1, E10, 3T3-L1-hERRα. Bottom panel, Expression of exogenous human ERRα mRNA validated by qPCR. (B–D) Stable expression of ERRα up-regulates adipogenic marker genes during 3T3-L1 differentiation. 3T3-L1 clones were maintained in the differentiation medium as described in Fig. 1. mRNA levels of the aP2 (B), PPARγ (C), and PGC-1α (D) in each clone at indicated times were examined by qPCR and the results were shown as fold change over the expression level in each clone at day 0. (E) Oil-Red-O staining of 3T3-L1 clones.

Taken together, gain- and loss-of-function study for ERRα reveals that this nuclear receptor positively regulates the expression of adipogenesis-related genes as well as its coactivator PGC-1α, and functions as a promoting factor for 3T3-L1 differentiation.

Discussion

In the present study, we showed that ERRα mRNA expression was up-regulated in response to the adipogenic induction including IBMX, Dex, and insulin in 3T3-L1 and DFAT-D1 as well as C3H10T1/2 cells. Under this differentiation condition, PGC-1α and PGC-1β expression was also increased in parallel with ERRα in those cells. ERRα knockdown by the specific siRNA repressed the adipogenesis-related induction of aP2, PPARγ, and PGC-1α in 3T3-L1 cells. Furthermore, stable expression of ERRα in 3T3-L1 cells significantly up-regulated adipogenesis-related genes and increased triglyceride accumulation during differentiation. These results provide the first evidence that ERRα positively regulates the expression of adipogenesis-related genes during adipocyte differentiation.

ERRα is predominantly expressed in mitochondria-rich tissues such as brown adipose tissue and cardiac myocytes and to play a critical role in the regulation of gene expression involved in mitochondria biogenesis, oxidative phosphorylation, and β-oxidation of fatty acids [20–22]. ERRα itself is not a constitutively active receptor and no small lipophilic ligand has been identified for the receptor. Instead, PGC-1α and PGC-1β have been identified as potential protein ligands for ERR family [8,9]. PGC-1α has been originally identified as an interacting factor for PPARγ [23] and can potentially activate many nuclear receptors. Mice lacking either PGC-1α or ERRα exhibit phenotypes with being lean and resistant to high fat diet-induced obesity [7,24], suggesting that PGC-1α and ERRα function in the same signal pathway. It is also confirmed that PGC-1α mRNA expression in brown fat of ERRα knockout mice is almost half of the expression in wild-type mice [25].

PGC-1β is considered as a more ERR-specific coactivator and protein ligand that may regulate the ERR-mediated transcription [9,26,27]. PGC-1β plays a critical role particularly in energy production in brown fat. PGC-1β transgenic mice are lean, of elevated energy expenditure, and resistant to high fat diet-induced obesity [9]. Although the precise function of PGC-1β in adipogenesis remains to be studied, our results suggest that PGC-1β may also be involved in adipogenesis.

Recently, ERRα has been also shown to regulate the transcription of the nuclear receptor corepressor RIP140/NRIP1 that mediates an inhibitory feedback mechanism to control the adipogenesis-related gene expression during differentiation [28,29]. Thus, ERRα may function as a key regulator in both stimulatory and inhibitory mechanisms for adipogenesis.

ERRβ and ERRγ expression was induced in DFAT-D1 and C3H10T1/2 cells but not in 3T3-L1 cells in the present study. The difference of gene expression may be related to each cell-specific character that represents distinct stages of adipogenesis. Further study will reveal the roles of these receptors during adipogenesis.

In summary, the present study shows that ERRα is a novel adipogenic marker involved in the regulation of the expression of differentiation-related genes. These findings would have physiological relevance that ERRα can be potentially used as a molecular target for the treatment of obesity-related diseases.

Acknowledgments

We thank for Dr. T. Katagiri (Saitama Medical University) for technical advice. We are also grateful to T. Hishinuma, K. Chida and W. Satoh for their technical assistance. This work was supported in part by Grants-in-Aid from the Ministry of Health, Labor and Welfare; from the Japan Society for the Promotion of Science; from The Promotion and Mutual Aid Corporation for Private Schools of Japan. This work was supported in part by Grants of the Genome Network Project and the DECODE from the Ministry of Education, Culture, Sports, Science and Technology of Japan.

References

[1] Y. Shi, P. Burn, Lipid metabolic enzymes: emerging drug targets for the treatment of obesity, Nat. Rev. Drug Discov. 3 (2004) 695–710.
[2] E.E. Kershaw, J.S. Flier, Adipose tissue as an endocrine organ, J. Clin. Endocrinol. Metab. 89 (2004) 2548–2556.
[3] V. Giguère, N. Yang, P. Segui, R.M. Evans, Identification of a new class of steroid hormone receptors, Nature 331 (1988) 91–94.
[4] D.J. Heard, P.L. Norby, J. Holloway, H. Vissing, Human ERR, a third member of the estrogen receptor-related receptor (ERR) subfamily of orphan nuclear receptors: tissue-specific isoforms are expressed during development and in the adult, Mol. Endocrinol. 14 (2000) 382–392.
[5] H. Hong, L. Yang, M.R. Stallcup, Hormone-independent transcriptional activation and coactivator binding by novel orphan nuclear receptor ERR3, J. Biol. Chem. 274 (1999) 22618–22626.
[6] R. Sladek, J.A. Bader, V. Giguere, The orphan nuclear receptor estrogen-related receptor α is a transcriptional regulator of the human medium-chain acyl coenzyme A dehydrogenase gene, Mol. Cell. Biol. 17 (1997) 5400–5409.
[7] J. Luo, R. Sladek, J. Carrier, J.A. Bader, D. Richard, V. Giguere, Reduced fat mass in mice lacking orphan nuclear receptor estrogen-related receptor α, Mol. Cell. Biol. 23 (2003) 7947–7956.
[8] J.M. Huss, R.P. Kopp, D.P. Kelly, Peroxisome proliferator-activated receptor coactivator-1α (PGC-1α) coactivates the cardiac-enriched nuclear receptors estrogen-related receptor-α and -γ. Identification of novel leucine-rich interaction motif within PGC-1α, J. Biol. Chem. 277 (2002) 40265–40274.
[9] Y. Kamei, H. Ohizumi, Y. Fujitani, T. Nemoto, T. Tanaka, N. Takahashi, T. Kawada, M. Miyoshi, O. Ezaki, A. Kakizuka, PPARγ coactivator 1β/ERR ligand 1 is an ERR protein ligand, whose expression induces a high-energy expenditure and antagonizes obesity, Proc. Natl. Acad. Sci. USA 100 (2003) 12378–12383.
[10] D. Knutti, A. Kralli, PGC-1, a versatile coactivator, Trends Endocrinol. Metab. 12 (2001) 360–365.
[11] Z. Wu, P. Puigserver, U. Andersson, C. Zhang, G. Adelmant, V. Mootha, A. Troy, S. Cinti, B. Lowell, R.C. Scarpulla, B.M. Spiegelman, Mechanisms controlling mitochondrial biogenesis and respiration through the thermogenic coactivator PGC-1, Cell 98 (1999) 115–124.
[12] K. Yagi, D. Kondo, Y. Okazaki, K. Kano, A novel preadipocyte cell line established from mouse adult mature adipocytes, Biochem. Biophys. Res. Commun. 321 (2004) 967–974.
[13] K. Horie-Inoue, K. Takayama, H.U. Bono, Y. Ouchi, Y. Okazaki, S. Inoue, Identification of novel steroid target genes through the combination of bioinformatics and functional analysis of hormone response elements, Biochem. Biophys. Res. Commun. 339 (2006) 99–106.
[14] H. Niwa, K. Yamamura, J. Miyazaki, Efficient selection for high-expression transfectants with a novel eukaryotic vector, Gene 108 (1991) 193–199.
[15] H. Green, M. Meuth, An established pre-adipose cell line and its differentiation in culture, Cell 3 (1974) 127–133.
[16] A.K. Student, R.Y. Hsu, M.D. Lane, Induction of fatty acid synthetase synthesis in differentiating 3T3-L1 preadipocytes, J. Biol. Chem. 255 (1980) 4745–4750.
[17] S.M. Taylor, P.A. Jones, Multiple new phenotypes induced in 10T1/2 and 3T3 cells treated with 5-azacytidine, Cell 17 (1979) 771–779.
[18] T. Katagiri, A. Yamaguchi, T. Ikeda, S. Yoshiki, J.M. Wozney, V. Rosen, E.A. Wang, H. Tanaka, S. Omura, T. Suda, The non-osteogenic mouse pluripotent cell line, C3H10T1/2, is induced to differentiate into osteoblastic cells by recombinant human bone morphogenetic protein-2, Biochem. Biophys. Res. Commun. 172 (1990) 295–299.
[19] E.D. Rosen, B.M. Spiegelman, Molecular regulation of adipogenesis, Annu. Rev. Cell Dev. Biol. 16 (2000) 145–171.
[20] V.K. Mootha, C. Handschin, D. Arlow, X. Xie, J. St Pierre, S. Sihag, W. Yang, D. Altshuler, P. Puigserver, N. Patterson, P.J. Willy, I.G. Schulman, R.A. Heyman, E.S. Lander, B.M. Spiegelman, Errα and Gabpa/b specify PGC-1α-dependent oxidative phosphorylation gene expression that is altered in diabetic muscle, Proc. Natl. Acad. Sci. USA 101 (2004) 6570–6575.
[21] J.M. Huss, I.P. Torra, B. Staels, V. Giguere, D.P. Kelly, Estrogen-related receptor α directs peroxisome proliferator-activated receptor α signaling in the transcriptional control of energy metabolism in cardiac and skeletal muscle, Mol. Cell. Biol. 24 (2004) 9079–9091.
[22] S.N. Schreiber, R. Emter, M.B. Hock, D. Knutti, J. Cardenas, M. Podvinec, E.J. Oakeley, A. Kralli, The estrogen-related receptor α (ERRα) functions in PPARγ coactivator 1α (PGC-1α)-induced mitochondrial biogenesis, Proc. Natl. Acad. Sci. USA 101 (2004) 6472–6477.
[23] P. Puigserver, Z. Wu, C.W. Park, R. Graves, M. Wright, B.M. Spiegelman, A cold-inducible coactivator of nuclear receptors linked to adaptive thermogenesis, Cell 92 (1998) 829–839.
[24] J. Lin, P.H. Wu, P.T. Tarr, K.S. Lindenberg, J. St-Pierre, C.Y. Zhang, V.K. Mootha, S. Jager, C.R. Vianna, R.M. Reznick, L. Cui, M. Manieri, M.X. Donovan, Z. Wu, M.P. Cooper, M.C. Fan, L.M. Rohas, A.M. Zavacki, S. Cinti, G.I. Shulman, B.B. Lowell, D. Krainc, B.M. Spiegelman, Defects in adaptive energy metabolism with CNS-linked hyperactivity in PGC-1α null mice, Cell 119 (2004) 121–135.
[25] J.A. Villena, M.B. Hock, W.Y. Chang, J.E. Barcas, V. Giguere, A. Kralli, Orphan nuclear receptor estrogen-related receptor α is essential for adaptive thermogenesis, Proc. Natl. Acad. Sci. USA 104 (2007) 1418–1423.
[26] J. Lin, P.T. Tarr, R. Yang, J. Rhee, P. Puigserver, C.B. Newgard, B.M. Spiegelman, PGC-1β in the regulation of hepatic glucose and energy metabolism, J. Biol. Chem. 278 (2003) 30843–30848.
[27] J. St-Pierre, J. Lin, S. Krauss, P.T. Tarr, R. Yang, C.B. Newgard, B.M. Spiegelman, Bioenergetic analysis of peroxisome proliferator-activated receptor γ coactivators 1α and 1β (PGC-1α and PGC-1β) in muscle cells, J. Biol. Chem. 278 (2003) 26597–26603.
[28] D. Nichol, M. Christian, J.H. Steel, R. White, M.G. Parker, RIP140 expression is stimulated by estrogen-related receptor α during adipogenesis, J. Biol. Chem. 281 (2006) 32140–32147.
[29] G. Leonardsson, J.H. Steel, M. Christian, V. Pocock, S. Milligan, J. Bell, P.W. So, G. Medina-Gomez, A. Vidal-Puig, R. White, M.G. Parker, Nuclear receptor corepressor RIP140 regulates fat accumulation, Proc. Natl. Acad. Sci. USA 101 (2004) 8437–8442.

The Prostate 67:1029 – 1037 (2007)

Cytochrome P450 2B6 is a Growth-Inhibitory and Prognostic Factor for Prostate Cancer

Jinpei Kumagai,[1] Tetsuya Fujimura,[1] Satoru Takahashi,[1]* Tomohiko Urano,[2] Tetsuo Ogushi,[1] Kuniko Horie-Inoue,[3] Yasuyoshi Ouchi,[2] Tadaichi Kitamura,[1] Masami Muramatsu,[3] Bruce Blumberg,[4] and Satoshi Inoue[2,3]

[1]*Department of Urology, The University of Tokyo, Hongo, Bunkyo-ku, Tokyo, Japan*
[2]*Department of Geriatric Medicine, Faculty of Medicine, The University of Tokyo, Hongo, Bunkyo-ku, Tokyo, Japan*
[3]*Research Center for Genomic Medicine, Saitama Medical University, Yamane, Hidaka-shi, Saitama, Japan*
[4]*Department of Developmental and Cell Biology, University of California, Irvine, California*

BACKGROUND. Cytochrome P450s (CYPs) influence the biological effects of carcinogens, drugs and hormones including testosterones. Among them, Cytochrome P450 2B6 (CYP2B6) plays a critical role in the deactivation of testosterone. In the present study, we examined CYP2B6 expression in human prostate tissues and prostate cancer.
METHODS. Immunohistochemical analysis was performed in 98 benign and 106 malignant prostate tissues and patients' charts were reviewed for clinical, pathologic and survival data. We also investigated whether stable expression of CYP2B6 in LNCaP (human prostate cancer cell line) influences cellular proliferation.
RESULTS. CYP2B6 was abundantly expressed in the normal epithelial cells compared to the prostate cancer cells. Significant immunostaining of CYP2B6 was found in 75 of 106 samples (71%), in the cytoplasm of cancerous tissue samples. CYP2B6 immunoreactivity was inversely correlated with high Gleason score ($P < 0.001$). Decreased immunoreactivity of CYP2B6 significantly correlated with poor prognosis ($P < 0.0001$). Univariate and multivariate hazard analyses revealed a significant correlation of decreased CYP2B6 expression with poor cancer-specific survival ($P = 0.0028$ and 0.0142, respectively). Furthermore, overexpression of CYP2B6 in LNCaP cells significantly decreased testosterone-induced proliferation.
CONCLUSIONS. These results demonstrated that decreased expression of CYP2B6 might play a role in the development of prostate cancer, and be useful as the prostate predictor for human prostate cancer. *Prostate 67: 1029–1037, 2007.* © 2007 Wiley-Liss, Inc.

KEY WORDS: **testosterone; proliferation and prognosis**

INTRODUCTION

Prostate cancer is one of the most common malignancies in the world. There is abundant evidence that androgens influence the development and progression of prostate cancer [1–3]. Since most of prostate cancer is androgen-dependent, standard treatment for metastatic prostate cancer patients is androgen deprivation therapy (ADT). However the beneficial effects of ADT are transient and prostate cancer progresses to recurrent cancer. Recent reports showed that levels of testosterone and its metabolites, dihydrotestosterone (DHT) and androstenediol, were still sufficiently high to activate the androgen receptor in recurrent prostate

Abbreviations: ADT, androgen deprivation therapy; CYPs, Cytochrome P450s; DHT, dihydrotestosterone; GS, Gleason score; IR, immunoreactivity; PSA, prostate-specific antigen.

Grant sponsor: Ministry of Health, Labour and Welfare; Grant sponsor: Japan Society for the Promotion of Science; Grant sponsor: Genome Network Project; Grant sponsor: Ministry of Education, Culture, Sports, Science and Technology; Grant sponsor: Promotion and Mutual Aid Corporation for Private Schools.

*Correspondence to: Satoru Takahashi, MD, Department of Urology, Faculty of Medicine, The University of Tokyo, 7-3-1 Hongo, Bunkyo-ku, Tokyo 113-8655, Japan. E-mail: tsatoru@med.nihon-u.ac.jp

Received 2 November 2006; Accepted 7 March 2007
DOI 10.1002/pros.20597
Published online 23 April 2007 in Wiley InterScience (www.interscience.wiley.com).

cancer during ADT [4,5]. The presence of testosterone and its metabolites in recurrent prostate cancer is likely to be significant in prostate cancer progression.

Cytochrome P450s (CYPs) play an important role in biotransformation of xenobiotics such as pharmaceutical drug, environmental contaminants. In addition, these enzymes metabolize endogenous compounds such as steroid hormones [6]. In the liver CYP2B6 hydroxylates testosterone, which results in the deactivation of the hormonal function. It also metabolizes drugs including anti-cancer prodrugs [7]. CYPs have also been detected in extrahepatic tissues, such as the intestine, lung, kidney and brain [8], and breast cancer tissues [9–11]. It was reported that CYP bioactivates anti-cancer prodrug ifosfamide [9] in breast cancers and that the expression of CYPs including CYP2B6 was lower in the tumor tissue than in the adjacent normal tissue [10,11]. The prostate expresses several enzymes involved in androgen metabolism. Since androgens are substrates for multiple CYPs (e.g., CYP2B6, CYP3A4) we undertook to study the expression of this enzyme family in prostate tissues. There are some data from RT-PCR analysis concerning the expression of CYP1A1, CYP1A2, CYP1B1, CYP2B6, and CYP3A4 in human prostate [12,13]. However the expression of CYPs has not been well studied in benign prostate tissues and prostate cancer at the protein level. Since hepatic CYP2B6 is important in testosterone deactivation, we investigated its expression in human prostate tissues using immunohistochemistry. We examined the potential clinical significance of this expression and the influence of CYP2B6 overexpression on the proliferation of the LNCaP cells.

MATERIALS AND METHODS

Antibody and Expression Plasmid Constructs

An anti-CYP2B6 rabbit polyclonal antibody was purchased from Research Diagnostics, Inc. (Flanders, NJ); anti-FLAG M2 antibody and anti-β-actin antibody was from Sigma (St. Louis, MO); and anti-rabbit IgG Alexa Fluor 594 and anti-mouse IgG Alexa Fluor 488 were from Molecular Probes (Invitrogen, Carlsbad, CA). The cDNA encoding amino-terminal FLAG-tagged human CYP2B6 was amplified from the IMAGE-clone, NIH MGC 195 (Open Biosystems), subcloned into a mammalian expression vector pcDNA3 (Invitrogen) and the resulting FLAG-tagged CYP2B6 expression plasmid (pcDNA3-CYP2B6-FLAG) was verified by DNA sequencing.

Cell Culture and Transfection

COS7 cells were cultured in Dulbecco's modified Eagle's medium (DMEM) containing 10% FBS. LNCaP (Human prostate cancer cell line) was purchased from American Type Culture Collection (Manassas, VA). LNCaP was maintained in RPMI1640 media supplemented with 2 mM glutamine, 1% nonessential amino acids, 100 U/ml streptomycin/penicillin and 10% fetal calf serum (FCS). Transfection was performed by using FuGENE6 (Roche, Indianapolis, IN) according to the manufacturer's instruction.

Immunofluorescence Staining

Cells were grown on 12-mm circle cover glasses (Fisher) in 24-well plates. After 16 hr, living cells were washed three times with phosphate-buffered saline (PBS), fixed with 4% paraformaldehyde/0.1 M phosphate buffer for 5 min at room temperature, washed once with PBS, and permeabilized with 0.2% Triton-X 100 in PBS for 10 min. After another washing step with PBS and blocking in 3% bovine serum albumin (BSA)/TBST (100 mM Tris–HCl pH 8.0, 150 mM NaCl, 0.05% Tween 20) for 30 min, cells were first incubated with rabbit anti-CYP2B6 antibody (1:200) and mouse anti-FLAG M2 antibody (1:500) in 3% BSA/TBST for 1 hr at room temperature, washed three times with PBS, subsequently incubated with anti-rabbit IgG Alexa Fluor 594 (1:2,000) and anti-mouse IgG Alexa Fluor 488 (1:2,000) in 3% BSA/TBST for 1 hr at room temperature. Nuclei were stained with DAPI (4′,6-diamidino-2-phenylindole). After cells were washed three times with PBS, cover glasses were mounted in 1.25% DABCO, 50% PBS, 50% glycerol and visualized using a digital microscope (VH-8000, Keyence, Japan).

Western Blot Analysis

Western blot analysis was performed using cellular protein extracts. Cells were rinsed twice with ice-cold PBS and lysed in 200 μl Nonidet P-40 lysis buffer (50 mM Tris–HCl [pH 7.4], 150 mM NaCl, 10 mM NaF, 5 mM EDTA, 5 mM EGTA, 2 mM sodium vanadate, 0.5% sodium deoxycholate, 1 mM dithiothreitol [DTT], 1 mM phenylmethylsulfonylfluoride [PMSF], 2 μg/ml aprotinin and 0.1% Nonidet P-40), and the lysates were cleared by centrifugation at 15,000*g* for 15 min at 4°C. Total protein lysate (20 μg) was fractionated on sodium dodecyl sulfate (SDS)-12.5% polyacrylamide gels, and electrophoretically transferred onto polyvinylidene difluoride (PVDF) membranes (Immobilon, Millipore Co., Bedford, MA).The membranes were blocked in Tris-buffered saline (TBS) with 5% skim milk for 30 min, then incubated with 5 ml each of 1:500 diluted anti-CYP2B6 antibody or 1:1,000 diluted anti-FLAG M2 antibody (Sigma) at room temperature for 3 hr. Each membrane was washed in TBS with 0.1% Tween 20 and incubated with 1:5,000 diluted horseradish peroxidase-conjugated donkey anti-rabbit immunoglobulin G (Ig G) or 1:5,000 diluted horseradish peroxidase-conjugated sheep anti-mouse Ig G (Amersham Pharmacia Biotech, Arlington Heights, IL) at room temperature for 1 hr. Bands were visualized with the chemiluminescence-based ECL plus detection system (Amersham Pharmacia Biotech). The membranes were exposed to X-ray film. All experiments were performed a minimum of three times.

Tissue Selections and Patient Characteristics

Formalin-fixed, paraffin-embedded sections were obtained from 106 patients who underwent radical prostatectomy for prostatic adenocarcinoma between 1987 and 2001. We obtained informed consent from all the patients. The age of the patients ranged from 52 to 78 years (mean 66.8 ± 6.0), and pretreatment serum PSA (prostate-specific antigen) level ranged from 2.2 to 136 ng/ml (mean 16.9 ± 19.5). The pathological stages included B (n = 33), C (n = 59) and D_1 (n = 14). Prostatic tissue sections submitted for this study contained 98 benign and 106 cancerous foci. The cancerous lesions consisted of tumors with Gleason score (GS) 6 (n = 22), 7 (n = 41), 8 (n = 20), 9 (n = 22), and 10 (n = 1), which was evaluated by two trained pathologists. Thirty-five patients (33%) were treated with surgery alone, whereas the remaining patients received adjuvant anti-androgen therapy. Patients were followed postoperatively by their surgeons at 3-month intervals to 5 years and yearly thereafter. Mean patient follow-up period was 82 ± 39 months (range 10–192). During the follow-up period, 77 patients (73%) are alive with no evidence of the disease and 12 (11%) are alive with biochemical or clinical recurrence. Eleven patients (10%) died from prostate cancer and 6 (6%) died from other diseases during the follow-up period.

Immunohistochemistry

Immunohistochemical analysis was performed employing the streptavidin–biotin amplification method using a peroxidase catalyzed signal amplification system: CSA system (DAKO, Carpinteria, CA) as previously described [14]. CSA was used following the manufacturer-supplied protocol. Six μm tissue-sections were deparaffinized, rehydrated through a graded ethanol series, and rinsed in PBS. For antigen retrieval, the sections were autoclaved at 120°C for 15 min in citric acid buffer (2 mM citric acid and 9 mM trisodium citrate dehydrate, pH 6.0). After blocking endogenous peroxidase with 0.3% H_2O_2, the sections were incubated in 10% bovine serum for 10 min. Application of the polyclonal antibody for CYP2B6 (1:200 dilution) was followed by sequential 15-min incubations with biotinylated link antibody, streptavidin–biotin–peroxidase complex, amplification reagent, and streptavidin-peroxidase. The antigen-antibody complex was visualized with 3,3′-diaminobenzidine (DAB) solution (1 mM DAB, 50 mM Tris–HCl buffer pH 7.6, and 0.006% H_2O_2). For negative controls, normal rabbit IgG was used instead of the primary antibodies. As positive controls, sections of human normal liver were immunoassayed with the primary antibodies in the same manner as described above.

Immunohistochemical Assessment

Immunostained slides were evaluated for the proportion (0, none; 1, <1/100; 2, 1/100 to 1/10; 3, 1/10 to 1/3; 4, 1/3 to 2/3; 5, >2/3) and the intensity (0, none; 1, weak; 2, moderate; 3, strong) of positively stained cells [15]. The total scores of immunoreactivity (0–8) were obtained as the sum of the proportion and the intensity. For immunohistochemical assessment, two investigators (TF and JK) evaluated the tissue sections independently. If the IR score (immunoreactivity score) differed between the two investigators, a third investigator (ST) evaluated the samples an average IR score was adopted. Since almost all benign foci showed >5 of IR scores for CYP2B6, we defined IR score 5 as a cutoff for positive immunoreactivity of CYP2B6.

Generation of LNCaP Stably Expressing CYP2B6-FLAG

LNCaP was transfected with an expression vector, pcDNA3-CYP2B6-FLAG or vector alone using FuGENE6. G418 resistant cells were selected and several independent clones were isolated.

3-(4,5-Dimethylthiazol-2-yl)-5-(3-Carboxymethoxyphenyl-2-(4-Sulfophenyl)-2H-Tetrazolium (MTS) Assay

Cell growth rate was measured using a MTS proliferation assay (Cell Titer 96 AQueous One Solution Cell Proliferation Assay, Promega, Madison, WI). The assay was performed according to manufacturer's instructions. Five thousand cells were seeded in 96-well plates and cultured in RPMI supplemented with 10% FBS for 48 and 72 hr. Before testing, 10 μl of MTS reagent was added and the cells were incubated for a further 4 hr at 37°C. The optical density (OD) was measured at a wavelength of 490 nm by a microplate reader (Bio-Rad model 550, Japan). Each time point was performed in quadruplicate wells and each experiment was repeated at least three times. To evaluate effects of testosterone on the growth of LNCaP-CYP2B6-FLAG or LNCaP-Vector clones, the cells were cultured in phenol-red free medium with 10% charcoal-stripped FBS for 48 hr

before experiments. Then 5,000 cells were seeded in 96-well plates and cultured with either vehicle control or testosterone at a dose of 10^{-10} or 10^{-8} M for 48 hr. Percent increase of OD compared with vehicle control was calculated.

Statistical Analysis

Correlations between IR score and clinicopathological characteristics (age, pretreatment serum PSA level, pathological stage and GS) were evaluated using the Student's *t*-test or chi-square test. Cancer-specific survival curves were obtained by the Kaplan–Meier method and verified by the log rank (Mantel-Cox) test. The comparisons between OD of LNCaP clones were evaluated using the Student's *t*-test. Statistical assessment was analyzed by Stat View-J 5.0 software (SAS Institute, Cary, NC) and *P* values less than 0.05 were regarded as statistically significant.

RESULTS

Immunofluorescence Staining of Transfected COS7 Cells

We transiently transfected COS7 cells using pcDNA3-CYP2B6-FLAG and immunostained with anti-CYP2B6 and anti-FLAG M2 antibodies. The anti-CYP2B6 antibody revealed a cytoplasmic staining pattern in CYP2B6-FLAG overexpressed COS7. This expression pattern was shared with the anti-FLAG antibody (Fig. 1A), demonstrating that the protein was located in the cytoplasm.

Validation of CYP2B6 Antibody by Western Blot Analysis

We next transiently transfected COS7 cells using CYP2B6-FLAG expression plasmid for Western blot analysis. As expected, the CYP2B6 antibody detected a 53-kDa band in pCDNA3-CYP2B6-FLAG transfected COS7. A band of apparently the same size was detected by the FLAG M2 antibody (Fig. 1B arrow head).

Immunohistochemistry

Diffuse, but intense CYP2B6 immunostaining was detected in the cytoplasm of benign prostate epithelium. In contrast, immunoreactivity of CYP2B6 was low in the cancer cells. In addition, immunoreactivity of high GS prostate cancer was markedly less than low GS prostate cancer (Fig. 2). The results for the expression of CYP2B6 in the human prostate tissues are shown in Figure 3. When an IR score ≥ 5 was defined as positive, positive CYP2B6 immunoreactivity was identified in 96 (98.0%) benign prostate epithelium cases. Among the 63 low GS prostate cancer cases, positive CYP2B6 immunoreactivity (IR score ≥ 5) was observed in 55 cases (87.3%). Of the 43 high GS prostate cancer cases, positive CYP2B6 immunoreactivity was observed in 20 cases (46.5%). Therefore, a strong association exists between high GS prostate cancer and low CYP2B6 immunoreactivity.

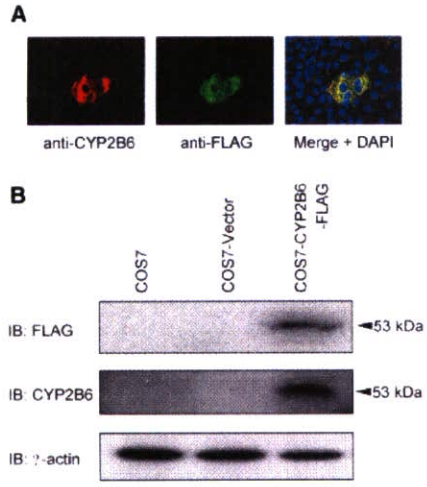

Fig. 1. Immunofluorescence staining of transfected COS7 cells and validation of CYP2B6 antibody by Western blot analysis. A: COS7 cells were grown on cover glasses, transiently transfected with CYP2B6-FLAG expression plasmid, fixed with paraformaldehyde and stained with anti-CYP2B6 antibody and anti-FLAG antibody. Nuclei were counterstained with DAPI. Signals from CYP2B6 (left panel) and signals from FLAG (middle panel) antibody shared an identical subcellular distribution. Merged images are shown on the right panel. Scale bars, 20 μm. B: Cell extracts from untransfected, pcDNA3 empty plasmid transfected, and pcDNA3-CYP2B6-FLAG transfected COS7 cells were resolved by SDS-PAGE and transferred to PVDF membrane. Blot was probed with the anti-CYP2B6 polyclonal antibody (1:500), anti-FLAG antibody (1:1,000) and anti-β-actin antibody (1:1,000). CYP2B6 antibody detected a 53-kDa band in pcDNA3-CYP2B6-FLAG transfected COS7 cells, which was coincided with a band detected by anti-FLAG antibody.

Correlation of CYP2B6 Expression With Clinicopathological Characteristics in Prostate Cancer

This association between CYP2B6 and GS, led us to evaluate the potential correlation between CYP2B6 immunoreactivity and clinicopathological characteristics. Age, pretreatment serum PSA level, GS and pathologic stage) were evaluated (Table I). CYP2B6 immunoreactivity was significantly lower in high GS

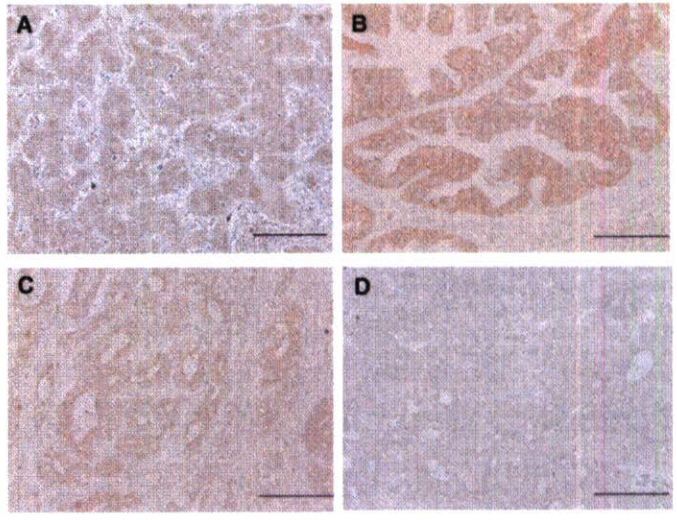

Fig. 2. Expression of CYP2B6 in human liver and benign prostate tissue, low GS and high GS prostate cancer. **A**: Strong staining (intensity: 3) of CYP2B6 was identified in liver. **B**: Strong staining (intensity: 3) of CYP2B6 was identified in benign epithelium. **C**: Moderate immunoreactivity (intensity: 2) was identified in low GS prostate cancer (GS 6). **D**: Weak immunoreactivity of CYP2B6 (intensity: 1) was observed in high GS prostate cancer (GS 9). Scale bars, 100 μm.

cancer (GS 8–10) than in low GS cancer (GS 2–7) ($P < 0.001$).

Figure 4 shows a cancer-specific survival curve prepared by the Kaplan–Meier method. Fifteen of 31 (48.4%) CYP2B6-negative cases had died from prostate cancer during the follow-up period. Patients with CYP2B6-negative prostate cancer had significantly worse cancer-specific survival than those with CYP2B6-positive prostate cancer ($P < 0.0001$, log rank test). Table II shows the prognostic value of PSA, pathological stage, GS and CYP2B6 immunoreactivity in univariate and multivariate proportional analyses for cancer-specific survival. In univariate analyses, CYP2B6 immunoreactivity was significantly ($P = 0.003$) related to cancer specific survival as well as the GS ($P = 0.014$) and pathological stage ($P = 0.035$). In multivariate analysis, among four parameters, only CYP2B6 immunoreactivity retained independent prognostic significance ($P = 0.014$). The relative risk for cancer specific mortality was 14.0 (95% CI 1.69–115.4) for patients with CYP2B6-negative prostate cancer.

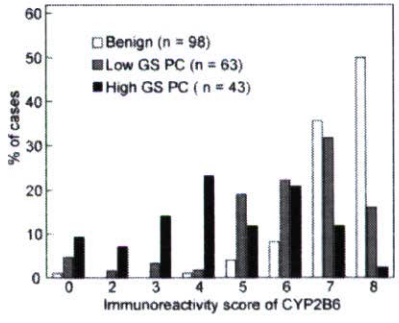

Fig. 3. Immunoreactivity score of CYP2B6 in human benign, low GS prostate cancer and high GS prostate cancer. Positive immunostaining (IR score ≥ 5) was observed more frequently in benign prostate than prostate cancer tissue and more frequently in low GS prostate cancer than in high GS prostate cancer.

Generation of LNCaP Stably Expressing CYP2B6-FLAG

To explore whether constitutive CYP2B6 expression influences cancer cell proliferation in human prostate cancer cell line, we generated LNCaP stably expressing human CYP2B6-FLAG protein and LNCaP clones with the vector (LNCaP-Vector clone #1 and #4). We selected two LNCaP-CYP2B6-FLAG clones #2 and #3 that express CYP2B6-FLAG protein as confirmed by Western blotting using anti-FLAG M2 antibody (Fig. 5A). Further we confirmed protein expression of

TABLE I. Relationship Between Expression of CYP2B6 and the Clinicopathological Findings in PC (n = 106)

	Immunoreactivity of CYP2B6[a]		
	Negative (n = 31)	Positive (n = 75)	*P* value
Age	66.2 ± 5.6	66.9 ± 6.1	0.59
Serum PSA (ng/ml)	19.2 ± 19.3	13.7 ± 12.7	0.08
Gleason score			
2–7	8 (12.7)	55 (87.3)	**<0.001**
8–10	23 (53.5)	20 (46.5)	
Pathological stage			
B, C	24 (22.6)	68 (77.4)	0.07
D1	7 (50)	7 (50)	

[a]IR score 0–4 and 5–8 were defined as negative and positive immunoreactivity, respectively.

LNCaP-CYP2B6-FLAG stable clones by immunofluorescence staining (Fig. 5B). Almost all stable cells expressed CYP2B6-FLAG protein, and the immunoreactivity detected by the anti-FLAG antibody and anti-CYP2B6 antibody were indistinguishable.

MTS Proliferation Assay of LNCaP

Proliferation of LNCaP cells was determined by MTS assay. The proliferation of LNCaP-CYP2B6-FLAG stable clones was significantly reduced after 48 and 72 hr incubation compared to vector clones ($P < 0.0001$) (Fig. 5C). The result indicated that stable expression of CYP2B6 decreased the proliferation of cultured prostate cancer cells. This is consistent with the immunohistochemical results that showed decreased expression of CYP2B6 was associated with a poor prognosis.

Inhibitory Effect of CYP2B6 on Testosterone-Induced Growth

To determine whether effects of testosterone were inhibited by expression of CYP2B6, growth of LNCaP-CYP2B6-FLAG and LNCaP-Vector clones were assayed after testosterone treatment. MTS assay showed that the percent increase of OD was significantly decreased in LNCaP-CYP2B6-FLAG stable clones after 48 hr incubation at doses of 10^{-10} M ($P < 0.0001$) and 10^{-8} M ($P = 0.012$) of testosterone compared to vector clones (Fig. 5D). These data indicated that testosterone-induced growth was inhibited by CYP2B6 expression clearly.

DISCUSSION

In human liver, CYP2B6 ranges between 2 and 10% of the total P450 content [16]. Moreover, CYP2B6 is involved in the metabolism of nearly 25% of drugs on the market today [17]. CYPs expressed in the liver are well known to play pivotal roles in the metabolism of endobiotics, xenobiotic and pharmaceutical drugs. However, CYPs are also expressed in extra-hepatic tissues. Recent years have seen an increased interest in investigation into the presence, function and regulation of CYPs in such tissues, particularly in tumors. CYP1B1 is reported to be overexpressed in human prostate cancer and it was postulated that it contributes to the development or progression of prostate cancer by activating pro-carcinogens [18]. A few reports are available on the expression of CYP2B6 mRNA in prostate [13]. Despite the important role of CYP2B6 in hepatic deactivation of testosterone, extra-hepatic expression of CYP2B6 protein has not been extensively studied, particularly in prostate cancer. Therefore, we studied the expression of CYP2B6 in human prostate tissues using immunohistochemistry and evaluated its clinical significance.

In the present study, we demonstrated CYP2B6 expression in human benign and malignant tissues by immunohistochemical analyses. CYP2B6 immunoreactivity was low in prostate cancer cells, whereas intense and diffuse CYP2B6 immunoreactivity was found in the normal or hyperplastic prostate epithelium. In univariate analysis, CYP2B6 immunoreactivity, GS and pathological stage were significantly related to cancer specific survival, but pretreatment PSA was not associated with cancer-specific survival. Pretreatment serum PSA level is generally an established prognostic

TABLE II. Univariate and Multivariate Proportional Hazard Analyses of Cancer-Specific Survival (n = 106)

	Univariate			Multivariate		
Variable	Hazard ratio	95% index	*P* value	Hazard ratio	95% index	*P* value
PSA (>10 vs. ≤10)	0.79	0.23–2.8	0.73	0.75	0.17–3.26	0.69
Gleason score (high vs. low[a])	13.4	1.71–105.2	**0.014**	5.46	0.61–49.6	0.13
Pathological stage (D1 vs. B, C)	3.8	1.01–12.9	**0.035**	2.02	0.47–8.2	0.34
CYP2B6 (negative vs. positive[b])	23.1	2.94–181.5	**0.0028**	14	1.69–115.4	**0.014**

[a]High Gleason score: 8–10, low: 2–7.
[b]IR score 0–4 and 5–8 were defined as negative and positive immunoreactivity, respectively.

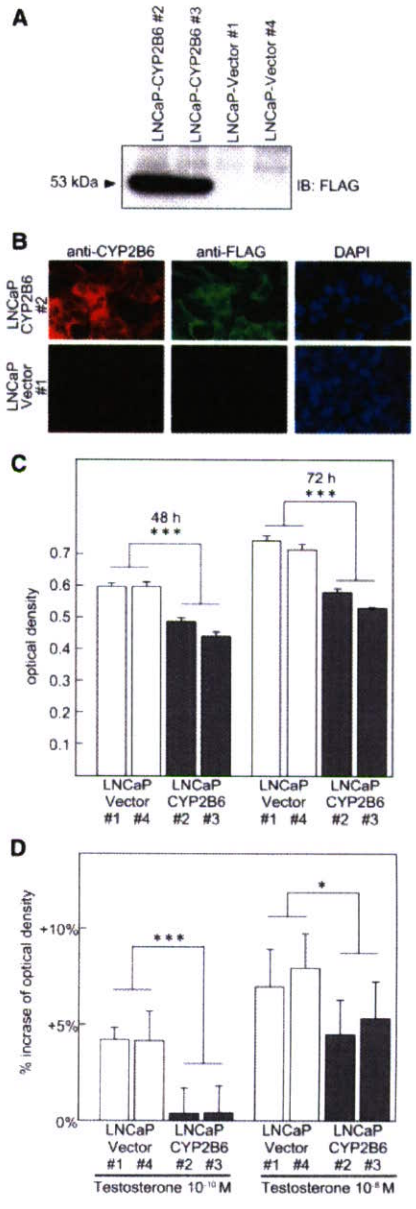

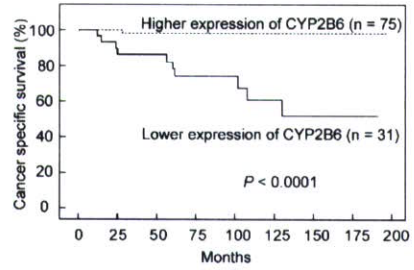

Fig. 4. Cancer-specific survival in 106 prostatic cancer patients relative to the immunoreactivity of CYP2B6. Cancer-specific survival of 31 patients with negative CYP2B6 expression (IR score < 5) was significantly worse than that of 75 positive expression cases (IR score ≥5) ($P < 0.001$).

Fig. 5. Overexpression of CYP2B6 decreases growth of LNCaP cells. **A**: Western blot analysis of LNCaP stably expressing CYP2B6-FLAG (LNCaP-CYP2B6-FLAG) or empty vector (LNCaP-Vector). CYP2B6-FLAG protein was overexpressed in LNCaP-CYP2B6-FLAG clones. LNCaP-Vector clones were used for control. **B**: Immunofluorescence staining of LNCaP. Almost all cells expressed CYP2B6-FLAG protein in LNCaP-CYP2B6-FLAG clone #2 (upper panel). CYP2B6 immunoreactivity was not detected in LNCaP-Vecter cells as shown in lower panel. **C**: Proliferation of LNCaP stable clones was determined by MTS assay. Cell proliferation was evaluated after 48 and 72 hr incubation. ***$P < 0.0001$, compared to vector controls. **D**: Proliferative effects of testosterone were determined by MTS assay. Percent increase of OD was significantly decreased in LNCaP-CYP2B6-FLAG stable clones after 48 hr incubation compared to vector clones at doses of 10^{-10} and 10^{-8} M testosterone. ***$P < 0.0001$, *$P < 0.05$, compared to vector controls.